Monday, July 27, 1998
POSTER SESSION
5:30 p.m. Edmund Burke Theatre Concourse

MARTIAN AND SNC METEORITES

Head J. W. III Smith D. Zuber M. MOLA Science Team
Mars: Assessing Evidence for an Ancient Northern Ocean with MOLA Data

Varela M. E. Clocchiatti R. Kurat G. Massare D.
Glass-bearing Inclusions in Chassigny Olivine: Heating Experiments Suggest Nonigneous Origin

Boctor N. Z. Fei Y. Bertka C. M. Alexander C. M. O'D. Hauri E.
Shock Metamorphic Features in Lithologies A, B, and C of Martian Meteorite Elephant Moraine 79001

Flynn G. J. Keller L. P. Jacobsen C. Wirick S.
Carbon in Allan Hills 84001 Carbonate and Rims

Terho M.
Magnetic Properties and Paleointensity Studies of Two SNC Meteorites

Britt D. T.
Geological Results of the Mars Pathfinder Mission

Wright I. P. Grady M. M. Pillinger C. T.
Further Carbon-Isotopic Measurements of Carbonates in Allan Hills 84001

Burckle L. H. Delaney J. S.
Microfossils in Chondritic Meteorites from Antarctica? Stay Tuned

CHONDRULES

Srinivasan G. Bischoff A.
Magnesium-Aluminum Study of Hibonites Within a Chondrulelike Object from Sharps (H3)

Mikouchi T. Fujita K. Miyamoto M.
Preferred-oriented Olivines in a Porphyritic Olivine Chondrule from the Semarkona (LL3.0) Chondrite

Tachibana S. Tsuchiyama A.
Measurements of Evaporation Rates of Sulfur from Iron-Iron Sulfide Melt

Maruyama S. Yurimoto H. Sueno S.
Spinel-bearing Chondrules in the Allende Meteorite

Semenenko V. P. Perron C. Girich A. L.
Carbon-rich Fine-grained Clasts in the Krymka (LL3) Chondrite

Bukovanská M. Nemec I. Šolc M.
Study of Some Achondrites and Chondrites by Fourier Transform Infrared Microspectroscopy and Diffuse Reflectance Spectroscopy

Semenenko V. P. Nittler L. R. Girich A. L.
The Krymka Chondrite (LL3): A Graphite-containing Fragment and Isotopic Composition of Its Graphite Crystals

Semenenko V. P. Girich A. L.
The Nature of Graphite-containing Fragments in the Krymka (LL3) Chondrite

IRON METEORITES

Budka P. Z. Viertl J. R. M. Schumaker T. B.
Image Analysis Reveals New Information About the Meteoritic Widmanstatten Structure

Ponganis K. V. Marti K.
Nitrides in Iron Meteorites

Budka P. Z. Viertl J. R. M.
Digital Image Techniques Provide New Insights into Meteorite Microstructural Development

Grokhovsky V. I. Kozlov E. A. Karkina L. E. Teplov V. A.
Trasmission Electron Microscope Study of Kamacite in Coarse-structured Iron Meteorites

Righter K. Chabot N. L.
Silicate and Metal Phases in the Queen Alexandra Range 94411 Iron Meteorite

ACHONDRITES

Fioretti A. M. Molin G.
Frontier Mountain 95028: A New Low-Shock Ureilite Close to Allan Hills 78019

Fioretti A. M. Molin G.
Alabandite in Ureilite Frontier Mountain 95028

Floss C.
Iron-, Magnesium-, and Manganese-bearing Phosphates in the Lodranite Graves Nunataks 95209

Goodrich C. A.
Queen Alexandra Range 93148: A Unique Achondrite

Weber I. Bischoff A. Langenhorst F.
Preliminary Results of Microstructural Transmission Electron Microscopy Investigations of Distinct Fine-grained Components Within the Ureilite Hammadah Al Hamra 064

Singh U. K. Sisodia M. S. Shukla A. D. Chakraborty S. Suthar K. M. Dixit M. H. Shukla P. N. Bhandari N.
Lohawat Howardite: Chemical and Mineralogical Characteristics and Cosmogenic Records

Floss C. Fogel R. A. Crozaz G. Weisberg M. Prinz M.
Sulfide/Silicate Melt Partitioning During Enstatite Chondrite Melting

CHONDRITES

Costa T. V. V. Vieira V. W. Araújo M. A. B. Souza Azevedo I. Scorzelli R. B.
Mössbauer Spectroscopy Evidence of Different Degrees of Aqueous Alteration in Two CM Chondrites: Niger (I) and Murchison

Biryukov V. V. Ulyanov A. A.
Textures and Bulk Chemistry of Dark Inclusions in the Reduced CV3 Chondrite Efremovka

Biryukov V. V. Korotaeva N. N. Krot A. N. Ulyanov A. A.
Mineralogy and Classification of Dark Inclusions in the Reduced CV3 Chondrite Efremovka

Gardinier A. Robert F. Behar F. Largeau C. Derenne S.
Preliminary Geochemical Study of Insoluble Organic Matter from the Orgueil Meteorite

Schultz L. Scherer P. Spettel B. Wlotzka F. Zipfel J. Schlüter J. Merchel S. Herpers U. Newton J. Franchi I. A. Pillinger C. T. Leya I. Neumann S. Neupert U. Michel R. Kubik P. W. Synal H.-A. Bonani G. Hajdas I. Ivy-Ochs S. Suter M.
Ten New Meteorites from the Ténéré Desert (Niger): Classification, Noble Gases, Cosmogenic Radionuclides, and Terrestrial Ages

Stepniewski M. Borucki J. Siemiatkowski J.
New Data on the L5(S1) Chondrite Baszkówka (Poland)

Chikami J. El Goresy A. Janicke J.
Chemical Zoning Profiles of Daubreelites in Enstatite Chondrites

Weber H. W. Schultz L.
Noble Gases in the Antarctic R Chondrites Mount Prestrud 95410, 95411, and 95412

Bourot-Denise M. Perron C.
Shock-induced Transformations in an EH3 Chondrite

Kallemeyn G. W. Ebihara M. Latif S.
Prompt-Gamma Analysis and Instrumental Neutron Activation Analysis Studies of a New Reduced L Chondrite

Bridges J. C. Franchi I. A. Sexton A. S. Pillinger C. T.
Oxygen-Isotopic Exchange in Unequilibrated Ordinary Chondrites

Bischoff A. Weber D. Bartoschewitz R. Clayton R. N. Mayeda T. K. Schultz L. Spettel B. Weber H. W.
Characterization of the Rumuruti Chondrite Regolith Breccia Hughes 030 (R3–6) and Implications for the Occurrence of Unequilibrated Lithologies on the R-Chondrite Parent Body

Paliwal B. S. Vaya V. K. Shukla A. D. Chakraborty S. Suthar K. M. Dixit M. H. Shukla P. N. Bhandari N.
Cosmogenic Records in the Didwana-Rajod Meteorite

Kallemeyn G. W.
Further Studies of Antarctic R Chondrites

Mittlefehldt D. W. Lindstrom M. M.
Petrology and Geochemistry of Large Metaigneous Inclusions from L Chondrites

IMPACT CRATERS AND EJECTA

Abels A. Mannola P. Lehtinen M. Bergman L. Pesonen L. J.
New Observations of the Properties of the Lumparn Impact Structure, Åland Islands, Southwestern Finland

Abels A. Pesonen L. J. Deutsch A. Bischoff L. Lehtinen M.
A Geographic Information System-based Characterization of the Söderfjärden Impact Structure, Western Finland

Jones A. P. Heuschkel S. Claeys P.
Comparison Between Carbonate Textures in Chicxulub Impact Rocks and Synthetic Experiments

Abbott J. I. Hough R. M. Gilmour I. Pillinger C. T.
Carbon Chemistry of Suevites and Target Rocks at the Ries Crater, Germany

Skála R. Rohovec J.
Possibly Back-reacted Carbonates from Impact Craters: Evidence Through Magic-Angle-Spinning Nuclear Magnetic Resonance Spectroscopy

Turtle E. P. Melosh H. J.
Can Exponential Creep of Olivine Explain the Formation of the Ring Around Chicxulub?

DeCarli P. S.
Direct Synthesis of Diamond in the Laboratory and in Impact Craters

Ivanov B. A.
Large Impact Crater Formation: Thermal Softening and Acoustic Fluidization

Blom R. G. McHone J. F. Crippen R. E.
Possible 770-Meter-Diameter Impact Crater Detected by Satellite: Yemen Arab Republic

Buchanan P. C. Koeberl C.
Planar Deformation Features in Quartz Grains from the Manson Impact Structure, Iowa

McHone J. F. Killgore M.
Impact-produced Surface Craters on Sikhote-Alin Irons

Grieve R. A. F. Kreis K. Therriault A. M. Robertson P. B.
Impact Structures in the Williston Basin

Aggrey K. Tonzola C. Schnabel C. Herzog G. F. Wasson J. T.
Beryllium-10 in Muong Nong-type Tektites

Kieffer S. W. Claeys P.
Emplacement and Thickness of the Chicxulub Ejecta

Monteiro J. F. Munha J. Ribeiro A.
Impact Ejecta Horizon near the Cenomanian-Turonian Boundary, North of Nazaré, Portugal

Isachsen Y. W.
Metallic Spherules and a Microtektite Support the Interpretation of a Buried Impact Crater Beneath Panther Mountain in the Central Catskill Mountains, New York

OTHER TOPICS

Russell S. S.
A Survey of Calcium-Aluminum-rich Inclusions from R Chondrites: Implications for Relationships Between Meteorite Groups

Ruzmaikina T. V.
Accretional Shock Processing of Dust Aggregates in the Inner Solar Nebula

Gilmour J. D. Bridges J. C. Hutchison R. Turner G.
Iodine-Xenon Analysis of an Igneous Clast from Julesberg: Evidence of Shock Disturbance

Lavielle B. Gilabert E. Soares M. R. Vasconcellos M. A. Z. Poupeau G. Canut de Bon C. Cisternas M. E. Scorzelli R. B.
Noble Gas and Metal Studies in the Vaca Muerta Mesosiderite

Maurette M. Mellini M. Silen J. Tabacco I. Morbidelli A. Chatila R.
Meteorites at Dome C? A Project for the Automated Search for Meteorites with a Planetary Exploration Robot Equipped with Two Radars

Pillinger C. T. Pillinger J. M.
Wold Cottage and Its Influence on Reports of the Pettiswood and Evora Meteorites

Petaev M. I. Wood J. A.
The CWPI Model of Nebular Condensation: Effects of Pressure on the Condensation Sequence

Cyr K. E. Sharp C. Lunine J. I.
Nebular Water Distribution and Nebular Chemistry

Gilabert E. Lavielle B. Neumann S. Gloris M. Michel R. Sudbrock F. Herpers U.
New Cross-Section Measurements of Proton-induced Production of Helium, Neon, and Argon in Iron and Nickel in the Energy Range from 159 to 1600 MeV

Leya I. Baur H. Busemann H. Wieler R. Gloris M. Neumann S. Michel R. Herpers U.
Measurement of Cross Sections for the Proton-induced Production of Helium and Neon Isotopes from Magnesium, Aluminum, and Silicon

Reedy R. C.
Variations in Solar-Proton Fluxes over the Last Million Years

Šolc M. Stork R.
Loosely Bound Matter on the Surface of Small Bodies: Models of Its Motion

Burbine T. H. Binzel R. P. Bus S. J.
"Basaltic" Asteroids in the Main Belt: Are They Fragments of Vesta?

Stork R. Borovicka J. Bocek J. Šolc M.
Peculiar Features of Alpha Monocerotid TV Spectra

Fioretti A. M. Molin G. Reniero G. Piacenza B. Serra R.
Magnetic Cosmic Spherules from the Great Sand Sea (Western Desert, Egypt): A New Example of Eolian Concentration and Trapping

Flynn G. J. Keller L. P. Jacobsen C. Wirick S.
Carbon and Potassium Mapping and Carbon-Bonding-State Measurements on Interplanetary Dust Particles

Flynn G. J. Sutton S. R. Kehm K. Hohenberg C. M.
Volatile Contents of Large and Small Interplanetary Dust Particles from L2036: Comparison of Zinc and Helium Heating Indicators

Koscheev A. P. Panin I. A. Ott U.
Thermal Modification of Synthetic Nanodiamonds as an Analog of Meteoritic Diamond Grains

Gallino R. Lugaro M. Arlandini C. Busso M. Straniero O.
Isotopic Composition of Zirconium and Molybdenum in Single Silicon Carbide Presolar Grains: Asymptotic Giant Branch Model Prediction and Measurements

Lugaro M. Gallino R. Busso M.

Isotopic Composition of Heavy Elements in Single Silicon Carbide Grains: Asymptotic Giant Branch Model Prediction — The Case of Strontium and Barium

Lee P. Cassidy W. A. Apostolopoulos D. Deans M. Foessel A. Krause C. Parra J. Pedersen L. Schwehr K. Whittaker W. L.

Search for Meteorites in the Patriot Hills Area, Ellsworth Mountains, West Antarctica

MARS: ASSESSING EVIDENCE FOR AN ANCIENT NORTHERN OCEAN WITH MOLA DATA. J. W. Head III[1], D. Smith[2], M. Zuber[3], and the MOLA Science Team, [1]Department of Geological Sciences, Brown University, Box 1846, Providence RI 02912, USA (James_Head_III@Brown.edu), [2]Goddard Space Flight Center, Greenbelt MD 20771, USA, [3]Massachusetts Institute of Technology, Cambridge MA 02139, USA.

Several workers have documented evidence on Mars for the presence during its history of water precipitation and runoff, ground ice and groundwater, emergence of subsurface water at slow to catastrophic rates to form channels, and standing bodies of water ranging in scale from lakes to oceans. The Mars Orbiter Laser Altimeter (MOLA) instrument provides very high resolution altimetric data along individual profiles and global high-density altimetric data to characterize regional slopes, roughness, surface features and morphologies. We have been using these data to characterize the northern lowlands, to search for evidence of the presence of an ancient ocean or lakes, and to assess hypothesized coastal geomorphologic features. This assessment addresses the following questions: 1) Do proposed shorelines lie at a constant topographic datum, and if not, could variations be due to subsequent tilting? 2) Is there evidence for a regional change in slope at proposed shorelines? 3) Are surface roughnesses at various scales consistent with the presence of an ocean? 4) Is there topographic evidence in the vicinity of the proposed shorelines for features interpreted to represent coastline processes? 5) Is there topographic evidence for features associated with the proposed emplacement, behavior, and loss of an ocean, in terms of features associated with erosion, deposition, flooding, shoreline migration, freezing, and loss? MOLA data show that one of the shorelines mapped by Parker et al. (JGR, 98, 11061, 1993) occurs within a few hundred meters of the same level at the majority of profiles crossing the boundary. MOLA data also show that the surface is extremely smooth and flat in the northern latitudes. At all longitudes between latitudes 80N and 55N the surface is about -4 km and very level (except in Tharsis, where the surface appears tilted up toward the south). The smoothness is very extensive and extends from the polar terrain toward the equator in several regions. Point to point roughness data and rms slope data show regions of smoothness that are linked to geologic units and their boundaries. Changes in regional slope and roughness show positive correlations with areas proposed to be ancient shorelines in several of the profiles. Thus, MOLA data reveal several lines of evidence that are consistent with the presence of a regional standing body of water in the northern lowlands in the past history of Mars.

GLASS-BEARING INCLUSIONS IN CHASSIGNY OLIVINE: HEATING EXPERIMENTS SUGGEST NON-IGNEOUS ORIGIN. M. E. Varela[1], R. Clocchiatti[2], G. Kurat[3], and D. Massare[2], [1]UNS-CONICET, Dipartimento. de Geologia, San Juan 670, 8000 B. Blanca, Argentina, [2] Laboratoire Pierre Süe, CEA-CNRS, F-91191 Gif sur Yvette Cedex, France, [3]Naturhistorisches Museum, Postfach 417, A-1014 Vienna, Austria.

Multiphase (minerals plus glass) inclusions in olivine of the Chassigny achondrite have been extensively studied [1–3].These inclusions are widely believed to be residuals of the parental melt which was trapped during growth of the olivine from the melt. Under the assumption that Chassigny is a cumulate rock and the glass-bearing inclusions represent the parent magma, the calculated chemical composition of the initial trapped melt resembles that of terrestrial boninite lavas [2]. Subsequent closed system cooling of these trapped melts will produce an assemblage of daughter crystals and a quenched glass. However, based on petrographic features and on the chemical composition of glasses of all types of inclusions in Chassigny olivine [4] proposed that the multiphase inclusions could have been formed by heterogeneous trapping of its constituents rather then by trapping of a parental melt.

Three types of glass inclusions are present in the Chassigny olivine: pure glass, monocrystal and multiphase inclusions (glass, glass plus one mineral or glass plus several minerals, respectively). Glass/mineral ratios are highly variable. The primary petrographic nature of the inclusions suggests that they are very likely samples of the ambient phases that exist during the growth of Chassigny olivine. If the parental melt would be trapped contemporaneously into two inclusions in a given host phase and some phases grow in one inclusion but not in the other, the chemical composition of the glasses in these inclusions must be differ from each other. However, this is not the case with the glasses in the three types of inclusions in Chassigny olivine which all have very similar compositions.

Heating experiments allow to reverse the processes that occurred inside the inclusion during cooling. The phases formed after the closed system evolved will dissolved in the melt during heating. Thus, after quenching, the chemical composition of the glass in a heated residual melt inclusion will be different from that of an unheated one. Heating experiments were performed in a Pt-Pt_{90} Rh_{10} heating stage in a hot He atmosphere as oxygen getter [5] with quenching times (from 1200°C to 500°C) of less than 1 s. The optimum condition runs lasted for approximately 8 hours each with final temperatures of 900°, 1000°, and 1200°C, respectively, which were held for thirty minutes. The final temperature of 1200°C exceeds the "accumulation" temperature of 1140°C estimated for Shergotty and Zagami shergottites [6] (other members of the SNC group). Thus, at 1200°C some reactions between glass (melt) and the host can be expected. However, there was no reaction the case of glass-bearing inclusions in Chassigny olivine.

Table: Averaged electron microprobe analyses (wt%) of glasses in heated glass-bearing inclusions Number in brackets is the number of glass inclusions heated.

T(fin)	900°C (7)	1000°C (6)	1200°C (6)
SiO_2	69.9	71.1	70.0
TiO_2	0.15	0.12	0.20
Al_2O_3	17.6	16.4	16.8
FeO	1.18	2.08	3.28
MnO	0.06	0.04	0.11
MgO	0.83	0.52	1.16
CaO	0.81	1.24	1.31
Na_2O	3.67	3.78	3.62
K_2O	4.53	4.10	3.19
Total	99.03	99.38	99.67

The composition of glasses inside the heated inclusion and close to the inclusion walls remains rich in SiO2, Al_2O_3, and K_20 and poor in FeO and MgO (Table). The compositional similarity between heated and unheated glassy and multiphase inclusions indicates that the latter are not the product of a melt evolution after closed system cooling. Therefore, the glass of glass-bearing inclusions in olivine is not a residual melt but rather is an independent phase which was trapped either with or without mineral phases giving rise to the three inclusion types present.

Acknowledgments: This work was support by LPS (CEA-CNRS) in France, FWF in Austria and CONICET in Argentina.

References: [1] Floran R. J. et al., (1978) *GCA, 42*, 1213–1229. [2] Johnson M. C. et al., (1991) *GCA, 55*, 349–366. [3] Righter et al. (1997) *LPSC XXVIII*, 1181–1182. [4] Varela M. E. et al., (1997) *Meteoritics and Planet. Sci., 32*, Suppl., A130–A131.[5] Zapunnyy S. A. et al. (1989) *Geochem Internat., 26*, 120–128. [6] Stolper E. and McSween H. Y. Jr. (1979) *GCA, 43*, 1475–1498.

SHOCK METAMORPHIC FEATURES IN LITHOLOGIES A, B, AND C OF MARTIAN METEORITE EETA 79001; N. Z. Boctor[1], Y. Fei[1], C. M. Bertka[1], C. M. O'D Alexander[2], and E. Hauri[2], [1]Geophysical Laboratory, Carnegie Institution of Washington, 5241 Broad Branch Rd., NW, Washington, DC 20015; [2]Department of Terrestrial Magnetism, Carnegie Institution of Washington, 5241 Broad Branch Rd., NW, Washington, DC 20015.

EETA 79001 consists of two distinct basaltic lithologies. Lithology A, a highly vesicular fine ground basalt containing olivine megacrysts, and lithology B, a coarse grained ferroan basalts. Between the two lithologies there are pockets of quenched impact melts designated lithology C. Though it is agreed that EETA 79001 is metamorphosed by impact [1,2] a systematic study of its shock history is lacking [3]. We have provided evidence of vitrification and high pressure phase transitions in olivine megacrysts in lithology A (4) and concluded that it is an impact melt. We here report additional features from lithology A, describe shock effects in lithologies B and C, and use pertinent SHOCK wave data to construct the shock history of EETA 79001. In addition to the fine grained aggregates of iron-rich and iron poor olivine described by [4] in shocked olivine megacrysts from lithology A, we observed within some megacrysts alternating lamellae of iron-rich and iron-poor olivine and myrmekite-like intergrowths of the two olivine phases. The olivine compositions plot in the two phase loop where α olivine and γ spinel coexist in the Mg_2SiO_2–Fe_2SiO_4 system at high-pressure [5,6]. The γ phase inverted to the α olivine on decompression. Hugoniot data on olivine show a mixed phase region at pressures of 50–100 GPa [7,8]. The vitrification observed in some megacrysts would occur at pressures ~55 GPa [9].

Shock metamorphic features in lithology B are represented by kinking and deformation lamellae in pigeonite which would require peak pressures ~28 to 34 GPa [3] and melting and incipient vesiculation of plagioclase at shock pressure ~45 GPa. Incipient melting of pyroxene occurred and would require peak pressure of ~60 Gpa. Melt veinlets enclosing nearly isotropic grains of pyroxene composition, similar to those tentatively identified as majorite by [1] are also present. Raman spectra of these grains, however, show Raman peaks at 677 and 1011 cm^{-1} which are characteristic of pyroxene.

In lithology C plagioclase glass pockets are more vesicular relative to plagioclase in lithology B and show a flow structure. Mafic glass pockets show chilled margins and are partially devitrified. They also show a flow structure. The mafic glass formed at shock pressures >80 GPA (10). At such pressure the extensive impact melting that formed lithology A occurred.

References: [1] Steele and Smith (1982) *Proc.LPSC 13*, in *JGR,. 89*, B612. [2] McSween and Jarosewich (1983) *GCA, 47*, 1501. [3] Bischoff and Stöffler (1992) *Eur. J. Mineral., 4*, 707. [4] Boctor et al. (1998) *LPS XXIX*. [5] Katsura and Ito (1989) *J. Geophys. Res., 94*, 15663. [6] Bertka and Fei (1997) *J. Geophys. Res., 102*, 525. [7] Jeanloz (1980) *J. Geophys. Res., 83*, 3163. [8] Jackson and Ahrens (1979) *J. Geophys. Res., 84*, 3039. [9] Jeanloz et al. (1977) *Science, 197*, 457. [10] Schaal and Hörz (1977) *Proc. LSC 8th*, 1697.

CARBON IN ALLAN HILLS 84001 CARBONATE AND RIM. G. J. Flynn[1], L. P. Keller[2], C. Jacobsen[3], and S. Wirick[3], [1]Department of Physics, State University of New York–Plattsburgh, Plattsburgh NY 12901, USA, [2]MVA, Inc., 5500 Oakbrook Parkway, Norcross GA 30093, USA, [3]Department of Physics, State University of New York–Stony Brook, Stony Brook NY 11794, USA.

We have previously reported Scanning Transmission X-Ray Microscope (STXM) C mapping and X-ray Absorption Near Edge Structure (XANES) spectroscopic measurements on carbonate globule and opaque "rim material" from the ALH 84001 meteorite [1]. Percent-level organic carbon was found associated with both the carbonate globule and the "rim material" dominated by feldspathic glass, appearing opaque mainly because of the presence of chromites, and containing only minor amounts of the carbonate, magnetite, and sulfide which are major components in the rims described by McKay et al. [2]. Further, the organic compound in the globule was different from that in the opaque material [1].

To follow-up on those measurements, a carbonate globule with attached rim material was extracted from a freshly broken surface of a chip of ALH 84001 (ALH 84001,255). This sample was embedded in elemental S, a series of ultramicrotome thin sections were prepared and deposited on an SiO substrate. Several sections included a small (~2 × 2 μm) area of rim material attached to an ~8-μm globule fragment, preserving the spatial associations between the rim and the globule.

Transmission Electron Microscope examination of the section analyzed indicates it contains three distinct regions. Fine-grained rim material consisting of carbonate, magnetite, and rare sulfides, and coarse-grained carbonate in the globule interior are separated by a region containing coarse-grained, porous carbonate and sparse, fine-grained magnetite.

The rim material showed four strong π^* peaks. Three peaks, at 285 eV, 286.2 eV, and 288 eV, are similar to the peaks, at 284.8 eV, 286.5 eV, and 288.2 eV, detected in the carbonate globule from ALH 84001 examined previously [1]. Those peaks were associated with organic C by Fourier Transform Infrared spectroscopic examination of that globule [1]. The fourth peak, at 290 eV, is indicative of carbonate. In each C-XANES spectrum we can measure the ratio of the absorption at 290 eV to that at 288 eV to monitor the ratio of carbonate to organic C. A comparison of the average C-XANES spectrum over the carbonate globule with the average over the rim indicates that the rim has a higher ratio of organic C to carbonate than does the globule. We were unable to isolate regions in the rim which showed only the organic or only the carbonate absorption feature(s), suggesting that organic C is intimately mixed with the carbonate on the scale of ~100 nm.

The same three organic absorption peaks occur with roughly the same peak height ratios in both the rim and the globule. This indicates that, in this sample, the rim and the globule contain the same type(s) of organic compound(s). Analyses of individual carbonates within the globule showed weak, but distinct, organic absorptions accompanying the strong carbonate absorption, indicating the presence of the organic component either within or associated with the large carbonates. The porous carbonate beneath the rim exhibits the same four C-XANES absorptions, and the average spectrum of the porous carbonate is indistinguishable from that of the core carbonate.

These new measurements confirm our earlier results indicating that relatively high concentrations (percent level) of organic C are spatially associated, at the 100-nm scale, with the carbonates in ALH 84001. They differ from the earlier results in that this sample of rim material, consisting of fine-grained carbonate, magnetite, and sulfides, contains an organic component that is identical in its C-XANES spectrum to that of the carbonate globule to which it is attached. The earlier opaque sample, dominated by feldspathic glass and chromite, has a C-XANES spectrum which differs in absorption peak energies and structure from these rim and globule samples.

References: [1] Flynn G. J. et al. (1998) *LPS XXIX*. [2] McKay D. S. et al. (1996) *Science*, *273*, 924–927.

MAGNETIC PROPERTIES AND PALEOINTENSITY STUDIES OF TWO SNC'S. M. Terho, Palkkatilankatu 1-3 L 193, SF-00240 Helsinki, Finland (mauri.terho@sci.fi).

Magnetic properties and paleointensities have been studied from Zagami and EETA 79001.138 shergottites. Both samples were small fragments. Weight of Zagami (from Finnish collection) was 2,89 g and weight of EETA 79001.138 (from LPI) was 5,47 g [1].

The petrophysical properties of the samples show similarities. The densities of samples were 3071 kg/m^3 (Zagami) and 3124 kg/m^3 (EETA 79001). The porosity of samples is 7,23% (Zagami) and 7,97% (EETA 79001) [1].

The magnetic susceptibility of samples is also quite similar 1237×10^{-6} SI (Zagami) and 1977×10^{-6} SI (EETA 79001). The anisotropy of magnetic susceptibility is quite the same 1,07 (Zagami) and 1,02 (EETA 79001) and magnetic foliation dominates in both samples [1]. Thermal behavior of magnetic susceptibility shows Curie-points 590ºC for both samples and equal mineralogical chances happened during heating from 20ºC up to 720ºC.

The hysteresis properties are, again, quite similar. Remanent magnetisation is 55 A/m (Zagami) and 65 A/m (EETA79001). Coercivity and coercivity of remanence are 18,1 mT and 100 mT for Zagami and 22,2 mT and 88,5 mT for EETA 79001. The ratio between remanence and saturation magnetisation behaves in the same way: 0,33 for Zagami and 0,36 for EETA 79001. The hard of magnetisation [2] is 3,6% for Zagami and 4,4% for EETA 79001.

The intensity of anhysteretic remanent magnetisation (ARM) is just as high in both samples: 0,43 A/m for Zagami and 0,36 A/m for EETA 79001. The saturation field is also the same for both samples (150 mT), though the 50%-value ($B_{½}$) is higher for EETA 79001 (56 mT) than for Zagami (30 mT). According to Lowrie-Fuller test the magnetic domain behaves as SD/PSD in Zagami, but in EETA 79001 the domain behaves as SD/PSD in the field lower than 45 mT and above it behaves as MD.

The intensity of natural remanent magnetisation (NRM) of Zagami (11 A/m) is much higher than the intensity of EETA 79001 (0,073 A/m). A.f. demagnetisation up to 150 mT shows that NRM of both samples has only one component and it is stable. The intensity of NRM after 150 mT demagnetisation is two times higher in EETA 79001 (30%) than in Zagami (15%).

Three separate paleointensity tests (Thellier double heating, Shaw-method, ARM-NRM) and four of their applications have been used to determine the strenght of paleofield. Paleointensity for Zagami is much higher than paleointensity for EETA 79001. In the case of Zagami the paleointensity varies from 64 μT (Coe) to 3161 μT (CPM) whereas paleointensity in the case of EETA 79001 varies from 0,6 μT (Kono) to 13,4 μT (Thellier and Coe). The reliability of determinations is quite good. The temperature range for Thellier and Coe is 150°–300ºC for EETA 79001 and 300°–550ºC for Zagami and the field range for non-heating methods is 0–150 mT for EETA 79001 and 0–100 mT or 20–150 mT for Zagami.

Though the paleointensity results vary much depending on the technique of determination, the big difference between the paleofields measured from Zagami and from EETA 79001 suggests that the intensity of magnetic field in Mars is not homogenous, but may vary in large scale [3].

All the measurements have been made by the author in Geological Survey of Finland in 1992–1997. The author wishes to acknowledge the help and direction of L. J. Pesonen, K. A. Kinnunen, M. Lehtinen, M. Leino, M. Lindström, S. Mertanen and R. Puranen. This work has been supported by Oskar Öflunds Stiftelse and Vilho, Yrjö and Kalle Väisälä Foundation grants.

References: [1] Terho M. (1997) *M. Sc. Thesis. Univ. Helsinki*, 59 pp. [2] Morden S. J. (1990) *Ph.D. Thesis Univ. Newcastle upon Tyne.*, 123. [3] Terho M. et. al (1996) *Earth, Moon and Planets, 72*, 225–231.

GEOLOGICAL RESULTS OF THE MARS PATHFINDER MISSION. D. T. Britt, Lunar and Planetary Laboratory, University of Arizona, Tucson AZ 85721, USA.

Perhaps the most surprising finding by Pathfinder was the consistant pattern of high-silica rocks measured by the APXS [1]. The SiO_2 compositions ranged from 52.2–61.2 wt% and were strongly anti-correlated with sulfur content, suggesting that the lower silica rocks were depleted by a weathering process that increased the sulfur content of the surface rind [1]. All the analyzed rocks at the site fit on a trend line of increasing silica with decreasing sulfur, which can be extrapolated to a "sulfur-free" composition of 62 wt% SiO_2. There is a similar spectral correlation with the higher-silica, less sulfur-rich rocks appearing refresher, darker, and less weathered. The implication of these data are that the rocks of the Pathfinder site have very similar compositions and may be from the same geologic unit. The variation in reflectance spectra and APXS results are probably due entirely to the effects of differing exposure to local weathering. The results also suggest that the rocks at the Pathfinder are not the hoped-for highlands material, but are part of a locally extensive unit composed of late stage fractionated magma similar to Icelandite. These are magmas with silica contents in the Andesite range but not associated with subduction processing. These compositions are characteristic of late-stage volcanism of fractionated basaltic precursors that can be laterally extensive but volumetrically relatively minor. This unit may be associated with the nearby Ridged Plains Material of Hesperian Age.

A second surprising result the was the lack of well-defined spectral features in the rocks (and the soils). There are no apparent orthopyroxene features in the 0.9–1.0 μm region, as might have been expected from shallow bands seen in the Martian Dark Region spectra. APXS analysis suggests that the rocks are Fe rich and may have a mineralogy with significant high-Fe clinopyroxene, which has band minima outside the IMP wavelength range. These rocks are mineralogically and morphologically consistant with an igneous origin although a sedimentary origin cannot be ruled out [1].

FURTHER CARBON ISOTOPIC MEASUREMENTS OF CARBONATES IN ALH 84001 I. P.Wright[1], M. M.Grady[1,2], and C. T.Pillinger[1], [1]Planetary Sciences Research Institute, Open University, Walton Hall, Milton Keynes MK7 6AA, England (i.p.wright@open.ac.uk), [2]Natural History Museum, Cromwell Road, London SW7 5BD, England (m.grady@nhm.ac.uk).

We have previously suggested that the (somewhat unexpected) results obtained from sequential acid etching of one particular sample of ALH 84001 could be due to the presence of organic materials surrounding individual carbonate grains [1]. Indeed, taking the evidence and conclusions of McKay et al. [2] at face value, and assuming the operation of past life on Mars, we had speculated that the organic materials in question could be due to a biofilm [1], an observation in keeping with features documented by electron microscopy [3]. Whilst the relevance of biofilms in a sample from Mars goes without saying [e.g. 4], it is clearly going to be necessary to constrain the meteoritical phenomena as tightly as possible. As such it seemed appropriate to consider this issue further.

In order to comprehend the results from our original acid dissolution experiments, which involved reclaiming unreacted material at each stage, a further sample of ALH 84001 (subsample 106) was treated, but in this case residual materials were *not* reclaimed after each period of etching. Rather, the meteorite was reacted sequentially with acid but *without* removal of any residues. In this new set of experiments the CO_2 released after the first 12 hours at 25•C amounted to 12.1 ppm C with $\delta^{13}C$ of +14.5‰ (compared to 12.8 ppm C and $\delta^{13}C$ of +6.8‰ in the original experiment). For completeness note that the $\delta^{18}O_{SMOW}$ value obtained herein was +18.7‰, assuming calcite, compared to +15.1‰ previously [1]. The CO_2 released during the next 12 hours, this time at 75•C, was equivalent to 170.6 ppm C with $\delta^{13}C$ of +40.9‰ (21.3 ppm C and $\delta^{13}C$ of -5.6‰ previously). After a further period at the same temperature the overall C yield for all steps was nearly 200 ppm with $\delta^{13}C$ of +38.7‰ (compared to 43.7 ppm C and $\delta^{13}C$ of -1‰ for the original experiment). So, in other words, it would seem that provided the sample under investigation is not removed from the acid during sequential etching, the overall yield of CO_2 is compatible with that expected, i.e. about 280 ppm C, on the basis of total carbon measurements [5]. The overall $\delta^{13}C$ value is exactly what would be anticipated from the bulk of the carbonates in ALH 84001 [5].

So, there are two things to contemplate. Firstly, we can re-evaluate the results from the original study confident that they are real (although still difficult to understand). This necessarily means considering further the role of organic materials during the dissolution process. Secondly, we need to explain the difference in $\delta^{13}C$ obtained from the first and subsequent extractions. In our experiments the first extractions were carried out at 25°C, with subsequent ones at 75°C. So, it is not merely time that is important here, but temperature as well. It is known that the composition of the carbonates plays a part here, with Ca-rich minerals reacting ahead of Mg-rich varieties. Future ion probe measurements should enable carbon isotopic data to be related directly to carbonate chemistry. In the meantime it is already known that there are wide variations in the carbon isotopic composition of the carbonates in ALH 84001 [1,6,7]. The results presented here would seem to confirm this.

The question to address is whether or not the variation in C isotopic composition of carbonates in ALH 84001 represents a primary effect which, in consequence, would have martian connotations. In this regard it should be stressed that meteorites collected from Antarctica are prone to becoming contaminated by terrestrial weathering products. From many other studies these are known to have $\delta^{13}C$ around 0±10‰. Thus, it is entirely probable that the CO_2 released during the preliminary acid etch herein, or in the previous investigation [1], is predominantly from the reaction of Antarctic weathering products. If so, it is apparent that the bulk of the carbonates in ALH 84001 have $\delta^{13}C$ values of about +40‰, which seems to be at odds with results from other studies [e.g. 6,7].

References: [1] Wright I. P. et al. (1997) *LPS, XXVIII,* 1589–1590. [2] McKay D. S. et al. (1996) *Science, 273,* 924–930. [3] McKay D. S. et al. (1997) *LPS XXVIII*, 919–920. [4] Gibson E. K. et al. (1998) *LPS XXIX*, abstract #1433. [5] Grady M. M. et al. (1994) *Meteoritics, 29*, 469. [6] Jull A. J. T. et al. (1995) *Meteoritics, 30,* 311–318. [7] Jull A. J. T. et al. (1997) *JGR (Planets), 102,* 1663–1669.

MICROFOSSILS IN CHONDRITIC METEORITES FROM ANTARCTICA? STAY TUNED. L. H. Burckle[1] and J. S. Delaney[2], [1]Lamont Doherty Earth Observatory of Columbia University, Palisades NY 10064, USA (burckle@LDEO.columbia.edu), [2]Department of Geological Sciences, Rutgers University, 610 Taylor Road, Piscataway NJ 08854-8066 (jsd@rci.rutgers.edu).

Controversies surrounding the alleged occurrence of Martian life forms in a meteorite recovered from Antarctica require that the Antarctic environment be critically assessed as a source of terrestrial biogenic contaminants. Carbon isotopic evidence that terrestrial organics have indeed invaded the ALH 84001 achondrite is compelling. However, the vector by which they were introduced into the meteorite is not well defined. The organic molecules recognized provide limited information about the original host. For example, they may be introduced as discrete organic molecules by some ice/water transportation mechanism or by eolian processes. They may also be a by-product of the breakdown of microscopic life forms that were transported and lodged in the meteorite during their residence on the Antarctic ice. The East Antarctic Icefield, from which most Antarctic meteorites have been concentrated and collected, is a locus for portions of the global circulation pattern. Two atmospheric processes are capable of transporting terrestrial biotic remains onto the East Antarctic Plateau; (a) atmospheric lows form off the Antarctic coast and occasionally penetrate far inland and (b) the polar cell which transports air (and micrometer-sized particles) from lower latitudes through the upper atmosphere to the south polar region where it descends. This air spreads out radially across the plateau as inversion winds and, at the margin of the plateau becomes katabatic winds that are easily capable of displacing even gravel sized particles. Indeed, such winds are known to transport meteorites across the blue ice fields and are a major contributor to the deflation of the blue ice surface. It is reasonable to suggest that micrometer to millimeter sized objects are also easily transported. Because microfossils from both the Southern Ocean and more northerly sources have been identified in Antarctic ice at South Pole Station and at Station Dome C [1,2], we suggest that global circulation plays a role in transporting microfossils (diatoms and opal phytoliths) onto the Antarctic continent. We further suggest that the occurrence of such microfossils on the East Antarctic Plateau may be used to address some questions concerning alleged martian life forms as well as high southern latitude atmospheric circulation. Many recent microfossils still contain associated organic materials and represent a readily identifiable source of contaminants in meteorites. The importance of these microfossils has also been recognized in the Transantarctic Mountains where implausible climate change models have been falsified by the recognition of air borne microfossils [3,4]. A search for similar microfossils has been initiated treating the Antarctic meteorite collections as potential hosts. The initial study involves small ordinary chondrites of high metamorphic grade for which there is absolutely no evidence or even a suggestion that extraterrestrial life forms may be present. The meteorites are chosen to be somewhat fractured so that good sites are available to trap windblown particles. The unbroken main masses of the meteorites are transported to a clean room and the storage bags unsealed there. The meteorite is then immersed in double distilled water and sonified to dislodge dust from the cracks and surface. This dust is transferred to microscope slides under clean room conditions, and examined microscopically for microfossils. The initial work involves two chondrites each from Allan Hills and the Queen Alexandria Range; results will be reported at the Dublin meeting. If microfossils from mid-latitude sources are identified then we suggest that other micrometer scale particles such as smog, perhaps with associated PAH, from Southern hemisphere cities may also occur in Antarctic meteorites. If sufficient microfossils are present in individual meteorites they may be concentrated for extraction and characterization of their organic fractions.

References: [1] Burckle L. H. et al. (1988) *Geology, 16,* 326–329. [2] Kellogg D. E. and Kellogg T. B. (1996) *Geology, 24,* 115–118. [3] Bleakley N. (1996) Msc. thesis, Victoria University of Wellington, 273 p. [4] Burckle L. H. and Potter Jr., N. (1996) *Geology, 24,* 235–238.

Mg-Al STUDY OF HIBONITES WITHIN A CHONDRULE-LIKE OBJECT FROM SHARPS (H3). G. Srinivasan[1] and A. Bischoff [2]. [1]Earth Science and Solar System Division, Physical Research Laboratory, Ahmedabad 380 009, India. [2]Institut für Planetologie, Wilhelm-Klemm-Str. 10, D-48149 Münster, Germany, bischoa@nwz.uni-muenster.de.

Calcium-aluminum-rich inclusions (CAIs) and chondrules are important constituents of primitive meteorites, however, the relationships between these objects are not absolutely clear. Many authors have suggested that CAIs, Al-rich chondrules, and normal ferromagnesian chondrules would represent a continuum of compositions and, thus, could be genetically related (e.g., [1,2]). Chemical mixing calculations suggest that CAI fragments mixed with normal ferromagnesian chondrules reproduce the bulk composition of Al-rich chondrules [3]. Further, CAIs from primitive chondrites have initial $^{26}Al/^{27}Al$ of ~ 5×10^{-5} [4,5,6] and Al-rich objects have lower $^{26}Al/^{27}Al$ of $\leq 1 \times 10^{-5}$ (e.g., [6,7]). If the ^{26}Al distribution in the nebula was homogeneous, then the observed $^{26}Al/^{27}Al$ values imply that Al-rich objects formed about two million years after the formation of CAIs, however this interpretation has been questioned by some authors [8].

We have initiated mineralogical, isotopic and trace-elemental studies of several inclusions from Sharps (H3) ordinary chondrite to (i) further investigate the ^{26}Al abundances in CAIs and chondrules from ordinary chondrites, and (ii) to decipher possible genetic relationships between CAIs, Al-rich chondrules and ferromagnesian chondrules. The inclusions were documented using an JEOL 840A electron microscope at the University of Münster and Mg-Al analyses and trace element studies are in progress using the Cameca ims-4f ion microprobe at PRL.

The Sharps chondrule-like object (SCI) is 150 μm in diameter and consists of an irregularly-shaped hibonite-spinel-rich inclusion embedded in a nepheline-like mesostasis of the host object (Fig. 4d of [9]). The host consists of CaO-rich and CaO-poor pyroxene, olivine, CaO-rich plagioclase, and Fe-Ni blebs [9]. The second refractory inclusion in Sharps (SCII) is a fine-grained round object of 100 μm in diameter rimmed by Ca-rich pyroxene. It consists of fassaite (TiO_2: ~10–14 wt%), CaO-rich pyroxene, spinel (FeO: ~2-8 wt%) and a nepheline-like phase. The third inclusion SCIII is an elongated object (250 × 60 μm) rimmed by CaO-rich pyroxene. One melilite grain (Mg-free; about 10 × 10 μm) is located in the interior adjacent to a tiny garnet. Small (≤5 μm) grains of perovskite/ilmenite are also present. (see Fig.4c of [9]).

We have carried out Mg-Al isotope studies of the hibonite grains and the nepheline-like phase in SCI. Ion probe measurements were difficult due to the small grain size and the possibility of contamination by surrounding Mg-rich phases. Contamination from the surroundings was minimised by using low primary ion beam current and by collecting secondary ions through a small aperture. The Al/Mg values in hibonite range from 30-50 and none of the grains show resolvable ^{26}Mg excess. The initial $^{26}Al/^{27}Al$ in this object is $<5\times10^{-6}$.

The absence of ^{26}Al in hibonite implies that these grains were formed several million years after the initial formation of CAIs. Alternatively, the Mg isotopic systematics was reset by late stage secondary processes. The igneous texture of the host object clearly indicates that the inclusion experienced partially melting after initial formation [9]. If the Mg-Al system was reset by partial melting event then it implies that this event took place several million years after the initial formation of CAIs. Therefore, the formation of chondrule-like host took place several million years after the formation of CAIs. Further work on these objects is in progress.

References: [1] Scott E. R. D. et al. (1982) *LPS XIII*, 704. [2] Bischoff A. and Keil K. (1983) *Nature, 303*, 588–592; [3] Srinivasan G. et al. (1997) *Meteoritics & Planet. Sci., 32*, A123–A124. [4] Lee et al.(1976) *JGR, 3*, 109–112. [5] MacPherson et al. (1995) *Meteoritics & Planet. Sci., 30*, 365-386. [6] Russell S. S. et al. (1996) *Scienc,e 273* 757–762. [7] Hinton R. and Bischoff A. (1984) *Nature, 308*, 169–172. [8] Wood J. (1996) *Meteoritics & Planet. Sci., 31*, A154–A155. [9] Bischoff A. and Keil K. (1984) *GCA, 48*, 693–709.

PREFERRED-ORIENTED OLIVINES IN A PORPHYRITIC OLIVINE CHONDRULE FROM THE SEMARKONA (LL3.0) CHONDRITE. T. Mikouchi, K. Fujita, and M. Miyamoto, Mineralogical Institute, Graduate School of Science, University of Tokyo, 7-3-1 Hongo, Bunkyo-ku, Tokyo 113-0033, Japan (mikouchi@min.s.u-Tokyo.ac.jp).

Semarkona (LL3.0) is known as one of the least thermally equilibrated ordinary chondrites and many works have been performed to understand formation processes of chondrites in the early solar system [e.g., 1,2]. We have analyzed the thin section of Semarkona (USNM 1805-10) and found a large porphyritic olivine chondrule (~7 mm across) showing a preferred oriented texture of olivine within it (Fig. 1). The olivine phenocrystic grains in this chondrule are euhedral (hexagonal) and embedded in mesostasis glass with abundant microcrystallites. To testify whether olivine grains in this large chondrule really have a preferred orientation or not, we measured angles between the longer dimensions of the euhedral crystals and the base line set in an enlarged optical photomicrograph of this chondrule. About 60 individual euhedral crystals showing well-developed hexagonal shapes are measured and the result is shown in Fig. 2. This clearly suggests that olivine grains in this chondrule have a preferred orientation. We then analyzed chemical compositions of these olivine grains by electron microprobe. Olivines are zoned in chemical composition and the core compositions are as magnesian as Fa_9. Thus, this large chondrule belongs to a type II porphyritic olivine chondrule. A few types of chemical zoning patterns are observed in these olivines, which is consistent with a report of type II porphyritic chondrules by [2]. There is also no difference in major and minor element contents from the other type II porphyritic olivine chondrules in the studied thin section. This means that this large chondrule experienced the same thermal history as the others and rules out an exotic origin of this chondrule. The shape of this chondrule is not perfectly spherical, but slightly flattend. The flattend direction is nearly parallel to the preferred-oriented direction of olivine grains. Therefore, compaction of this chondrule might cause a preferred orientation of olivine grains within it when the chondrule was still soft. The presence of cracks parallel to this direction (Fig. 1) is also consistent with such compaction. However, we can not rule out the other processes producing a preferred orientation of olivines in this chondrule.

Acknowledgment: We thank Drs. G. J. MacPherson and T. J. McCoy for the sample.

References: [1] Jones R. H. and Scott E. R. D. (1990) *Proc. LPSC 19th*, 523–536. [2] Jones R. H. (1989) *GCA*, *54*, 1785–1802.

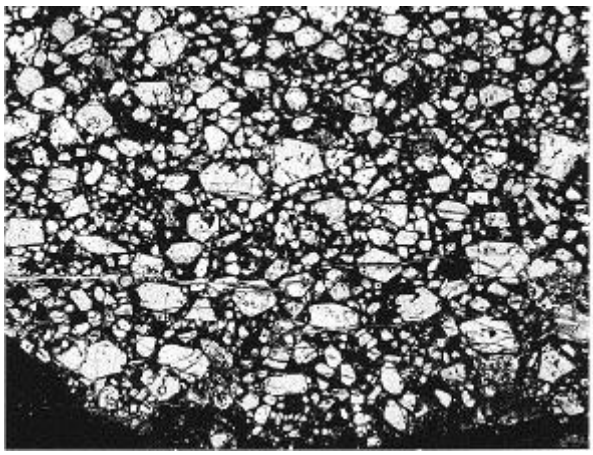

Fig. 1. Photomicrograph of a porphyritic olivine chondrule in Semarkona. The field of view is about 3 mm.

Fig. 2. Angles between longer dimensions of olivine crystals and the base line. The base line is set almost perpendicular to the bottom line of Fig. 1.

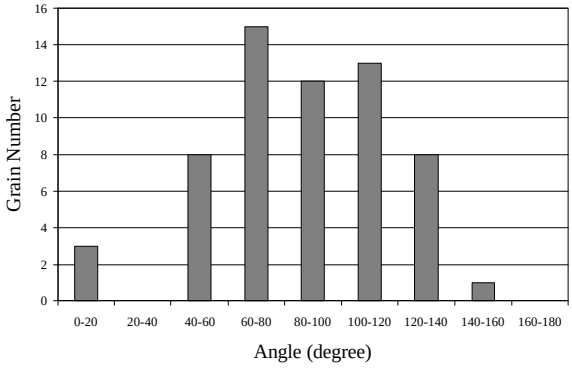

MEASUREMENTS OF EVAPORATION RATES OF SULFUR FROM IRON-IRON SULFIDE MELT. S Tachibana and A. Tsuchiyama, Department of Earth and Space Science, Graduate School of Science, Osaka University, Toyonaka, 560-0043, Japan (tachi@ess.sci.osaka-u.ac.jp; akira@ess.sci.osaka-u.ac.jp).

Introduction: We carried out evaporation experiments on Fe-FeS melt and obtained evaporation rates of sulfur from Fe-FeS melt. The Fe-FeS eutectic temperature is about 988°C (1261K), and this temperature could be achieved in the inner region of the solar nebula, and it should be also achieved during the chondrule formation. It is of importance to understand evaporation kinetics of Fe-FeS melt for discussion on the origin of troilite in meteorites, especially in chondrules.

Experimental: Evaporation experiments were done in a gold image furnace (ULVAC-RHV-E44VHT), in which samples were heated by infrared light focused with gold mirrors [1]. Troilite powder synthesized from pyrrhotite ($Fe_{0.886}S$) was used as a starting material. The powder was pressed into a pellet (3mm in diameter and ~2mm in height), and its weight was adjusted to 50 ± 0.1mg. An alumina ring (3mm in inner diameter) was used to hold a melt droplet instead of the conventional Pt-wire loop method because Pt reacts with Fe. Experiments were carried out at 1100° and 1200°C and at $p(H_2)=10^{-4}$ and 10^{-5}bar for different duration from 0 to 150min. Heating duration was measured after the furnace temperature achieved to the experimental temperature.

Results: The weight of the melt droplet decreases with heating duration. The residual sulfur content was calculated from the weight loss assuming that only sulfur evaporates from the melt. The higher temperature, the larger evaporation rates of Fe-FeS melt. Within the compositional range of total melt (34.2–29.3 wt% of S at 1100°C, 36.5–27 wt% of S at 1200°C), the higher sulfur content in the melt, the larger evaporation rates.

Discussion on evaporation kinetics: If the chemical reaction on the surface of the melt droplet controls the evaporation, the evaporation rate of sulfur is expressed by the Hertz-Knudsen equation;

$$J(S) = \Sigma\, \alpha_i\, (p_i^e - p_i) / (2\pi\, m_i\, kT)^{0.5},$$

where p_i^e is the equilibrium vapor pressure of i-th S-bearing gas, p_i is the ambient gas pressure of i-th gas in the surrounding gas atmosphere, m_i is the molecular weight of i-th gas, k is the Boltzman constant, T is the absolute temperature, and α_i is the evaporation coefficient. α_i shows the kinetic barrier for evaporation of i-th gas. Evaporation proceeds without any kinetic constraints when α is unity.

The equilibrium vapor pressure of S-bearing gas with Fe-FeS melt depends on the sulfur activity in the melt [2]. Dominant S-bearing gas species under the present experimental conditions are S_2 and HS. Hence, J(S) can be expressed approximately by the sum of $J(S_2)$ and J(HS). The experimental data cannot be fitted by the ideal evaporation rate of sulfur (α_{S2}, $\alpha_{HS} = 1$), while they can be fitted by the rates with α_{S2} = 0.035 – 0.09 and α_{HS} = 0.001. This indicates the existence of the kinetic barrier for evaporation. The $p(H_2)$ dependence of evaporation rates seems not to be large. This suggests that the contribution of $J(S_2)$ to J(S) is larger than that of J(HS) because the evaporation reaction of S_2 ($S(l)=1/2S_2(g)$; l:liquid, g:gas) does not include hydrogen. The larger contribution of $J(S_2)$ to J(S) can be explained by the presence of the larger kinetic barrier ($\alpha_{S2}>\alpha_{HS}$) for evaporation of HS than that for evaporation of S_2 as suggested in [1].

References: [1] Tachibana, S. and Tsuchiyama, A. (1998) *GCA*, in press. [2] Nagamori et al. (1970) *Trans. JIM*, *11*, 190–194.

SPINEL-BEARING CHONDRULES IN THE ALLENDE METEORITE. S. Maruyama[1], H. Yurimoto[2], and S. Sueno[3], [1]Venture Business Laboratory, University of Tsukuba, Tsukuba Ibaraki 305-8573, Japan (maruyama@arsia.geo.tsukuba.ac.jp), [2]Department of Earth and Planetary Sciences, Tokyo Institute of Technology, Meguro, Tokyo 152-8551, Japan (yuri@geo.titech.ac.jp), [3]Institute of Geoscience, University of Tsukuba, Tsukuba, Ibaraki 305-8571, Japan (sueno@arsia.geo.tsukuba.ac.jp).

Chondrules and Ca, Al-rich inclusions (CAIs) could have formed compound objects among the same constituents [1]. No compound chondrule-CAI objects have been recognized. However, recently Misawa and Fujita [2] found a barred-olivine chondrule (BOC) containing a coarse, subhedral spinel grain from the Allende meteorite. From the similarity of the composition, this spinel grain may be a relict CAI mineral. This evidence indicates that some CAIs and chondrule precursors coexisted in the same region of the solar nebula. Study of chondrules including spinels may clarify the genesis of chondrules and the relationship between chondrules and CAIs. *In-situ* O isotopic measurements were carried out for two chondrules including spinel grains of the Allende meteorite.

Oxygen isotopic measurements were performed with the TiTech Cameca ims 1270 SIMS instrument using a ~5-μm-diameter Cs^+ beam and an electron flood gun to compensate for electrostatic charging on sample surface. The mass resolution power was set to ~6000 to resolve ^{17}O from the interference of ^{16}OH. Secondary ion signals were detected with an electron multiplier (EM). Measurements were made by magnetic scanning through the following mass sequences; the $^{16}O^-$ tail (15.9915amu), $^{16}O^-$, $^{17}O^-$, $^{16}OH^-$, and $^{18}O^-$. Measurements of the $^{16}O^-$ tail and ^{16}OH were performed for correction of the ^{16}OH contribution on ^{17}O peaks. This correction is always less than 0.5‰. Data were corrected for deadtime and the instrumental mass fractionation by utilizing a terrestrial spinel standard.

The O isotopic compositions of spinels included in these chondrule are plotted on the carbonaceous chondrule anhydrous minerals (CCAM) line (Fig. 1). The O isotopic compositions of olivines and pyroxenes in these chondrules are in general agreement with previous observations [3, 4, 5].

A1-2b-1 is a typical BOC surrounded by porphyritic olivine rim. A coarse, subhedral spinel grain is embedded in the core part. The composition of the spinel is the almost pure $MgAl_2O_4$. From the chemistry and the texture, it is uncertain whether the spinel is the relict CAI mineral.

The O isotopic compositions of the spinel grain are close to those of coexisting olivines, and are quite different from those of spinels in CAIs (Fig. 1). It is certain that the spinel grain is the primary phase which crystallized during the chondrule-forming event.

AL95-2-1-CDL.1 is classified into independent consorting compound chondrules of [6]. The primary chondrule is dominated by olivine and pyroxene. The secondary chondrule can be categorized as a plagioclase-olivine inclusion (POI) [7].

The O isotopic compositions of the spinel grains in the POI are similar ^{16}O-excess to those of CAI spinels [8]. The origin of the spinel grain may be directly related to CAI precursors or CAIs itself from the similarity of ^{16}O-enrichment.

From O isotopic compositions, spinels in chondrules can be obviously distinguished between CAI-related and CAI-unrelated. It is difficult to judge whether spinels in chondrules are CAI-related or not from the similarity of the chemistry.

References: [1] Rubin A. E. (1994) *Nature, 368,* 691. [2] Misawa K. and Fujita T. (1994) *Nature, 368,* 723. [3] Hervig R. L. and Steele I. M. (1992) *LPSC XVII,* 364. [4] Weinbruch S. et al. (1993) *GCA, 57,* 2649–2661. [5] Hiyagon H. (1996) *Meteoritics and Planet. Sci., 31,* A62. [6] Wasson J. T. et al. (1995) *GCA, 59,* 1847. [7] Sheng Y. J., Hutcheon I. D., and Wasserburg G. J. (1991) *GCA, 55,* 581. [8] Maruyama S., Yurimoto H., and Sueno S. (1998) *LPSC XXIX*, Abstract #1342.

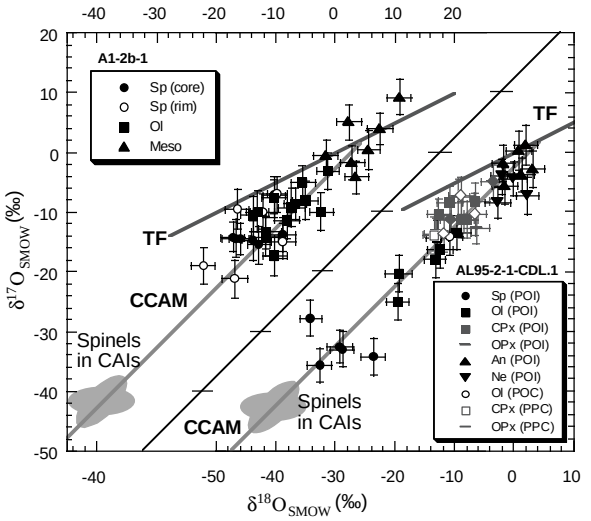

Fig. 1. O isotopic compositions of individual phases of chondrules. TF = Terrestrial Fractionation, CCAM = Carbonaceous Chondrule Anhydrous Minerals.

CARBON-RICH FINE-GRAINED CLASTS IN THE KRYMKA (LL3) CHONDRITE. V. P.Semenenko[1], C. Perron[2], and A. L.Girich[1], [1]State Scientific Centre of Environmental Radiogeochemistry, National Academy of Sciences of Ukraine, Palladina 34A, Kyiv-142, 252180, Ukraine, [2]Laboratoire de Minéralogie, CNRS-ESA 7058, Museum National d'Histoire Naturelle, 75005 Paris, France.

Fine-grained matrix material is found in unequilibrated ordinary chondrites filling interchondrule space or rimming chondrules [1]. It more rarely occurs as lithic clasts [2]. Here we present data on two clasts and a vein-like interchondrule area of unusually large sizes, which we observed in Krymka, and are mainly composed of fine-grained matrix-like material.

The two clasts (~3 × 4.5 mm^2) and the vein (~1 × 10 mm^2) have gross characteristics similar to each other and to previously described matrix lumps [2], but differ in some of their mineralogical features. They are black, chondrule-free and made of a very fine-grained groundmass (<1 μm) containing more or less uniformely distributed coarse grains (<50 μm) of silicates, Fe-Ni metal, chromite and very rarely troilite. The groundmass mainly consists in FeO-rich silicates. The average composition, as measured by broad beam electron microprobe, is roughly similar to that of interchondrule matrix in Krymka [1], but the FeO content is significantly lower in the two large clasts. As is usual for this kind of material, the totals are systematically low (89–92 wt%). The S content of one of the clasts (1.5 wt%) is the same as that measured in Krymka in rims around chondrules and around a carbonaceous clast [3]. It is very low (0.08 wt%) in the other two.

The coarse silicate grains vary in size from a clast to the other. They have an inhomogeneous composition and are mainly composed of olivine (Fa_{2-41}), Ca-poor ($Fs_{1.4-30}En_{68-98}Wo_{0-9}$) and Ca-rich ($Fs_{2.6-29}En_{44-61}Wo_{10-53}$) pyroxenes. Feldspatic grains are extremely rare. Many of the olivine grains are zoned, displaying a thin FeO-rich rim. The metal particles have awaruite (56-60% Ni and 2.0–2.7% Co), taenite (41–54% Ni and 0.2–1.3% Co) and rarely kamacite (3.3–4.8% Ni and 1.2–4.5 Co) composition. Spongy metal grains contain many silicate, chromite and phosphate inclusions.

The most noticeable characteristics of these objects is the ubiquitous presence of C-rich material. C-rich areas were searched among those appearing darkest on BSE images, and identified by EDS. At least the largest of these areas seem to be made of nearly pure C. The C-rich material is located within the groundmass as irregular areas (<4 × 25 μm^2) and as intergranular filling with poorly defined outlines, and inside coarse metal and silicate grains (especially spongy grains) as well delineated areas (<2 μm). We noted a few rimmed, coarse silicate grains with cataclastic structure, having C-rich material introduced in the cracks. Although we cannot absolutely rule it out, it seems unlikely that all these occurences of C are due to terrestrial contamination.

The presence in Krymka of the rock fragments described here implies that a fine-grained, C-rich, silicate dust experienced agglomeration together with high-temperature silicate grains, before accretion of the Krymka parent-body. It is noteworthy that C-rich clasts have already been found in the Krymka chondrite [3,4] which has otherwise a bulk C content rather low for a primitive type 3 ordinary chondrite (0.27% [5]). These clasts include a carbonaceous clast [3] and graphite-rich clasts [4] They have textures and mineral compositions quite different from those of the clasts described here, and the size, morphology and siting of their C-rich material are also markedly different. In particular, the graphite-rich clasts contain large, apparently well-crystallized graphite crystals [4]. However, it may not be impossible to make them by processing of matrix material, including more or less intense heating, and sulfurization of Fe-Ni metal. All together, C-rich clasts in Krymka may thus be witnesses of the (probably pre-accretion) evolution of the same material. More data are obviously needed on both bulk and mineral compositions of these various objects.

Acknowledgment: This work was supported by INTAS grant 93-2101-ext.

References: [1] Huss G. R. et al. (1981) *GCA, 45,* 33–51. [2] Brearley A. J. et al. (1989) *GCA, 53,* 2081–2093. [3] Semenenko V. P. (1996) *Meteoritics and Planet. Sci., 31,* A126–A127. [4] Semenenko V. P. and Girich A. L. (1995) *Min. Mag., 59,* 443–454; Semenenko V. P. and Girich A. L. (1998) this volume. [5] Moore C. B. and Lewis C. F. (1967) *JGR, 72,* 6289–6292.

STUDY OF SOME ACHONDRITES AND CHONDRITES BY FOURIER TRANSFORM INFRARED MICROSPECTROSCOPY AND DRIFTS. M. Bukovanská[1], I. Nìmec[2], and M. Šolc[3], [1]National Museum, Václavské nám. 68, 115 79 Prague 1, Czech Republic (ais@nm.anet.cz), [2]Department of Inorganic Chemistry, Charles University, Albertov 2030, 128 40 Prague 2, Czech Republic (agnemec@prfdec.natur.cuni.cz), [3]Institute of Astronomy, Charles University, Prague, Czech Republic (solc@mbox.troja.mff.cuni.cz).

Fourier transformed infrared (FTIR) spectra of basaltic achondrites Padvarninkai, Stannern, Jonzac eucrites and EET 83251 howardite, ordinary chondrites Pribram H5, Suchy Dul L6, Lissa L6, Sazovice L5, Zebrak H5 and several others were measured for the future comparison of their characteristic infrared spectral features with the higher resolution spectra of some asteroids.

Experimental: FTIR spectra of the whole rock were recorded by the method of diffuse reflectance spectroscopy (DRIFTS) on a Mattson Genesis FTIR spectrometer (4 cm^{-1} resolution, triangular apodization) in the 400–4000 cm^{-1} region. Powdered meteorites were mixed with KBr in a ratio 1:20 and homogenized. Pure powdered KBr was used as a background surface.

Fourier transform infared spectra of a very small objects (20–50 μm in diameter) in meteorites mineralogically studied by first of the authors (various kinds of igneous inclusions and clasts in achondrites as well as chondrules and matrix in chondrites) were collected by a Mattson Quantum infrared microscope (reflection mode) with a Mattson Infinity FTIR spectrometer in the 675–4000 cm^{-1} region (4 cm^{-1} resolution, triangular apodization). Obtained reflectance spectra were processed using Kramers-Kronig transformation and compared with transmission spectra in [1].

Results: Basaltic achondrites are mixtures of pyroxene (both ortho- and clinopyroxene, mostly pigeonite, in case of EET 83251 also in some inclusions with Mg-rich diogenitic orthopyroxene and olivine) with plagioclase (bytownite - anorthite) and small amount of silica, ilmenite, chromite, metalic NiFe etc. All of them have strong 960–966 cm^{-1} spectral band, typical for pyroxenes (both ortho- and clinopyroxenes). Another pyroxene characteristic spectral band is 1058–1075 cm^{-1}, unfortunately very close to anorthite ~1080 cm^{-1}. Spectral band ~990 cm^{-1}, typical for bytownite, can be clearly observed. The lower frequency region exhibits an important spectral band ~580 cm^{-1}, typical for bytownite and anorthite.

Spectra of two measured parts of Stannern differ in amount of pyroxenes (band 968 cm^{-1}) and plagioclases (band 677 cm^{-1}). Six Padvarninkai spectra from clasts, matrix and glassy veins differ in presence of pyroxene bands at 960–965 cm^{-1}, which are shifted to lower wavenumbers by ~10 cm^{-1} in parts rich in plagioclases. A set of EET 83251 howardite spectra (see Fig. 1) has well pronounced pyroxene band (960–969 cm^{-1}) which is slightly shifted (955–957 cm^{-1}) in the spectra from places with higher content of plagioclases. Band at ~1080 cm^{-1} typical for anorthite is possible to find beside pyroxene 1070 cm^{-1} band in some spectra. Typical olivine bands 984–985 cm^{-1} and 881 cm^{-1} exhibit a good possibility of olivine detection in basaltic achondrites spectra.

Spectra of chondrites Pribram, Zebrak, Suchy Dul, Sazovice and others differ mainly in content of olivine and pyroxene. The presence of well pronounced spectral bands 983–989 cm^{-1} (olivine) and 960–969 cm^{-1} (pyroxenes) are in agreement with the mineralogical observation of in situ measured parts of chondrites. Ca-rich cpx could be proved probably in spectra showing the band 906–907 cm^{-1}. According to [2] hypersthene and augite can be distinguished in the chip and powder spectra. We were not able to distinguish H from L chondrites, hopefully we will get reasonable results with the method, described by [3].

Conclusions: Infrared spectra collected from various mineralogically different places of achondrites and chondrites samples (rough cut surface and polished thin section) can be used for the determination of the main mineral phase. We could distinguish olivine- and pyroxene-rich parts in chondrites and dominated plagioclase, pyroxene and olivine phases in achondrites.

Acknowledgments: This work was supported by the Grant Agency of the Czech Republic and FWF in Austria. We are grateful to Prof. Dr. Gero Kurat for very useful comments.

References: [1] Van der Marel H.W. and Beutelspacher H. Atlas of Infrared spectroscopy of clay minerals and their admixtures. Elsevier (1976). [2] Bishop J. L. et al. (1997) LPSC XXVIII, electr. vers. [3] Feely K. C. and Christensen P. R. (1997) LPSC XXVIII, electr.vers.

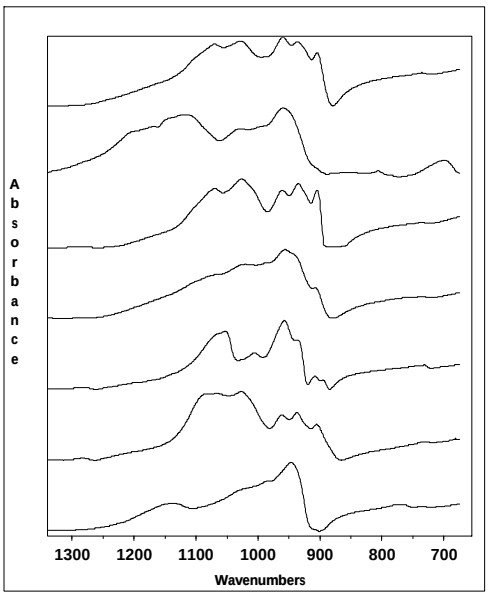

Fig. 1. IR spectra of different parts of EET 83251 howardite obtained by FTIR microspectroscopy.

THE KRYMKA CHONDRITE (LL3): A GRAPHITE-CONTAINING FRAGMENT AND ISOTOPIC COMPOSITION OF ITS GRAPHITE CRYSTALS. V. P. Semenenko[1], L. R. Nittler[2], and A. L. Girich[1], [1]State Scientific Centre of Environmental Radiogeochemistry National Academy of Sciences of Ukraine, Palladina 34A, Kyiv-142, 252180, Ukraine, [2]Carnegie Institution of Washington, 5241 Broad Branch Road NW, Washington DC 20015, USA.

The search for and examination of different morphological types of graphite in meteorites allows us to understand what kinds of material were present within the solar nebula and probably during the presolar period [1,2]. Seven graphite-containing fragments found in the Krymka chondrite belong to an exotic kind of preterrestrial material [3,4] due to the presence of regular graphite crystals and other C-rich material. The mineralogical insight into the nature of the fragments [5] has to be confirmed by isotopic data for the graphite and C-rich material. Here we present the first isotopic results for one of the fragments which contains the largest graphite crystals ($<100 \times 7$ μm).

In contrast to the other graphite-bearing fragments [3,4], the fragment studied here, N6, has the lowest level of oxidation, corresponding to that of equilibrated LL-chondrites, a lower quantity of sulfide and metal, absence of a rim of primitive silicate material and the highest concentrations of TiO_2 in chromite. The fragment displays a metamorphic appearing texture with homogeneous mineral compositions (excluding metal). It contains: mainly olivine (Fa_{26}), Ca-poor pyroxene ($Fs_{23}En_{75}Wo_2$), plagioclase (Ab_{81}), minor quantities of Ca-rich pyroxene ($Fs_{32}En_{26}Wo_{42}$), chromite with 1.38% MgO, 7.50% Al_2O_3 and 4.40% TiO_2, Cl-apatite (3.82% Cl and 1.49% F), troilite, large and small graphite crystals, C-rich material and rare grains of Ni-rich taenite with variable concentrations of Ni (52.1–59.2%) and Co (0.95–1.80%) and kamacite (4.07% Ni and 2.87% Co).

In general the graphite crystals have lamella shape and differ by size, location and origin. C-rich material is found as irregular areas inside feldspar and as abundant veins. The fragment contains direct evidence of shock formation of C-rich veins after metamorphism of the primary rock. In contrast to the other fragments the olivine, pyroxene and feldspar in N6 are "clean" and do not contain inclusions of C-rich material. Dispersed (?) C which is present inside minerals of some graphite-containing fragments is also absent.

The mineralogy of fragment N6 testifies that it is genetically connected to the other graphite-containing fragments [3–5]. The large graphite crystals were formed from a C-bearing melt, and the small ones as a result of metamorphism. The stage of metamorphism, which promoted to complete rectification of minerals from dispersed (?) C and C-rich inclusions, corresponds to that of the fragments N1 and N5 and is higher than in the rest. The fragment probably experienced the influence of hot fluids bearing S, Cl, and F, although not as remarkably as for the other ones. After agglomeration with the Krymka host, the fragment was altered by shock which resulted in mechanical brecciation and redistribution of C-rich material.

The isotopic compositions of C and N were measured in three large graphite crystals with an ion microprobe. The results are shown in Fig. 1 (2σ errors), along with the ranges of isotopic compositions of graphite (associated with metal) in other chondrites [6,7]. The three grains all have $\delta^{13}C_{PDB}$ values close to 0, and N-isotopic ratios within errors of normal. These $\delta^{13}C$ values are higher than those of graphite measured in other UOCs [6,7] and most organic material found in primitive meteorites [8], but are similar to graphite in CR chondrites [7]. Whether the difference between these graphite grains and those in other UOCs reflects primordial heterogeneity or variable isotopic fractionation arising from different formation mechanisms of the different types of graphite is unknown. Additional isotopic analyses of graphite grains and other carbonaceous material in N6 and in the other Krymka fragments should help resolve their origin.

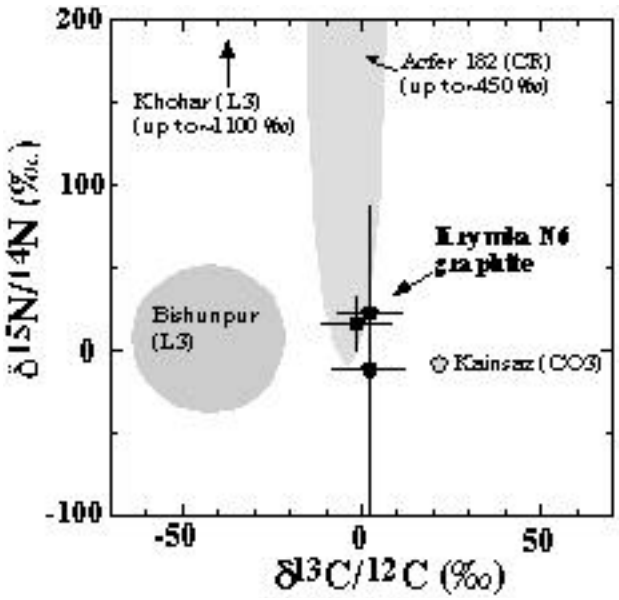

Fig. 1.

Acknowledgments: The mineralogical part of this work was supported by the Smithsonian Institution (Washington).

References: [1] Zinner E. K. et al. (1990) *Lunar Planet. Sci., 21,* 1379–1380. [2] Zinner E. K. et al. (1995) *Meteoritics, 30,* 209–226. [3] Semenenko V. P. and Girich A. L. (1995) *Mineral. Mag., 59,* 443–454. [4] Semenenko V. P. and Girich A. L. (1996) *Meteoritics and Planet. Sci., 31,* A127. [5] Semenenko V. P. and Girich A.L. (1998), this volume. [6] Mostefaoui S. et al. (1997) *Lunar Planet. Sci., 27.* [7] Mostefaoui S. et al. (1996) *Meteoritics and Planet. Sci., 31,* A93. [8] Alexander C. M. O'D. et al. (1998), *Meteoritics and Planet. Sci.,* in press.

THE NATURE OF GRAPHITE-CONTAINING FRAGMENTS IN THE KRYMKA (LL3) CHONDRITE.

V. P. Semenenko and A. L. Girich, State Scientific Centre of Environmental Radiogeochemistry National Academy of Sciences of Ukraine, Palladina 34A, Kyiv-142, 252180, Ukraine.

Seven graphite-containing fragments have been indentified in the Krymka chondrite [5,6]. The fragments have uniform, fine-grained texture and are chondrule-free. They are friable, contain a rather high quantity of troilite, relatively homogeneous silicates, graphite crystals and C-rich material. Like the Krymka chondrules, in the most cases they are coated by a rim of fine-grained silicate material. The fragments differ by level of oxidation (basically corresponding to more oxidized material than equilibrated LL-chondrites), quantity of Ca-rich pyroxene, the presence of feldspar, magnetite, ilmenite, spinel, scapolite(?), Cl- or F-apatite, composition of minerals (especially chromite and metal), quantity and size of graphite crystals and distribution of C-rich material.

There are three kinds of carbon material: regular graphite crystals (large and small), C-rich material and dispersed(?) carbon. Small graphite crystals and C-rich material are present within seven fragments, while the large crystals and dispersed(?) carbon only in some. The large graphite crystals have a much larger size than that of the other minerals and show morphological signs of primary crystallization from a C-bearing melt. The small graphite crystals have a size which corresponds to that of the silicate grains and are located inside olivine and pyroxene grains or on a phase boundary of minerals. They contain evidences of a metamorphic growth. C-rich material (perhaps not graphitized but it is unclear) is found as irregular areas inside feldspar or feldspatic mesostasis (like that in ureilites [1]), as round inclusions inside the silicates, and as veins which intrude the phase boundaries and the silicates along fractures. Arrangement of the veins testifies to their genetical relationship with C-rich areas inside of feldspatic material and to their formation following a shock metamorphism of the Krymka parent body. It means the C-rich material has a low melting-point and is mobile. In a few fragments some carbon is present inside of feldspatic mesostasis, pyroxene and troilite, however the form of carbon is not known (possibly C-rich micro-inclusions which are not visible at high SEM-resolution or dispersed carbon).

Although many mineralogical details of the fragments remain unresolved, most of them may be explained as a result of the following processes: (1) Crystallization of minerals from a C-bearing melt followed by an enrichment of residual material in carbon. Carbonaceous matter like that of the mysterite-bearing fragments from Krymka [2–4,7] might have to be the precursor of this melt. (2) Metamorphism (progressive or regressive) and probably influence of hot fluids containing S, Cl, and F. (3) Fragmentation of a primary rock and agglomeration with chondrules in a range enriched by fine-grained silicate dust. (4) Shock metamorphism of the Krymka parent body. Formation of cracks and cataclastic areas in the fragments followed by mobilization and penetration of C-rich material into cracks and phase boundaries of grains.

Acknowledgments: This work was supported by the Smithsonian Institution (Washington). E. Jarosewich, G. MacPherson and S. Russell are gratefully acknowledged.

References: [1] Berkley J. L. et al. (1980) *GCA, 44,* 1579–1597. [2] Laul J. C. et al. (1973) *GCA, 37,* 329–358. [3] Lewis R. S. et al. (1979) *GCA, 46,* 897–903. [4] Semenenko V. P. (1996) *Meteoritics & Planet. Sci., 31,* 126–127. [5] Semenenko V. P. and Girich A. L. (1995) *Mineral. Mag., 59,* 443–454. [6] Semenenko V. P. and Girich A. L. (1996) *Meteoritics & Planet. Sci., 31,* 127. [7] Semenenko V. P. et al. (1991) *Geochimia, 8,* 1111–1121, in Russian.

IMAGE ANALYSIS REVEALS NEW INFORMATION ABOUT THE METEORITIC WIDMANSTATTEN STRUCTURE. P. Z. Budka[1], J. R. M. Viertl [2], and T. B. Schumaker[3], [1]2135 Morrow Avenue, Schenectady NY 12309, USA (75302.1764@compuserve.com), [2]1403 Clifton Park Road, Schenectady NY 12309, USA, [3]Rensselaer Polytechnic Institute, Troy NY, USA.

Count Von Widmanstatten revealed the meteoritic structure that bears his name in 1808 by etching. In 1813, Von Widmanstatten and Schreibers applied printer's ink to this surface to produce a direct typographical imprint—the first meteoritic "macrograph." [1] "Modern" metallurgical analysis tools of succeeding eras have been applied to the study of this very familiar microstructural morphology. From Sorby's first metallograph in the 1860s, to X-ray diffraction in the 1920s and 30s, to the microprobe beginning in the 1950s, from very low magnification to very high magnification, each analytical tool has made a contribution to our understanding of the meteoritic Widmanstatten structure. Similarly, today's image analysis tools can be of value in the microstructural analysis of metallic meteorites. This paper will use image analysis to present surprising new information about the formation of kamacite and the meteoritic Widmanstatten structure.

References: [1] Smith C. S. (1960) "A History of Metallography," The MIT Press, Cambridge, MA.

NITRIDES IN IRON METEORITES. K. V. Ponganis and K. Marti, Department of Chemistry, University of California at San Diego, 9500 Gilman Drive, La Jolla CA 92093-0317, USA.

Replicate analyses of metal phases in iron meteorites reveal that the N content varies greatly (Table 1) although in all cases these variations were outside experimental error. Sometimes this variation is accompanied by a difference in the $\delta^{15}N$ signature. In most cases N inventories in the metal samples were much higher than predicted by the solubility of N in Fe,Ni phases under a solar nebular environment [1]. The presence of small amounts of nitrides, which have been exsolved from the Fe,Ni phase, may account for this variation.

We prepared duplicate samples of IAB/IIICD iron meteorites as previously described [2] and analyzed for both N_2 and Xe. Xe is used as a monitor for inclusions such as silicates, graphites, carbides or trolite. The amounts of Xe were always at system blank levels. For these types of inclusions to alter the N content to the extent observed, the Xe content should be measurable.

Observed shifts in isotopic compositions might be, in part, due to $^{15}N_C$ contributions. For example, $^{15}N_C$-corrected values are given for Yanhuitlan [3]. One Yanhuitlan sample showed evidence for two distinct N signatures.

Nitrogen solubility in Fe is low at solar nebular P-T regions, Any Ni in Fe would decrease the N solubility even more, although other elements in the metal might offset this effect. Fegley [1] predicted that under solar nebular equilibrium condition at most 0.08 ppm N would dissolve in the metal phase. Most iron meteorites have N levels 10 times this or more.

If the N content was altered by a nitride inclusion at ppm levels, it would be very difficult to identify, except by N itself. Such small inclusions, even if they trap Xe, would (probably) not carry enough Xe to be detected. Nitrides have, in fact, been found in iron meteorites (roaldite [4] and carlsbergite [5]) and are probably ubiquitous throughout the irons even though total nitride amounts are small compared to other inclusions.

Fegley [1] suggested that N is initially stored in organic compounds, which during heating and processing, decompose to produce a local N pressure high enough to allow metal nitrides to exsolve from the metal phases. Specifically, during a cooling history a phase transition from α- to γ-Fe,Ni can be expected to exsolve nitrides since N and nitride solubilities decrease when going from the f.c.c. to b.c.c. forms [6].

Conclusions: The presence of unidentified nitrides is consistent with our Xe measurements. Small amounts of nitrides such as roaldite or carlsbergite can be expected to be below the detection limit for their Xe component. Nitrides probably exsolved during phase changes while the meteorite parent bodies cooled. The distinct isotopic signatures of N require separate local reservoirs.

Meteorite	**N ppm**	**$\delta^{15}N$**	**Ref**
IAB Canyon Diablo	3.9	–9.7	This work
	11.6	–62.4	This work
	20.2	–68.9	[7]
	45.0	–49.9	[7]
	48.8	–66.7	[7]
IAB Four Corners	44.9	–54.5	[8]
	117.6	–55.4	[8]
IAB Odessa	138.7	–67.0	[9]
	36.8	–62.3	This work
IIICD Cranbourne	6.7	–42.1	This work
	12.8	–23.4	This work
IVA Yanhuitlan	91.0	–26, –6	[3]
	0.28	–26	[3]

TABLE 1. Examples of N content variability in iron meteorites

References: [1] Fegley B.(1983) *JGR Suppl., 88*, A853–A868. [2] Ponganis K. V., Kohl C. P., and Marti K., (1998) *LPSC XXIX*, 1161–1162. [3] Mathew K. J. et al. (1998), in preparation. [4] Nielsen H. P. and Buchwald V. F. (1981) *LPSC XII*, 1343–1348. [5] Buchwald V. F. and Scott E. R. D. (1971) *Nature, 233*, 113–114. [6] Raghavan V. (1987) *Phase Diagrams of Ternary Iron Alloys. Part I.*, Delhi, Indian Institute of Metals. [7] Prombo C. A. and Clayton R. N. (1993) *GCA, 57*, 3749–3761. [8] Franchi I. A., Wright I. P., and Pillinger C. T., *GCA, 57*, 3105–3121. [9] Kim Y. (1994) Thesis, Dept. of Chemistry, University of California at San Diego: La Jolla. pp. 123.

DIGITAL IMAGE TECHNIQUES PROVIDE NEW INSIGHTS INTO METEORITE MICROSTRUCTURAL DEVELOPMENT. P. Z. Budka[1] and J.R.M. Viertl [2], [1]2135 Morrow Avenue, Schenectady NY 12309, USA (75302.1764@compuserve.com), [2]1403 Clifton Park Road, Schenectady NY 12309, USA.

Digital image techniques provide opportunities to wrest new and sometimes surprising information from old specimens as well as old micro and macro photographs. These techniques are applied to a variety of nickel-iron and pallasite specimens to reveal new information about microstructural evolution.

TRANSMISSION ELECTRON MICROSCOPE STUDY OF KAMACITE IN COARSE-STRUCTURED IRON METEORITES. V. I. Grokhovsky[1], E. A. Kozlov [2], L. E. Karkina [3], and V. A. Teplov [3], [1]Physico-Technical Department, Ural State Technical University - UPI, Ekaterinburg 620002, Russia (grokh@pcma.rcupi.e-burg.su), [2]Russian Federal Nuclear Center, Snezhinsk 454070, Russia, [3]Institute of Metal Physics, Ekaterinburg 620219, Russia.

The Fe meteorites display a wide range of secondary structures and the underlying causes and events must have been rather complex [1]: shock metamorphism, plastic deformation caused by atmospheric disruption, cycles of cooling and reheating, weathering . In this work we report new results obtained by transmission electron microscope (TEM) on kamacite of the coarse-structured iron meteorites with different nature of secondary structures.

The Sikhote-Alin and Bilibino iron meteorites was classified as coarsest octahedrite IIB, however in first case were used "fresh" individuals, fragments and shocked fragments samples, collected in 1987, 1997 expeditions, but in the second case the meteorite was found in alluvion that has been more 200,000 yr age. Electropolished thin sections of these samples were studied using a JEM 200 CX transmission electron microscope operating at 200 kV.

Sikhote-Alin: The kamacite has a abundand rhabdites and Neumann bands. TEM evidence of the high dislocation density in the kamacite is seen on both sides of the Neumann band boundary. The dislocation formed a cellular structure with 0,2 - 0,4 μm cell, and a major portion could be shown to be screw dislocations with Burgers vector 1/2 <111>. The wide cell boundaries are formed by a pairs of dislocation junction on reaction $1/2\ [11\bar{1}] + 1/2\ [1\bar{1}\,1] \rightarrow [100]$. Similar dislocation structure have been observed in Fe-Ni alloys after about 30% cold deformation [2]. The deformed fragment samples from impact holes show a elongated kamacite subgrains with the high densities of dislocations.

Bilibino: There are special features in microscopically grained kamacite that was formed by weathering-induced recrystallization. No shock effects were found in recrystallized kamacite by TEM. TEM shows unit dislocations and edge boundaries. Incoherent and semicoherent oxide precipitates was observed in new kamacite grains. The size and density of precipitates varied and are connected with distance from of reaction front.

Acknowledgments: This work was supported by RFFI grant 98-05-64822.

References: [1] Buchwald V.F. (1975) *Handbook of Iron Meteorites*, Univ. of California. [2] Ribin V. V. (1986) *High plastic deformation and fracture of metal*, Moscow. [3] Grokhovsky V. I. (1997) *Meteoritics and Planet. Sci., 32*, A52.

SILICATE AND METAL PHASES IN THE QUE94411 IRON METEORITE. K. Righter and N. L. Chabot, Lunar and Planetary Laboratory, University of Arizona, Tucson AZ 85721 (righter@lpl.arizona.edu, chabot@lpl.arizona.edu).

Introduction: Iron meteorite QUE94411 is an unusual silicate inclusion-bearing Fe. Although this meteorite contains mostly angular silicate inclusions of pyroxene, olivine, and feldspar [1], there are many spherical glassy inclusions that resemble chondrules. We have initiated a systematic study of the glassy spherules, silicate mineral inclusions and metal in order to better understand the conditions under which this meteorite formed, especially in comparison to the many other types of silicate inclusion-bearing Fe meteorites such as the IVA [2], IAB/IIICD [3], IIF [4], Mbosi [5], Bocaiuva [6] and Eagle Station Trio pallasites [7].

Petrography and Analyses: The polished thin section of 94411 contains many glassy spherules, which have a small range of diameters, from approximately 70 to 200 μm. The angular silicate mineral fragments are much more common and larger (1 to 2 mm). Altogether, the silicates comprise 15-20% of the section, the balance being composed of metal. Metal and silicate phases were analyzed using a CAMECA electron microprobe at the University of Arizona, using a variety of natural and synthetic standards and a point beam. Silicates were analyzed with 15 kV accelerating potential, 20 nA sample current, and 10 second counting times for major and minor elements, whereas metals were analyzed using 25 kV accelerating potential, 20 nA sample current, and 30 second (Fe, Ni) and 60 sec (P, Co) counting times.

Results: Metal compositions are variable, and overlap with the IIIA and IVA magmatic Fe meteorite groups, as well as the IA and anomalous irons in terms of Ni and P. Co/Ni and Ni contents show similarity to metal in the Bencubbin, Weatherford and Bocaiuva irons. Glass spherules are silica rich (52.4 to 54.1 wt% SiO_2), and alkali poor (Na_2O < 0.04 wt%). They are generally MgO-rich (44 to 45 wt%) and CaO-poor (0.8 to 1.5 wt%) and Al_2O_3-poor (0.85 to 1.85 wt%). Comparisons of these compositions to those of published chondrule compositions [8–14], show overlap with chondrules from the CM2 Murray (Fig. 1). Although E4 chondrules have equally high Mg#'s [10], their bulk MgO contents are lower, from 30 to 38 wt% MgO, and thus not a good match to the QUE94411 spherules. A connection between this Fe and carbonaceous chondrites would suggest a similarity to two other anomalous Fe meteorites - Mbosi and Bocaiuva - and the Eagle Station Trio pallasites, all of which show O isotopic compositions along the C3 chondrite line. This research is supported by NASA Grant NAG5-4084.

References: [1] Mason B. (1996) *Ant. Meteor. Newsletter, 19:1,* 17. [2] Ulff-Moller F. et al. (1995) *GCA, 59,* 4713–4728. [3] Choi B. et al. (1996) *59,* 593–612. [4] Kracher F. et al. (1980) *GCA, 44,* 773–787. [5] Olsen E. et al. (1996) *Met. and Planet. Sci., 31,* 633–639. [6] Malvin D. J. et al. (1985) *Meteoritics, 20,* 259–273. [7] Buseck P. R. (1977) *GCA, 44,* 711–740. [8] Gooding J. L. et al. (1980) *EPSL, 50,* 171–180. [9] Smith J. V. et al. (1983) *LPS XIV,* 714–715. [10] Grossman J. N. et al. (1985) *GCA, 49,* 1781–1795. [11] McCoy T. J. et al. (1991) *GCA, 55,* 601–619. [12] Rubin A. E. and Wasson J. T. (1986) *GCA, 50,* 307–315. [13] Rubin A. E. and Wasson J. T. (1988) *GCA, 52,* 425–432. [14] Rubin A. E. and Wasson J. T. (1987) *GCA, 51,* 1923–1937.

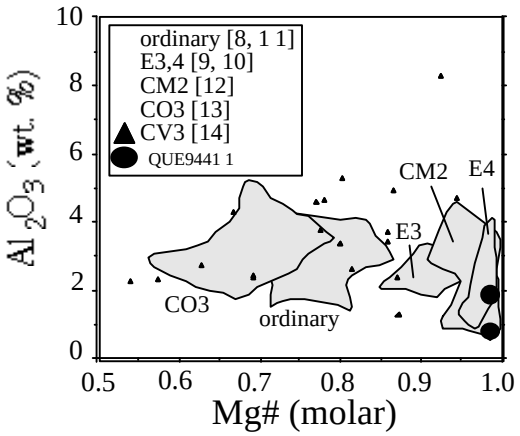

FRONTIER MOUNTAIN 95028: A NEW LOW-SHOCK UREILITE CLOSE TO ALLAN HILLS 78019.
A. M. Fioretti[1] and G. Molin[2], [1]C. S. Geodinamica Alpina, C.N.R., I-35122 Padova, Italy (anna@dmp.unipd.it), [2]Dipartimento di Mineralogia e Petrologia, I-35122 Padova, Italy (gmario@dmp.unipd.it).

Introduction: Ureilites are coarse-grained achondrites composed in various proportions of olivine, pigeonite (± augite, ± orthopyroxene) in a carbonaceous matrix. Ureilites display a wide range of petrographic texture, mineral composition and degree of shock [1]. Ureilite FRO95028 [2] belongs to the Euromet collection and was found during the XI Italian Expedition (1995/1996) at Frontier Mountain (Antarctica). One polished thin section (pts) of sample FRO 95028 was studied in transmitted and reflected light. The chemical compositions of mineral phases were determined using a WDS CAMECA-Camebax microprobe operating at 15kV with 15nA sample current for silicates and at 20kV with 15nA for metals and sulfides.

Petrography: Frontier Mountain 95028 consists of coarse-grained olivine (up to 2.5 mm) and pigeonite (up to 1.7 mm), with interstitial carbonaceous materials in the form of graphite. It is composed of 68% olivine, 20% pigeonite, and 12% graphite (modal proportion) with minor metal, troilite, Cr-rich iron sulfide, schreibersite and alabandite as accessory phases. Triple junctions are common. Silicates are anhedral to subeuhedral and display curved grain edges. Rare, small, rounded grains of pigeonite are enclosed in olivine. Graphite is well crystallized and makes up interstitial, sometimes interconnected patches which intrude along the boundaries between grains, sometimes surrounding and "detaching" rounded crystals. The contacts of graphite with olivine are lobed, with smooth embayments and cuspidae of graphite intruding along both crystal fractures and boundaries between adjacent crystals. At the contact with graphite, the outer rims of olivine are decorated with small (2–3 μm) grains of metal and sulfide. Swarms of metal and minor sulfide droplets also decorate subparallel planar fractures in olivine. Graphite shows prominent pressure lamellae, which suggest that it was deformed after crystallization.

Alteration is minor; thin limonitic veins are present inside main and minor fractures. Some of these areas display unusually high Cl contents (EDS) inside alteration products. Moderate fracturing in silicate, and prevalent sharp or smooth undulatory extinctions indicate [3], [4] a low degree of shock.

Mineral chemistry: Both olivine and pigeonite have uniform core compositions, ($Fo_{78.4}$ and $Wo_{8.1}En_{73.8}Fs_{18.1}$) with greatly reduced rims ($Fo_{95.3}$ and $Wo_{5.7}En_{90.8}Fs_{3.5}$) respectively. A further thin rim of almost pure enstatite ($Wo_{0.4}En_{96.3}Fs_{3.3}$) was observed at the contact of reduced olivine rim with graphite.

Two distinct metal compositons are observed with Ni 0.5–0.9 (wt%) and Ni 2.7–3 (wt%) respectively. Both troilite (Cr 0.3–0.6) and Cr-rich iron sulfide (Cr up to 12.6 wt%) are present. Schreibersite (Fe 79; P 13.6; Ni 5.6; Co 0.2; Cr 0.17; S 0.18 wt%) and alabandite (Mg 9.7; Fe 17.6; Mn 26.7; Ca 0.5; S 40.59) [5] have uniform compositions.

Discussion: Frontier Mountain 95028 displays major- and minor-element abundances of olivine and pigeonite in the range of ureilites ALHA 78019–ALHA 78262 [6] [7]. Both FRO 95028 and ALHA 78019 show rims of low-Ca pyroxene on olivine, whereas no reduced rim is reported on pigeonite in ALHA 78019. Frontier Mountain 95028 has a wider number of accessory phases that show quite variable compositions. The troilite of FRO 95028 and ALHA 78019 is comparable in composition, while Ni content of metal in FRO 95028 is lower than that in ALHA 78019 and ALHA 78062. The shock level of FRO 95028, although relatively low, is higher than that of ALHA 78019.

Conclusions: Modal abundances and major and minor element mineral compositions indicate that FRO 95028, ALHA 78019, and ALHA 78062 are very similar and suggest that they represent fragments which were very close to one another on the ureilite parent body. Differences in shock stage indicate either that the same shock event affected very close fragments to a different extent or a secondary event.

Acknowledgments: We thank EUROMET for providing the ureilite pts, the Italian Antarctic Research Programme (PNRA) for financial support, and C. A. Goodrich for helpful discussions.

References: [1] Goodrich C. A. (1992) *Meteoritics, 27,* 327–352. [2] *The Meteoritical Bulletin, No. 82.* [3] Berkley J. L. (1986) *Meteoritics, 21,* 169–189. [4] Bischoff A. and Stöffler D. (1992) *Eur. J. Mineral., 4,* 707–755. [5] Fioretti A. M. and Molin G., this volume. [6] Berkley et al. (1980) *GCA, 44,* 1579–1597.[7] Berkley J. L. and Jones J. H. (1982) *Proc. LPS 13th,* in *JGR, 87,* A353–A364.

ALABANDITE IN UREILITE FRONTIER MOUNTAIN 95028. A.M. Fioretti[1] and G. Molin[2], [1]C.S. Geodinamica Alpina, C.N.R., I-35122 Padova, Italy (anna@dmp.unipd.it), [2]Dipartimento di Mineralogia e Petrologia, I-35122 Padova, Italy (gmario@dmp.unipd.it).

Alabandite is the Mn-rich endmember of the cubic monosulfide series with the general formula (Mg,Mn,Fe)S, the Mg-rich endmember being niningerite. Alabandite is a quite uncommon mineral phase in meteorites, and has so far been found only in EL enstatite chondrites [1–3], and in enstatite achondrites [4,5].

FRO95028 has the petrographic texture, modal abundance and mineral composition typical of ureilites [6]. In FRO95028, one small (15 mm) interstitial grain of alabandite is found in contact with Cr-rich iron sulfide containing troilite flammae and associated with schreibersite. The occurrence and mineral chemistry of alabandite in a ureilite are documented here for the first time. Microprobe analyses (WDS) carried out on three spots give compositions very close to stoichiometry $(Mg_{0.318}Mn_{0.384}Fe_{0.249}Ca_{0.01}Cr_{0.021})S$ and show the rather homogeneous composition of the crystal, also confirmed by the MgKα, FeKα, MnKα scanning picture, indicating a mineral assemblage close to equilibrium. FRO 95028 alabandite has a distinct composition with higher Mg/Mn and Mg/Fe values than those of alabandites in enstatite achondrites and in EL chondrites (Fig. 1).

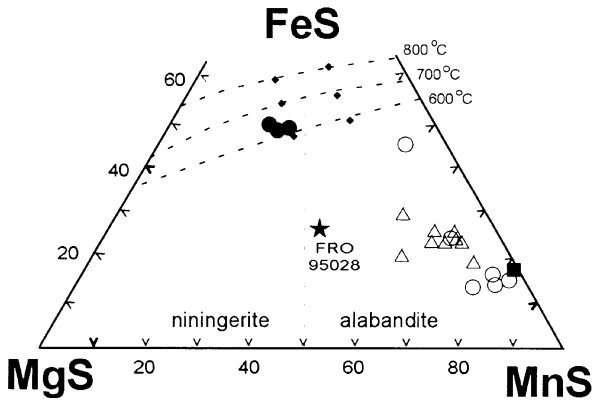

Fig. 1. Composition of alabandite (mol%) in FRO 95028 compared with alabandite in enstatite achondrite Peña Blanca Spring (full square) and EL chondrites. Data from [5] full square; [1] triangles; [2] open and full circles. Full circles indicate "alabandite" of EL chondrites LEW 87119, LEW 88714 and RKPA 80258, which actually plot in the field of niningerite. Small, full diamonds represent experimental data from [7].

Experimental data [7] indicate that the FeS content of alabandite in equilibrium with troilite is proportional to its minimum temperature of formation or of last equilibration, showing a linear correlation in the experimental range 600°–1000°C. Although no data are available for temperatures below 600°C, the small amount of FeS in FRO 95028 strongly suggests a low closing temperature, probably of the order of few hundred degrees for the intracrystalline troilite-alabandite Fe exchange reaction [3].

The presence of an alabandite crystal with this composition in FRO 95028 may be ascribed to a low-temperature crystallization during a slow cooling history of the rock under severe reducing conditions. This episode must be subsequent to the high closure temperature and fast cooling rate event observed in the range 800°–600°C [8], [9] on the basis of several lines of evidence such as the high Ca content in olivine, persistence of reduced forsteritic rims, the closure temperature for the intracrystalline Fe^{2+}-Mg ordering reaction, and TEM microtextures in pyroxene. A further slow cooling episode at low temperatures, when ion exchange reactions in silicates are virtually quenched, is therefore hypothesized.

Acknowledgments: We thank EUROMET for providing the meteorite samples, the Italian Antarctic Research Programme (PNRA) for financial support, and C. A. Goodrich for helpful suggestions.

References: [1] Keil K. (1968) *JGR, 73,* 6945–6976. [2] Zhang Y. et al. (1995) *JGR, 100,* 9417–9438. [3] Zhang Y. and Sears D. W. G. (1996) *Meteoritics & Planet. Sci., 31,* 647–655. [4] Ryder G. and Murali A. V. (1987) *Meteoritics, 22-4,* 495–496. [5] Lin et al. (1989) *LPS XX,* 572–573. [6] Fioretti A. M. and Molin G., this volume. [7] Skinner B. J. and Luce F. D. (1971) *Am. Mineral., 56,* 1269–1297. [8] Goodrich C. A. (1992) *Meteoritics, 27,* 327–352. [9] Tribaudino M. et al. (1997) *Meteoritics & Planet. Sci., 32,* 671–678.

IRON-, MAGNESIUM-, AND MANGANESE-BEARING PHOSPHATES IN THE LODRANITE GRAVES NUNATAKS 95209. C. Floss, McDonnell Center for the Space Sciences and Department of Earth and Planetary Sciences, Washington University, St. Louis MO 63130, USA (floss@howdy.wustl.edu).

Introduction: As part of an in-depth trace element study of the acapulcoite – lodranite suite of meteorites [1,2], ion microprobe measurements were made on the recently classified lodranite, GRA 95209 [3]. Examination of thin section ,39 revealed the presence of two large Fe,Mg,Mn-bearing phosphate grains. These grains were examined optically and by secondary electron microscopy, and the rare earth element (REE) compositions were measured by ion microprobe.

Results and Discussion: Graves Nunataks 95209 appears to consist of three lithologies, described by [4]: relatively metal-rich matrix, metal-poor regions, and a metal-rich sheet on the surface of the meteorite that extends into the interior [5]. Section ,39 consists of equigranular olivine and orthopyroxene grains, with abundant metal and minor clinopyroxene, plagioclase, and troilite. Rare chromite grains are present, but Ca-phosphates (merrillite and apatite) and schreibersite are not observed in this section, although they have been reported by others [4]. However, two large regions of Fe,Mg,Mn-bearing phosphates, one (area B) about 500 by 700 µm, the other (area D) 600 by 1100 µm, were found associated with the metal in section ,39. The areas were examined by secondary electron microscopy and major element compositions were measured by quantitative energy-dispersive X-ray analysis. Each region appears to contain two distinct phosphates, Ca-free and Ca-bearing; small metal grains are interspersed throughout.

The Ca-free phosphates have average compositions of $(Fe_{1.07}Mg_{1.70}Mn_{0.18})_{?=2.95}P_{2.00}O_8$ and $(Fe_{1.53}Mg_{1.06}Mn_{0.33})_{?=2.92}P_{2.02}O_8$ for areas B and D, respectively, corresponding to an ideal formula of $(Fe,Mg,Mn)_3(PO_4)_2$. Some analyses show minor amounts of Ni, which are probably due to contamination from adjacent metal grains. These phosphates are more Fe- and Mn-rich than previously reported farringtonites [e.g., 6,7], but contain significantly more Mg than graftonite [8]. Partially surrounding individual Ca-free grains, and lining adjacent metal grains, are thin rims of what appears to be chladniite. Average compositions are $Na_{1.93}Ca_{0.55}(Fe_{1.69}Mg_{4.46}Mn_{1.03})_{?=7.18}P_{6.08}O_{24}$ for area B and $Na_{1.98}Ca_{0.49}(Fe_{2.36}Mg_{3.50}Mn_{1.48})_{?=7.34}P_{6.06}O_{24}$ for area D. These are distinctly more Fe- and Mn-rich than the chladniite found in the Carlton (IIICD) iron meteorite [9], and approach the composition of johnsomervilleite, which has an ideal formula of $Na_2Ca(Fe,Mg,Mn)_7(PO_4)_6$ [10,11]. The presence of chladniite in GRA 95209 was noted by [4], but no analyses were reported.

Trace elements (e.g., the REE) were measured by ion microprobe in the phosphates. REE abundances are below detection limits in the Ca-free phosphates, but show a wide variety in three chladniite analyses. One grain is HREE-enriched with Lu ~ 100 x CI and has a negative Eu anomaly, another has a flat pattern at about 1× CI, and a third grain is LREE-enriched with a positive Eu anomaly.

Textures in the phosphates are suggestive of growth by reaction and replacement: Chladniite occurs primarily as thin rims around Ca-free grains or adjacent to larger metal grains, and small, corroded metal grains are present throughout both phosphates. The variable REE patterns noted in chladniite probably result from this replacement process. REE may have been imported together with Ca from surrounding phases such as plagioclase or pyroxene.

References: [1] Floss C. (1998) in *LPS XXIX*, Abstract #1237. [2] Floss C., this volume. [3] Mason B. (1997) *Antarctic Met. News.*, *20*, *1*, 9. [4] McCoy T. J. and Carlson W. D. (1998) in *LPS XXIX*, Abstract #1675. [5] Carlson W. D. and McCoy T. J. (1998) in *LPS XXIX*, Abstract #1541. [6] Bild R. W. (1974) *Contrib. Mineral. Petrol.*, *45*, 91. [7] Buseck P. R. and Holdsworth E. (1977) *Mineral. Mag.*, *41*, 91. [8] Olsen E. and Fredriksson K. (1966) *GCA, 30,* 459. [9] McCoy T. J. et al. (1994) *Am. Mineral.*, *79*, 375. [10] Araki T. and Moore P. B. (1981) *Am. Mineral.*, *66*, 827. [11] Rubin A. E. (1997) *Meteoritics & Planet. Sci*., *32*, 231.

QUEEN ALEXANDRA RANGE 93148: A UNIQUE ACHONDRITE. C. A. Goodrich. Max-Planck-Institut für Chemie, Postfach 3060, 55020 Mainz, Germany (goodrich@mpch-mainz.mpg.de).

Introduction: Queen Alexandra Range 93148 is a small (1.1 g), olivine-rich achondrite originally classified as a lodranite [1]. Righter and Delaney [2] studied thin-section QUE 93148,11 and found that the olivine (*mg* 85-86) contains small (~50 x 5 μ) lamellae which appear to consist of either a Cr_2O_3- and CaO-rich (19.3% and 9.7%, respectively) olivine, or a submicrometer mixture of chromite and Ca-rich pyroxene. These authors reported that the Cr_2O_3 and CaO contents of the host olivine (0.16% and 0.12%, respectively) are intermediate between those of ureilites and those of lodranites, acapulcoites or winonaites. Hence, QUE 93148 does not appear to be related to any of these groups. Mayeda and Clayton (pers. comm.) determined the oxygen isotopic composition of QUE 93148 to be $\delta^{18}O$=3.49, $\delta^{17}O$=1.67, which is very similar to that of Brachina, and thus suggests the possibility that QUE 93148 is an unusual brachinite.

The purpose of this work was to obtain precise Fe-Mn-Mg data (comparable to those of [3,4] for ureilites and lodranites) for QUE 93148 and brachinites, in order to determine if QUE 93148 is a brachinite. In the course of this work I also found that olivine in thin-section QUE 93148,14 contains a lamella which is much larger than those observed by [2] and which has a complex structure and composition. This lamella is described here.

Method: Precise Fe-Mn-Mg data for olivine in QUE 93148 and in 4 brachinites (Brachina, ALH84025, Reid 013, Hughes 026) were obtained following the method used by [3,4] for ureilites and lodranites. Three ureilites were used as internal standards to ensure comparability of the data with those of [3,4]. Compositions of phases in the lamella were determined by standard microprobe techniques.

Fe-Mn-Mg Relations: Olivine Fe/Mg-Fe/Mn trends among ureilites and among lodranites (Fig. 1) are characterized by a combination of Fe-loss (a trend of constant Mn/Mg ratio, which is interpreted as primary) and partial melting [4]. In contrast, brachinite olivine forms a tight Fe/Mg-Fe/Mn cluster, with a higher Mn/Mg ratio than that of lodranites or ureilites. QUE 93148 has a unique olivine Fe/Mg-Fe/Mn composition, with a Mn/Mg ratio (0.00424±0.00003) lower than that of any major group of primitive or evolved achondrites. It resembles that of olivine in the pyroxene pallasite Y8451, but a relationship to pyroxene pallasites is ruled out by oxygen isotopic composition [5]. I conclude that QUE 93148 is not a brachinite, and appears to be unique.

Lamella: One olivine crystal in QUE 93148,14 contains a single lamella, ~350 x 50 μ in size. It is largely parallel-sided, with pyramidal terminations, and has truncated-pyramidal projections. The lamella consists dominantly of a myrmekitic intergrowth of chromite (with ~6.3% MgO, 3.5% Al_2O_3 and 0.9% V_2O_3) and orthopyroxene (Wo 2.5, *mg* 84.5, with ~0.8% Cr_2O_3 and 0.3% Al_2O_3). However, in small patches restricted to the outer edges of the lamella, the intergrowth is a fine-scale, unresolvable mixture which appears to be chromite and high-Ca pyroxene, and resembles the lamellae composition reported by [2]. The lamella also contains three ~10 μ grains of high-Ca pyroxene (Wo ~44, *mg* 89.7, with ~0.7% Cr_2O_3 and 0.2% Al_2O_3). Using this composition, and that of the chromite, I calculate from broad beam analyses that the unresolvable areas contain 63-68% high-Ca pyroxene. There is also one ~30 μ crystal of Fe-Ni metal, and a trace of Fe-sulfide. A bulk composition (excluding metal and sulfide) for the lamella was determined by point counting (1040 points): ~40% SiO_2, 13% FeO, 20% Cr_2O_3, 1.2% CaO, 0.3% MnO, 25% MgO, 0.06% TiO_2, 1% Al_2O_3, and 0.3% V_2O_3. This composition is too Cr^{3+}-rich to represent an olivine. In addition, the texture of the lamella suggests that it was a melt. Therefore, perhaps this lamella represents a trapped liquid that assumed a negative olivine crystal shape [6], rather than an exsolution product. The composition calculated for the liquid (if representative), however, is unusual and its origin is unclear.

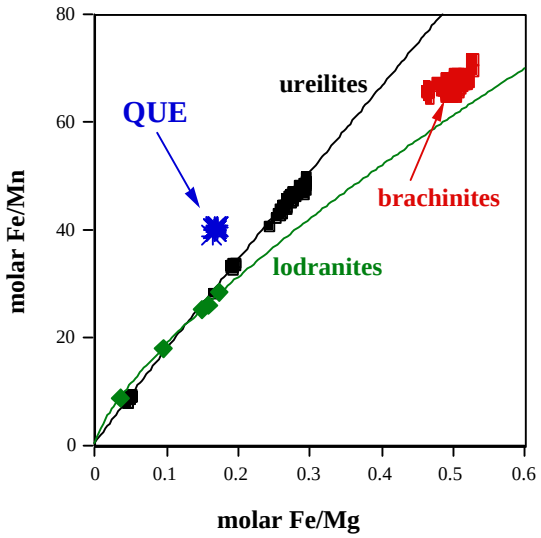

References: [1] Mason B. (1995) *Ant. Met. Newsletter, 18*, 1. [2] Righter K. and Delaney J. S. (1997) *Meteoritics and Planet. Sci., 32*, A108. [3] Goodrich C. A. et al. (1987) *GCA, 51*, 2255. [4] Goodrich C. A. (1998) *LPS XXIX*, Abstract #1044. [5] Boesenberg J. S. et al. (1995) *Meteoritics, 30*, 488. [6] Roedder E. (1984) *RIM, 12*, 15.

PRELIMINARY RESULTS OF MICROSTRUCTURAL TRANSMISSION ELECTRON MICROSCOPY INVESTIGATIONS OF DISTINCT FINE-GRAINED COMPONENTS WITHIN THE UREILITE HAMMADAH AL HAMRA 064. I. Weber[1], A. Bischoff[1], and F. Langenhorst[2], [1]Institut für Planetologie, Wilhelm-Klemm-Strasse 10, D-48149 Münster, Germany (sonderm@uni-muenster.de), [3]Bayerisches Geoinstitut, Universität Bayreuth, D-95440 Bayreuth, Germany.

Hammadah al Hamra 064 (HH064) is a medium-shocked (S3), poikilitic, bi-modal ureilite consisting of abundant olivine, augite and low-Ca pyroxene [1,2]. Fine-grained, carbon-rich interstitial material occurs along the grain boundaries of the mentioned phases, and along fractures and cleavage planes within these crystals. Weber and Bischoff [1] reported that HH064 belongs to the most pyroxene-rich ureilites. This meteorite was studied by transmission electron microscopy (TEM, JEOL JEM-3010, 300kV) in order to resolve the mineralogy within the fine-grained areas and within the reduction rims in olivines. The investigation was aimed to better understand the formation and evolution processes of this meteorite and the meteorite parent body.

Results: Two distinct fine-grained components were studied in detail by TEM and electron microprobe: a) the interstitial fine-grained, carbon-rich areas and b) the reduction rims in olivine.

Mineralogy of the fine-grained areas. The fine-grained areas occurring interstitial to the main silicates contain pyroxene (avg. $En_{88}Wo_9$) and low-Ni iron metal as phases large enough for microprobe analysis. The TEM observations show that the carbon-rich phase in these areas is basically graphite. Graphite occurs in the form of small flakes (40×160 nm in size), which show in high resolution images typical kinking of (0002) planes ($\approx$ 3.4 Å). Diffraction patterns from other constituents of the fine-grained areas revealed the occurrence of at least one highly disordered phase, which still has to be characterized in detail.

Mineralogy of the reduction rims. Electron microprobe investigations indicate that olivines in the reduction rims have a Mg content of Fo up to 97.5 mol%. These rims are riddled with tiny, mainly spherical metal grains. As an additional phase orthopyroxene ($En_{97}Wo_{\leq 1}$) preferentially occurs along the margins. Graphite is also present in these reduction rims. It occurs as small grains up to 200 nm in size.

Dark field imaging of olivine reveals the presence of dislocations originating at the spherical metal inclusions (Fig. 1). These dislocations probably represent misfit dislocations. They may formed during the growth of metal spherules as a result of the incoherence between the metal and olivine crystal lattices. In bright field images the orthopyroxene in the rims shows some transformation lamellae parallel the (100) plane. The electron diffraction pattern exhibits distinct streaking parallel to a*. These lamellae likely represent ortho-/clinoenstatite lamellae. Their formation is due to shearing along the (100) plane. Such shear forces could occur by different mechanisms, e.g., by a thermal (quenching from the protoenstatite field) or a deformation event.

Conclusions: Considering the origin of the ortho-/clinoenstatite lamellae it is difficult to distinguish between the two possibilities mentioned above. Assuming that the ureilites have a two-stage cooling history [2], the rapid cooling has certainly initiated the formation of a distinct amount of lamellae, which could have been further increased by a subsequent shock event. The high abundance of graphite in these ureilite and the Fa-content of 2.5 mol% in the reduction rims may indicate that the degree of reduction is not only dependent on the amount of carbon but preferentially due to rapid cooling.

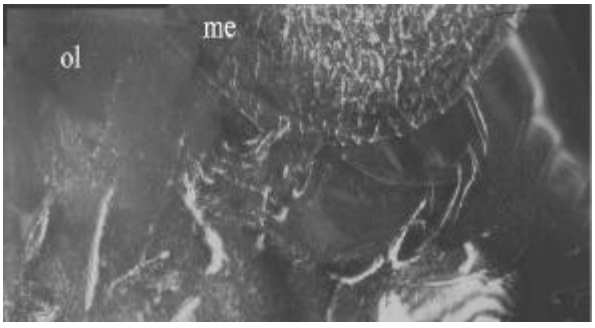

Fig. 1. Dark field image of olivine (ol) and spherical metal inclusions (me) with misfit dislocations (image width $\approx$ 1.6 µm).

References: [1] Weber I. and Bischoff A. (1998) *LPS XXIX*, Abstract #1365. [2] Goodrich C. A. (1992) *Meteoritics, 27*, 327–352.

LOHAWAT HOWARDITE: CHEMICAL AND MINERALOGICAL CHARACTERISTICS AND COSMOGENIC RECORDS. U. K. Singh[1], M. S. Sisodia[1], A. D. Shukla[2], S. Chakraborty[2], K. M. Suthar[2] , M. H. Dixit[2], P. N. Shukla[2], and N. Bhandari[2], [1]Department of Geology, J. N. V. University, Jodhpur 342 005 (bhandari@prl.ernet.in), [2]Physical Research Laboratory, Navrangpura, Ahmedabad 380 009, India.

Three rare stony meteorites (an enstatite chondrite, a howardite and an eucrite) have fallen in a period of 5 years within a distance of about 180–210 km from each other in the semi-desert region of western Rajasthan, India. Statistically it is a strange coincidence, firstly because of the nature of these meteorites, since they belong to rare groups, secondly because of the proximity of their fall and thirdly because of the short interval of time during which they fell. Normally, one meteorite is expected to fall over a 15000 sq km area in about 2000 years and the most probable i.e. abundant group of meteorites is that of ordinary chondrites. In addition, it may be noted that howardites and eucrites (HED) have related origin and it is believed that they belong to different depths of the same asteroidal bodies. The Didwana-Rajod enstatite chondrite and Piplia Kalan eucrite which fell in 1991 and 1996 respectively have been described previously [1–3]. Here we describe the howardite, of which a single fragment, weighing about 40 kg, which broke on impact, fell at Lohawat village, in Western Rajasthan on 30th October, 1994 at about 11 pm IST [4]. It is a heterogeneous polymict regolith breccia with a large variety and number of lithic fragments in a finely comminuted material, having appearance similar to Kapoeta. Two lithologies are prominent: one consisting of a fine grained light ash coloured angular and rounded fragments and the other, less abundant, of a dark glassy material, having dominantly feldspars. A dunitic fragment, probably of a diogenite, was also found and some fragments have eucritic mineral composition, consistent with the models that howardites are mixtures of eucrite and diogenite components. Many of these fragments and single mineral grains are rounded and some of them have well developed glassy rims. Several glassy (pyroxenitic) chondrule like objects , ranging in size from 1 mm to 7 mm were also found. Some minerals show definite shock effects as expected in impact breccias.

Chemical analysis gives concentrations of Fe(15.15%), Mg(9.28%), Al(4.22%), Ca(4.73%), K(0.0267 to 0.0366%) and Na(0.26%). These are similar to the values reported earlier [4].

Cosmic ray tracks and some radionuclides have been measured. The track density is found to range between 0.7 and $6 \times 10^6/cm^2$ in olivine and feldspar grains which were etched for 9 hours in boiling WN solution and for 30 minutes in boiling 1:2 NaOH respectively. Solar flare irradiated grains are extremely rare(<<1%). ^{22}Na and ^{26}Al activities measured, using whole rock gamma ray spectrometry, are 46 ± 5 dpm/kg and 77 ± 4 dpm/kg respectively.

We thank Mr. Rameshwar Lal Soni, Ramesh Tak and others of Lohawat village who helped us in collection of the meteorite fragments.

References : [1] Paliwal B. S. et al. (1997) *Current Science, 73,* 499–502. [2] Vaya V. K. et al. (1996) *Current Science, 71,* 253–257. [3] Shukla A. D. et al. (1998) *Meteoritics and Planet. Sci., 32,* 611–615. [4] Chattopadhyay B. et al. (1998) *J. Geol. Soc. India, 51,* 171–174.

SULFIDE/SILICATE MELT PARTITIONING DURING ENSTATITE CHONDRITE MELTING. C. Floss[1], R. A. Fogel[2], G. Crozaz[1], M. Weisberg[2], and M. Prinz[2], [1]McDonnell Center for the Space Sciences and Department of Earth and Planetary Sciences, Washington University, St. Louis MO 63130, USA (floss@howdy.wustl.edu), [2]American Museum of Natural History, Department of Earth and Planetary Sciences, New York NY 10024, USA.

Introduction: Aubrites are igneous rocks thought to have formed from an enstatite chondrite-like precursor [1]. Yet their origin remains poorly understood, at least partly because of confusion over the role played by sulfides, particularly oldhamite. CaS in aubrites contains high rare earth element (REE) abundances and exhibits a variety of patterns [2] that reflect, to some extent, those seen in oldhamite from enstatite chondrites [3]. However, experimental work suggests that CaS/silicate melt REE partition coefficients are too low to account for the high abundances observed [4,5] and do not explain the variable patterns. A related problem concerns the solubility of oldhamite under conditions of aubrite formation, as a relict origin has been proposed for some aubritic CaS [2,4]: phase equilibria experiments suggest that oldhamite readily dissolves in enstatite chondrite silicate melts [6]. In this initial work we re-examine the question of REE partitioning between sulfides and silicates during melting of natural enstatite chondrite material.

Results: Powdered samples of Indarch and Indarch + synthetic CaS were melted at temperatures between 1250°C and 1400°C [6]. We report here the first in situ (ion microprobe) determinations of sulfide/silicate melt partition coefficients using natural levels of the REE (i.e., those initially present in Indarch).

REE concentrations in enstatite, forsterite and metal are below detection limits. Glass has uniform REE concentrations and a flat pattern in each sample; abundances range from 0.5 to 10 x CI. Alabandite has a HREE-enriched pattern (Yb ~ 6 x CI) with a negative Eu anomaly. Natural alabandite exhibits a similar but steeper pattern [7], with LREE typically below detection limits [2,3]; this may be because our experimentally produced alabandite contains several wt.% Ca. Troilite is LREE-enriched (Ce ~ 5 x CI) with a small positive Eu anomaly. However, in aubritic troilite the REE are below detection limits [2,7], with concentrations more than two orders of magnitude lower than those observed here. Oldhamite (present only in CaS-saturated charges) has a flat REE pattern with abundances of about 0.5 x CI.

Discussion: Oldhamite/glass D values are close to 1 for most REE, consistent with previous results [4,5,6], and significantly lower than those expected based on REE abundances in aubritic oldhamite. In contrast, D values for FeS are surprisingly high (from about 0.1 to 1), given the low REE abundances of natural troilite. FeS/silicate partition coefficients reported by [5] are somewhat lower, but exhibit a similar pattern. Alkali loss from the charges, resulting in Ca-enriched glass, might provide a partial explanation for low oldhamite REE abundances, if the REE follow Ca, but cannot account for the elevated REE abundances in troilite. Sulfides in the Fe-Mg-Mn-Ca-S system can exhibit extensive re-equilibration to low temperatures unless cooled rapidly [8]; low temperature REE re-equilibration between troilite and oldhamite in aubrites may be a possible mechanism for enriching CaS in the REE. It is interesting to note that the REE pattern for troilite seen here is similar to one of the patterns observed in aubritic oldhamite [2]. However this mechanism cannot account for all oldhamite REE patterns and occurrences (e.g., [7]). Furthermore, FeS/CaS ratios in many aubrites may not be high enough to provide the strong enrichments observed in aubritic oldhamite. Additional work is clearly needed to resolve this problem, as well as the question of oldhamite solubility.

References: [1] Keil K. (1989) *Meteoritics, 24,* 195. [2] Floss C. and Crozaz G. (1993) *GCA, 57,* 4039. [3] Crozaz G. and Lundberg L. L. (1995) *GCA, 59,* 3817. [4] Lodders K. (1996) *Meteoritics & Planet. Sci., 31,* 749. [5] Dickinson T. L. and McCoy T. J. (1997) *Meteoritics & Planet. Sci., 32,* 395. [6] Fogel R. A. et al. (1996) *LPS XXVII,* 371. [7] Wheelock M. M. et al. (1994) *GCA, 58,* 449. [8] Skinner B. J. and Luce F. D. (1971) *Amer. Mineral., 56,* 1269.

MÖSSBAUER SPECTROSCOPY EVIDENCES OF DIFFERENT DEGREES OF AQUEOUS ALTERATION IN TWO CM CHONDRITES: NIGER (I) AND MURCHISON. T. V. V. Costa[1], V. W. Vieira[1], M. A. B. Araújo[1], I. Souza Azevedo[2], and R. B. Scorzelli[2], [1]Departomento de Física, Universidade Federal do Ceará, 60451-970 Fortaleza, Brazil, veve@fisica.ufc.br, [2]Centro Brasileiro de Pesquisas Físicas, Rua Xavier Sigaud 150, 22290-170 Rio de Janeiro, Brazil, scorza@cat.cbpf.br.

The Niger (I) meteorite is reported as a typical CM2 carbonaceous chondrite, with a composition very similar to that of Murchison (CM2). The iron content of these two meteorites is approximately 20 wt. %. ^{57}Fe Mössbauer spectroscopy (MS) reveals an intriguing difference between Murchison and Niger (I): Murchison MS does not reveal the presence of magnetite, whereas in the Niger (I), approximately 47% of the total iron can be attributed to magnetite.

The Niger (I) meteorite was investigated by ^{57}Fe MS at temperatures between 300 K and 16 K. The room temperature (RT) spectrum shows that besides Fe^{2+} and Fe^{3+} in paramagnetic compounds, the meteorite contains a large amount of magnetite, representing about 47% of the total spectrum area .

Using the area ratio of the two sextets of magnetite and assuming that the Debye-Waller factor (f) of the two sites is the same, we can obtain a relation between the degree of stoichiometry and the area ratios observed in the spectrum, which indicate that the magnetite present in Niger (I) is nearly stoichiometric.

The spectra obtained at 30 K and 16 K are typical of magnetite below the Verwey temperature (120 K). It should be noted that there is a slight increase in the contribution of the magnetic phase to the total spectrum from RT to 16 K. Scorzelli et al. [1] investigated the Niger (I) meteorite at lower temperatures, down to 4.2 K. At temperatures below 80 K they observed an increase in the intensity of the magnetic lines and a progressive decrease of the paramagnetic Fe^{3+} doublet, evidencing the presence of superparamagnetism. It has been suggested that about 15% of the iron in this meteorite is in the form of a superparamagnetic compound.

As far as we know, no other CM chondrite displays the amount of magnetite found in Niger (I). As mentioned before, the amount of magnetite in Murchison is not sufficient to be detected by Mössbauer spectroscopy. A substantial amount of magnetite is also found in the Orgueil CI carbonaceous chondrite [2]. In the RT Mössbauer spectrum of Orgueil, oxidized magnetite comprises ≈50% of the total area. In fact the Mössbauer spectra of Niger (I) at various temperatures resemble more the spectra of Orgueil than that of Murchison.

Much of the CM matrix material was probably produced by aqueous alteration of olivine, pyroxene, sulfide and metal. According to the literature, the abundance of cronstedtite and FESON is related to the degree of aqueous alteration and magnetite should be a product of alteration of FESON [3]. The Murchison meteorite contains abundant cronstedtite and FESON, so it is relatively unaltered when compared to other CM meteorites. The Mössbauer spectrum at 30 K of Niger (I) suggests that FESON represents ≈8% of the total iron, whereas in Murchison FESON constitutes ≈30% of the total iron [3]. The large amount of FESON present in Niger (I) seems to indicate that these two meteorites experienced different alteration conditions.

The origin of magnetite in Orgueil is controversial, but there are evidences that it was formed by aqueous alteration [4]. A detailed comparative study of the matrix of the Niger (I) and Orgueil meteorites would probably help to shed light on the process of formation of the low tempertaure mineral phases in carbonaceous chondrites.

References: [1] R. B. Scorzelli et al. (1996) P*roceed. LACAME 88,* 373–377. [2] M. B. Madsen et al. (1986) *Nature, 321,* 501–503. [3] K. Tomeoka et al. (1985) *GCA, 49,* 2149–2163. [4] K. Tomeoka et al. (1988) *GCA, 52,* 1627–1640.

TEXTURES AND BULK CHEMISTRY OF DARK INCLUSIONS IN THE REDUCED CV3 CHONDRITE EFREMOVKA. V. V. Biryukov and A. A. Ulyanov, Geological Faculty, Moscow State University, Moscow 119899, Russia (vvbir@geol.msu.ru).

Dark inclusions in the reduced CV3 chondrite Efremovka are mineralogically similar to the host meteorite, but experienced various degrees of late-stage, asteroidal alteration that resulted in formation of fayalitic olivine, kirschsteinite, salitic pyroxene, garnet, Ni- and Co-rich metal, phyllosilicates, and chromite [1]. At the same time, average sizes of chondrules and CAIs in these DIs (200 and 150 μm, respectively) are much smaller than those in the host Efremovka (730 and 790 μm, respectively), suggesting some size-sorting mechanism. The similar relationship was found for chondrules and CAIs in the Allende DIs and host Allende [2].

The observed differences in size distribution of chondrules and CAIs between DIs and their host CV meteorites could be explained by two models. 1) DIs formed from the CV-like material that experienced nebular size-sorting and accreted into separate parent bodies or into different parts of CV asteroid; it was subsequently altered, brecciated and incorporated into the host Efremovka. 2) DIs originated from a heterogeneously-altered CV3 parent body that experienced brecciation and alteration along tectonically active zones which had high fluid permeability. These processes may have produced secondary (asteroidal) size-sorting of chondrules and CAIs.

Unlike to the Allende DIs [2], there is no essential difference between bulk chemical composition for different types [1] of Efremovka DIs (Fig. 1). Moderately- and highly-volatile elements in the Efremovka and Allende DIs (Au, Na, K, As, Sb, Se, Cs) are highly-fractionated. All of these elements are mobile in low-temperature aqueous solutions under oxidized conditions. Mineralogical evidences indicate that alteration of the Allende and Efremovka DIs occurred under oxidized conditions. These include: presence of Fe^{3+}-rich garnet and chromite, preferential oxidation of Fe in the metal with enrichment of the residual metal in Ni and Co. Presence of minor phyllosilicates in the Efremovka DIs [3] may indicate that the alteration occurred at low temperatures, possibly during hydrothermal activity or hypergenes. Decreasing of concentration of alkali cations from Cs to Na probably is pointed to the sorbtion on phyllosilicates. Fractionation of Sb, As and Au is also consistent with hypergenesis conditions.

We infer that the Efremovka DIs possibly originated from the heterogeneously-altered CV asteroidal body. The alteration took place under low-temperature oxidized conditions and resulted in redistribution of moderately- and highly-volatile elements (Na, K, Au, As, Br, S, Se) between zones with different degrees of alteration. The alteration was followed by dehydration and brecciation.

Acknowledgments: This research was funded by grants of RFBR N96-05-65144 and program "Universities of Russia" N5305.

References: [1] Birjukov V. V. et al. (1998) this issue. [2] Buchanan P. C. et al. (1997) *GCA, 61*, 1733. [3] Krot A. N. et al. (1997) *LPS, XXVIII*, 769. [4] Krot A. N. et al. *GCA*, in press.

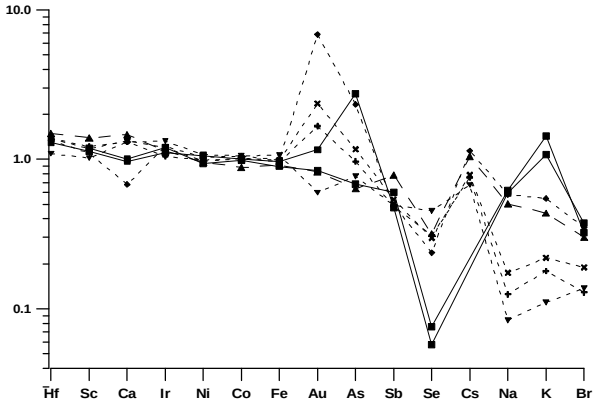

Fig. 1. CI normalized bulk chemical composition of DIs E39 and E53 in Efremovka CV3 (<) [4]; Allende DIs of type A (+), A/B (ρ), B (◆), C (6) and Allende host (5) [1]. (Cr=1)

MINERALOGY AND CLASSIFICATION OF DARK INCLUSIONS IN THE REDUCED CV3 CHONDRITE EFREMOVKA. V. V. Biryukov[1], N. N. Korotaeva[1], A. N. Krot[2], and A. A. Ulyanov[1], [1]Geological Faculty, Moscow State University, Moscow 119899, Russia (vvbir@geol.msu.ru) [2]Hawai'i Institute of Geophysics and Planetology, School of Ocean and Earth Sciences and Technology, University of Hawai'i at Manoa, Honolulu HI 96822, USA.

Dark inclusions (DIs) are fine-grained lithic clasts of chondritic materials, that experienced various degrees of alteration either in the solar nebula or in an asteroidal environment [1,2]. Recently, it has been suggested that the alteration process that affected DIs in CV chondrites was similar to that which altered the host meteorites [3]. In this paper, we present results of mineralogical and petrographic studies of several DIs in the reduced CV chondrite Efremovka, including previously described E39, E53, E80, E81, E82, E90 [4,5], and newly found E83 and E84.

Efremovka DIs have chondritic textures with distinct chondrules and CAIs. Primary chondrule and CAI minerals are replaced by secondary mineral assemblages, including fine-grained fayalitic olivine (Fa_{30-50}), kirschsteinite, chromite, phyllosilicates, Fe-Ni-Co metal (Co-taenite, Co-tetrataenite, Co-kamacite, wairauite), garnet(?), and salitic pyroxene. Because Efremovka DIs do not fit into the classification scheme proposed for the Allende DIs [3], we classified them exclusively based on the degree of alteration as weakly-, mildly-, and heavily-altered. The weakly-altered DI E53 contains incompletely-altered chondrules and CAIs with abundant relic minerals, including low- and high-Ca pyroxenes, forsteritic olivine, plagioclase, Mg-Al-spinel, and melilite. The mildly-altered DIs are the most common (E39, E81, E82, E83, E84, and E90). Chondrule and CAI textures are less distinct than in E53; most of the primary minerals are replaced by the secondary phases. A single heavily-altered DI, E80, almost does not contain relic minerals; chondrule pseudomorphs are barely visible; CAI pseudomorphs were not identified.

Although the mineralogy of the relict phases in Efremovka DIs is similar to those in chondrules and CAIs in the host meteorite, there are some differences in mineral chemistry, e.g., relic pyroxenes in CAIs from DIs contain significantly less Ti than most pyroxenes in the Efremovka CAIs. This either reflects a primary difference in mineral compositions between the DI and Efremovka CAIs or different resistance of primary CAI minerals to alteration. Relict forsteritic olivines in Type I chondrules in the DIs have lower Cr contents than those in the host meteorite, possibly reflecting diffusional loss of Cr to form chromites during metamorphism.

The observed secondary mineralization in Efremovka DIs differs from that in the Allende DIs [2], but is rather similar to that in the reduced CV chondrites Leoville and Vigarano [2]: it is dominated by very fine-grained fayalitic olivine closely associated with minor chromite and chlorite. Based on these observations, we infer that the presence of secondary fayalitic olivine in chondrules and CAIs in Efremovka DIs is consistent with the aqueous alteration-dehydration model. Kirschsteinite compositions in studied DIs are followed to the kirschsteinite-forsterite mixing line against to the kirschsteinite-monticellite composition common in meteorites. Garnets, which have been identified exclusively based on stoichiometry, are enriched in Fe and Ti, suggesting the presence of Ti-andradite and koharite ($Mg_3Fe_2Si_3O_{12}$) components and oxidized conditions during alteration. From weakly- to heavily-altered DIs, composition of garnet is changed from grossular-andradite to uvarovite-koharite-andradite. Amount of Fe^{3+} in chromite is increased with DIs alteration degree. High Ni and Co contents in metal grains indicate preferential oxidation of Fe during alteration. Excess of Co comparatively Ni may be produced by similar behavior of Fe and Co (they both are mobile in trivalent ions in aqueous solutions unlike Ni).

Acknowledgments: This research was funded by grants of RFBR N96-05-65144, program "Universities of Russia" N5305 and NASA grant NAG 5-4212. This is HIGP publication number 991 and SOEST publication number 4631.

References: [1] Kurat G. et al. (1989) *Zeitschr. Naturforsch., 44a,* 988. [2] Johnson C. A. et al. (1990) *GCA, 54,* 819. [3] Krot A. N. et al. (1995) *Meteoritics, 30,* 748. [4] Krot A. N. et al. (1997) *LPS XXVIII,* 769. [5] Biryukov V. V. et al. (1997) *LPS XXVIII,* 115.

PRELIMINARY GEOCHEMICAL STUDY OF THE INSOLUBLE ORGANIC MATTER FROM ORGUEIL METEORITE. A. Gardinier[1,2], F. Robert[1], F. Behar[2], C. Largeau[3], and S. Derenne[3], [1]Laboratoire de minéralogie, Museum National d'Histoire Naturelle, 61 rue Buffon 75005, Paris, France, [2]Division Géologie/Géochimie, Institut Français du Pétrole, 1 et 4 Avenue de Bois Préau; 92852 Rueil Malmaison, France, [3]Laboratoire de chimie bioorganique et organique physique, UMR CNRS 7573, Ecole Nationale Supérieure de Chimie de Paris, 11 rue Pierre et Marie Curie, 75231 Paris Cedex 05, France.

Numerous studies on the meteoritic soluble organic molecules in CCs have been reported in the literature leading to the identification of compounds such as amino acids, hydrocarbons, carboxylic acids and nitrogen compounds (e.g., Cronin et al. 1988). However, between 70% and 90% of the organic carbon consists in insoluble organic macromolecules. Althrough its specific structure, chemical parameters are often compared to those of terrestrial kerogens isolated from sedimentary rocks. Because of the technical difficulties linked to the study of insoluble organic compounds, the nature, structure and chemical composition of those meteoritic macromolecules are still not well known.

The aims of this study were to characterize the insoluble organic matter (OM) from the Orgueil meteorite and to determine the relationships between insoluble and soluble compounds. These relationships are of primordial importance to be known because they will give some hints on the synthesis of organic molecules in the early solar system.

Extractions with different solvents, base and acid hydrolyses were successively performed on the meteorites so as to recover the soluble OM. The final residue was further treated with HCl and HF in order to specifically isolate the insoluble OM. Special care to avoid any oxidation and ash formation was exercised. The insoluble OM was then submitted to global analysis as elemental analysis, solid state ^{13}C NMR and Fourier transformed infrared spectroscopy (FTIR), and degradative techniques as Rock-Eval pyrolysis and Curie point Pyrolysis GC-MS.

In order to quantify the different carbon types present in this insoluble OM, ^{13}C NMR spectra were recorded at 100 MHz using CP/MAS sequences at different contact times and spinning rates of 4, 5, and 10 kHz. Deconvolution of the spectra indicates the presence of non-protonated and protonated aromatic, and aliphatic carbons, but doesn't reveal carbonyl and carboxyl functions. All these types of carbon were quantified so as to derive a reliable aromaticity fraction of 0.45. The comparison between H/C ratio from elemental analysis (0.72) and the H/C ratio calculated from ^{13}C NMR data (1.25) indicates that either aliphatic carbons are overestimated or that aromatic carbons are underestimated. Since quaternary carbons located at the center of polyaromatic units are not affected by the polarization transfer, we can estimate that ca. 50% of the carbons, located at the center of polyaromatic units, are not detected via ^{13}C CP/MAS NMR.

Despite these results, FTIR indicates the occurrence of several oxygenated functions. In sight of these inconsistency, thermal degradatives methods have been used to show the nature of the constitutive moities. Rock Eval pyrolysis show that most of the released products are gaseous such as CO and CO2 (160 mg / g of Total Organic Carbon), the presence of ether groups which can be explain by those functional groups are not well detected by ^{13}C CP/MAS NMR. The other non hydrocarbon and hydrocarbon gases have not yet been studied.

This technique show also a relatively low thermal stability for the insoluble OM of Orgueil when compared with immature terrestrial kerogens (the cracking starts at 300°C and maximizes at 440°C).

Curie point Pyrolysis GC-MS indicate that the C6+ products (86 mg / g of TOC) chiefly correspond to aromatic compounds containing benzene, thiophene or phenol moieties, polycyclic hydrocarbons and aliphatic compounds (C8 to C18).

The insoluble OM of Orgueil thus appears to be thermally labile and constituted by monaromatic and polyaromatics units bounded with oxygen, sulfur and containing small aliphatic chains. Other complementary quantitative data on gases and C6+ products will allow us to propose a model of structure for this insoluble OM and to compare these products with the soluble OM extracted from the meteorite. The same approach will be followed for Murchison meteorite.

Reference: [1] Cronin J. R., Pizzarello S., and Cruikshank D. P. (1988) in *Meteorites and the Early Solar System* (eds. J. F. Kerridge and M. S. Matthews), pp. 819–857, University of Arizona.

TEN NEW METEORITES FROM THE TÉNÉRÉ DESERT (NIGER): CLASSIFICATION, NOBLE GASES, COSMOGENIC RADIONUCLIDES, AND TERRESTRIAL AGES. L. Schultz[1], P. Scherer[1], B. Spettel[1], F. Wlotzka[1], J. Zipfel[1], J. Schlüter[2], S. Merchel[1,3], U. Herpers[3], J. Newton[4], I. A. Franchi[4], C. T. Pillinger[4], I. Leya[5], S. Neumann[5], U. Neupert[5], R. Michel[5], P. W. Kubik[6], H.-A. Synal[6], G. Bonani[7], I. Hajdas[7], S. Ivy-Ochs[7], and M. Suter[7], [1]Max-Planck-Institut für Chemie, 55020 Mainz, Germany (schultz@mpch-mainz.mpg.de), [2]Universität Hamburg, 20146 Hamburg, Germany, [3]Abteilung Nuklearchemie, Universität zu Köln, 50674 Köln, Germany, [4]Planetary Science Research Institute, Open University, Milton Keynes, UK, [5]Zentrum für Strahlenschutz und Radioökologie, Universität Hannover, 30167 Hannover, Germany, [6]Paul Scherrer Institut c/o Institut für Teilchenphysik, ETH Hönggerberg, 8093 Zürich, Switzerland, [7]Institut für Teilchenphysik, ETH Hönggerberg, 8093 Zürich, Switzerland.

In March 1997 ten new meteorites were found in the Ténéré, a part of the Sahara located in Niger. The total recovered weight was about 37 kg, with the largest specimen of 27 kg. Table 1 gives the classification of these meteorites as obtained from mineralogical-petrographic investigation and the oxygen isotopic composition. Grein 002 is, according to its Si content in the metal, an EL chondrite, however, several bulk element concentrations do not allow a clear distinction between EL and EH.

We have measured concentrations and isotopic compositions of all noble gases. Furthermore, we have determined concentrations of long-lived cosmogenic nuclides ^{10}Be, ^{26}Al, and ^{36}Cl in bulk samples and magnetic fractions using accelerator mass spectrometry (AMS) after radiochemical separation. From the known ^{21}Ne radiation ages and ^{14}C terrestrial ages we corrected the measured radionuclide activities to production rates at time-of-fall, which allows us to compare directly our results with theoretical production rates [1].

To obtain terrestrial ages also ^{14}C in these chondrites was measured. Terrestrial ages are calculated from these values and depth dependent production rates taken from the physical model [1].

The O isotopic composition is strongly influenced by O from terrestrial weathering products. However, this effect is highly variable, as recorded by the H5 chondrites, suggesting either gross local variation in weathering conditions or different terrestrial ages.

The four H5 chondrites Tiffa 001 and 004 to 006 were found within a distance of about 10 km. They appear petrographically very similar and also their exposure ages agree within the limits of uncertainty (7.0 ± 0.5 Ma). The shielding conditions—represented by the cosmogenic ^{22}Ne/^{21}Ne ratio - are, however, very different. According to the radionuclide concentrations Tiffa 001 is probably not paired with the other three H5 specimens.

Carbon-14measurements indicate that many of these meteorites have terrestrial ages of 3400 to 5700 yrs. This is in agreement with the surface conditions of the find location. Neolithic artifacts found in the vicinity of the meteorites indicate that this part of the Sahara became arid only a few thousand years ago, providing the conditions for prolonged preservation. Only Adrar Madet, found under other surface conditions, has a terrestrial age of about 8000 years, while Grein 002 and Tiffa 003 are recent falls.

TABLE 1. Classification, shock and weathering grades of the investigated meteorites. (Names need to be approved by the Nomenclature Committee of the Meteoritical Society).

Name	Type	Shock	Weath.
Grein 001	H3	S2	W1
Grein 002	E4-5		W0
Grein 003	H6	S1	W1
Tiffa 001	H5	S2	W2
Tiffa 002	H4-5	S1	W3
Tiffa 003	L6	S3	W1
Tiffa 004	H5	S2	W2
Tiffa 005	H5	S2	W2
Tiffa 006	H5	S2	W2
Adrar Madet	H5-6	S2	W3

Acknowledgments: This study was partly supported by the Deutsche Forschungsgemeinschaft (DFG) and the Swiss National Science Foundation.

References: [1] Michel R. et al. (1996) *Nucl. Instr. Meth. Phys. Res., B113*, 434–444.

NEW DATA ON THE L5(S1) CHONDRITE BASZKÓWKA (POLAND). M. Stepniewski[1], J. Borucki[2], J. Siemiatkowski[3], [1]National Geological Institute, Rakowiecka 4, 00-975 Warszawa, Poland, [2]Pesztenska 3 m. 24 03-925 Warszawa, Poland, [3]National Geological Institute, Branch Station, Jaworowa 19, 53-122 Wroclaw, Poland.

The modal composition (electron microprobe analysis) of 14 olivine ($Fa_{26.1\ (25.0–28.0)}$) and 12 orthopyroxenes grains ($Fs_{22.3\ (20–23.2)}$) agree with published [1] data ($Fa_{25.8}$, $Fs_{23.2}$). The classification to the L-group was since confirmed by the O-isotope composition ($\delta^{17}O$ = +3.66 and $\delta^{18}O$ = +4.88; I. Franchi, Open Univ., Milton Keynes, UK).

Unfragmented chondrules (0.14–3 mm), making ~30% v/v of the meteorite, have smooth or rough surfaces and mostly microcrystalline rims. The plastic deformations are rather common. The other ~30% v/v of the meteorite is composed of the fragments of chondrules. However, fractures and/or fissures are missing in the unfragmented chondrules, so that process of fragmentation took place before the accretion of the Baszkówka parent body. Compound chondrules are composing ~10% v/v of the meteorite. The fine-grained mesostasis of some of chondrules is composed of the feldspar, feldspar-pyroxene, or feldspar-chromite aggregates.

The euhedral crystals of olivine and pyroxene were observed in the multiple hollows present in Baszkówka. Olivine crystals have the maximum length till ~0.X mm and very well developed crystal faces marked with sets of striae vertical to the Z-axis, effect of changing intensity of crystallization. The silicate crystal faces are decorated with multiple hollows (etch figures), particularly well developed on pyroxene faces, and having a regular symmetry on the chromite ones (Fig. 1).

The linear sequences of metal-troilite grains are giving the impression of partly broken, irregular veinlets. Other particular kinds of metal-sulphide grains are: (1) Aggregates (to >10 mm dia.) with troilite core, enveloped by a kamacite shell and a silicate rim. Olivine, pyroxene (angular or rounded) and rare plagioclases inclusions are present inside sulfide and metal. (2) Kamacite grains (to few mm dia.) with numerous angular or rounded pyroxene and olivine inclusions and silicate rims similar as above.

Few aggregates olivine-pyroxene-troilite-whitelockite (to ~0.2 mm) were found in the meteorite matrix. Four electron microprobe analysis permit to approximate the chemical formula of the phosphate: $(Ca_{8.7}Mg_{0.8}Na_{0.8}Fe_{0.1})(PO_{3.9})_7$. The presence of Fe-oxides in the matrix was confirmed during the SEM observations and microprobe analysis. The first analysis indicate the probable presence of wüstite, bunsenite and magnetite.

The analogies between Baszkówka and Mt. Tazerzait suggesting their affinity [3] are numerous: similar composition, significant porosity (density of Baszkówka: 2.9 g/cm^3), quantities of noble gases, and extraordinarily long exposure age [2]. Recent INAA analysis (R.Dybczynski, Institute of Nuclear Chemistry and Technology, Warsaw), the determinations of Hg (Nippon Instruments. Corp. Application. Lab., Osaka, Japan) 4.5 and 5.1 μgHg/g, as well as sulfur isotope composition $\delta^{34}S$= –1.25 and –1.18 (σ = 0.06) for Baszkówka and Mt. Tazerzait respectively (St.Halas, Lublin Univ., Poland) confirm the previous conclusions.

Conclusions. Observations confirm the probable origin of Baszkówka and Mt. Tazerzait from a common parent body, different from that of other L-chondrites. The growth of euhedral crystals in the voids of the chondrites and the etch figures on its faces, could be created by solutions on the Baszkówka-Mt. Tazerzait parent body.

Acknowledgments. We are grateful to E. Starnawska and L. Giro for the assistance of SEM interpretation and electron microprobe analysis. This study was supported by Polish Committee of Scientific Research; Grant 6PO4D 031 1.

References. [1] Wlotzka F. (1995) *Meteoritical Bulletin, 78,* 792. [2] Wlotzka F. (1997) *Meteoritics, 32,* A140–A141. [3] Stepniewski M. et al. (1996) *Meteoritic, 31,* A134–A135.

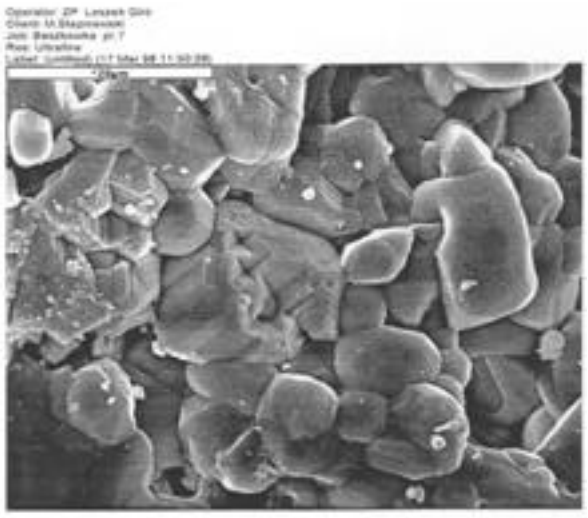

Fig. 1. Etch figures visible on the chromite grain in the center of the picture.

CHEMICAL ZONING PROFILES OF DAUBREELITES IN ENSTATITE CHONDRITES. J. Chikami[1,2], A. El Goresy[2], and J. Janicke[2], [1]Mineralogical Institute, Graduate School of Science, University of Tokyo, Hongo 7-3-1, Bunkyo-ku, Tokyo 113, Japan, [2]Max-Planck-Institut für Kernphysik, Postfach 103980, 69029 Heidelberg, Germany.

Introduction: The enstatite chondrites are the most reduced group among chondritic meteorites. Because of the reduced condition, enstatite chondrites sometimes contain daubreelites ($FeCr_2S_4$). Until now many researchers have studied daubreelites of enstatite chondrites [1,2]. But it has not been studied about the chemical zonings of daubreelites next to minerals, because of small size of grains. In this study, we have measured the zoning profiles of daubreelites next to various kinds of minerals and considered about the formation process of daubreelites in enstatite chondrites.

Results and discussion: We measured daubreelites in ALH77295, Y74370, Qingzhen (EH3), St. Marks (EH4) and MAC88180 (EL3).

1) daubreelite-troilite (ALH 77295, Qingzhen, Y 74370, St. Marks, MAC 88180). The chemical zonings from daubreelites to troilites show Cr and S decreasing and Fe increasing (In Y74370, some daubreelites show same chemical zonings, others do not show zoning). This is indicative of Fe diffusion from troilite into daubreelite and Cr and S diffusion from daubreelite into troilite. These zonings are in agreement with the reverse zoning from ningerite to troilite [3], zoning of sphalerite and young $^{39}Ar/^{40}Ar$ age (2.88 b.y.) [4]. These facts are strong evidence for planetary endogmatic process in both EL and EH. The reverse zoning of daubreelites may have resulted from thermal, probably planetary metamorphic episodes.

2) daubreelite-metal (Qinzhen, Y 74370). The chemical zoning from daubreelite to metal shows the same trend as those from daubreelite to troilite in Qingzhen. Fe is increasing (Fe: 12.66-14.70, 12.34-18.71 wt%) and Cr and S are decreasing (Cr: 35.24-34.70, 35.39-32.08, S: 43.46-43.14, 42.14-38.53 wt%). On the other hand, Y74370 daubreelites do not show chemical zonings to metal. El Goresy et al., classified one subgroup of EH as follows; Y74370, South Oman, Qingzhen, Kota Kota, Kiadun III, and St. Marks [2]. In this subgroup the meteorites follow an equilibration and evolution sequence; Y74370 the most primitive and St. Marks the most equilibrated. The different zoning profile between Y74370 and Qingzhen may suggest the different thermal history. This result is in agreement with daubreelite grains which do not show chemical zoning next to troilite in Y74370. But further study needs to explain about the different behavior among daubreelite-troilite, daubreelite-metal and daubreelite-silicate in Y74370.

3) daubreelite-hydrated Cr-sulfide (Qingzhen, ALH 77295). In Qingzhen, Cr, Fe, Zn contents are increasing towards hydrated-Cr sulfide (Cr: 34.1-35.3, 33.5-34.1, 34.2-34.4; Fe: 12.2-12.7, 12.5-12.5, 12.4-12.5; Zn: 7.82-8.03, 8.14-8.50, 8.62-8.70), while S contents are decreasing (S: 43.6-43.5, 44.9-44.5, 45.5-45.4 wt%). But in another grain, Fe content is increasing (Fe: 12.57-12.94 wt%) and Cr and S content are decreasing (Cr: 35.91-35.30, S: 43.83-44.22 wt%). In ALH77295, Fe is increasing (Fe: 14.15-14.47) and Cr and S are decreasing (Cr: 35.84-35.52, S: 43.88-43.76). The chemical zoning from daubreelite to hydrated Cr-sulfide is controversial probably because of heterogeneity of the reaction between Cr-sulfide and water.

4) daubreelite-sphalerite (ALH 77295). We found an evidence for diffusion of Zn from sphalerite to the coexisting daubreelite in ALH77295. Microprobe Zn-profiles in daubreelites display positive concentration slopes to the neighboring sphalerites. In addition, daubreelites coexisting with sphalerites in ALH 77295 show higher Zn contents than daubreelites in sphalerite-free assemblages.

5) daubreelite-silicate (Y 74370, St. Marks, MAC 88180). Cr and S are decreasing towards rim next to silicates. But Fe's behavior depends on each grain. It may have resulted from different kinds of silicate next to daubreelite grains.

6) daubreelite-alabandite (MAC 88180) Daubreelite next to alabandite shows Mn increasing and Fe, Cr, S decreasing. It has also resulted form thermal event like daubreelite-troilite.

References: [1] Keil K. (1968) *JGR, 73,* 6945–6976. [2] El Goresy A. et al. (1988) *Proc. NIPR Symp. Antarct. Meteorites, 1,* 65–101. [3] Ehlers K. and El Goresy A. (1988) *GCA, 52,* 877–887. [4] Müller N and Jessberger E. (1985) *LPSC XVI,* 595–596.

NOBLE GASES IN THE ANTARCTIC R-CHONDRITES MOUNT PRESTRUD 95410/411/412. H. W. Weber and L. Schultz, Max-Planck-Institut für Chemie, Abteilung Kosmochemie, D-55020 Mainz, Germany (schultz@mpch-mainz.mpg.de).

Rumuruti-chondrites (R-chondrites) have basically a chondritic chemical composition and form in a three-isotope plot of oxygen a distinct group with high $\Delta^{17}O$ values. They are characterized by a high modal abundance of olivine (70 ± 8 wt.%) and a low abundance of metallic FeNi [1]. With the exception of Rumuruti all R-chondrites are finds. We report here noble gas data of 3 specimens of the new R-chondrite Mount Prestrud (Table 1) which have been recovered recently from Antarctica. It was suggested that these three meteorites belong to one fall [2], a result that is corroborated by the gas analyses.

	PRE 95410	PRE 95411	PRE 95412
^{4}He	977000	1352000	1332000
	1061000	1622000	1644000
^{4}He/^{3}He	3268	3423	3364
	3205	3331	3439
^{20}Ne	8660	4437	9051
	9136	6443	10680
^{20}Ne/^{22}Ne	12.42	11.47	12.38
	12.38	11.76	12.35
^{22}Ne/^{21}Ne	26.70	23.60	26.97
	25.45	23.72	27.72
^{40}Ar	6763	5223	6235
	5822	5900	6321
^{40}Ar/^{36}Ar	24.86	28.39	22.69
	20.76	23.89	19.24
^{36}Ar/^{38}Ar	5.161	5.047	5.156
	5.154	5.074	5.126

Table 1. Noble gas concentrations (in 10^{-8} cm^3 STP/g) and selected isotopic compositions of Mt. Prestrud R-chondrites.

The noble gases of Mt. Prestrud are dominated by high concentrations of trapped solar gases. About 50% of R-chondrites are regolith breccias with solar gases [3], a high percentage compared to other meteorite groups (e.g. Aubrites: ~25%; H-chondrites: ~14%). Individual samples of Mt. Prestrud have different contributions of solar wind and solar energetic particles in their noble gas mixture.

The calculation of an exposure age is difficult because the cosmogenic component is masked by the large solar contributions. Assuming average shielding conditions an exposure age of (20 ± 5) Ma is calculated. Cosmic ray exposure ages of all R-chondrites range from 2.6 to 36 Ma. Similar ages are observed for most members of other chondrite groups.

The $^{84}Kr/^{132}Xe$ ratio in chondrites is a sensitive indicator of adsorbed atmospheric noble gases which are incorporated during weathering processes [4]. All Mt. Prestrud samples have $^{84}Kr/^{132}Xe$ values between 2.1 and 4.0 which could indicate the incorporation of atmospheric Kr and Xe (the least weathered fall Rumuruti has $^{84}Kr/^{132}Xe$=0.97; the air value is 27.8). Characteristic for all R-chondrites measured so far are variable and high $^{129}Xe/^{132}Xe$ ratios (up to 3.5 [3]). The Mt. Prestrud samples have values between 1.5 and 4.2.

Acknowledgments: We thank the Meteorite Working Group for providing samples as well as the National Science Foundation for supporting the ANSMET team.

References: [1] Kallemeyn G. W. et al. (1996) *GCA, 60*, 2243–2256. [2] Antarctic Meteorite Newsletter 20(2), 1997. [3]. Weber H. W. and Schultz L. (1993) *LPSC XXIX*, 1122–1123 (1998) [4] Scherer P. et al. (1994) in: *Noble Gas Geochem. Cosmochem.* (ed. J. Matsuda), 43–53.

SHOCK-INDUCED TRANSFORMATIONS IN AN EH3 CHONDRITE. M. Bourot-Denise and C. Perron, Laboratoire de Minéralogie, CNRS-ESA 7058, Muséum National d'Histoire Naturelle, 75005 Paris.

Sahara 97096 is an EH3 chondrite, found in 1997. It has been described recently [1], and our observations essentially agree with these. It can be classified among the most primitive enstatite chondrites, comparable to Qingzhen and Parsa. It contains olivine chondrules and type II chondrule fragments, with up to 22 wt% FeO in the pyroxene. Indications of shock effects have been noted [1]. Indeed, in one of the many fragments collected (Sahara 97158), we found an inclusion which shows strong and peculiar effects of shock heating. It is described here.

The roughly rectangular inclusion (Fig. 1) measures 8×5 mm^2 on our polished section, but it is cut by the edge of the section on 2 sides and the size of the complete inclusion is not known. It looks black, and has an overall silicate texture similar to the host chondrite, in particular it has abundant chondrules and chondrule fragments. However, the silicate composition, which is highly variable as in the host, appears to be on average more FeO-rich than the host. This is clear on BSE images. In addition, most measurements give FeO>1% (it is mainly <1% in the host) and values as high as 32% FeO have been obtained. The inclusion is entirely devoid of Fe-Ni metal. Rare large opaque nodules are made of sulfides only (mostly troilite and niningerite), while comparable nodules are abundant in the host and always comprise some metal. A multitude of tiny sulfide blebs indicates that a sulfide melt has been injected in almost every crack and interstice between silicate grains.

The inclusion is limited on one side by a 1.5 mm-wide, metal-rich band (M in Fig. 1), in which kamacite makes a nearly continuous network between silicate grains, chondrules and metal-sulfide nodules. This metal network appears dusty, with plenty of small silicate grains embedded in it. Perpendicularly to this feature, the only transition between the inclusion and the host is a thin vein of oldhamite (O in Fig. 1).

A wide vein (V in Fig. 1), about 140µm wide runs into the inclusion nearly perpendicularly to the metal-rich band. It is filled with various sulfides, including troilite, daubréelite, niningerite, sphalerite. Oldhamite fills the narrow end of the vein. Sulfide grains much larger than the tiny blebs already mentioned, appear to fill spaces in a 3.4×1.7 mm^2 porous region of the inclusion (S in Fig. 1), starting from the metal-rich band. Chondrules are rare in this region. Pockets of troilite, a few hundred µm across, with euhedral enstatite laths are dispersed in the inclusion.

Beyond this metal rich-band, the EH3 material appears undisturbed, except for a narrow vein nearly parallel to the band, filled with a metal-troilite intergrowth typical of shocked chondrites.

These observations are evidence that a shock-induced heating event caused localized percolation of the silicates by a metal-sulfide melt. The metal settled at the edge of the inclusion, while sulfides filled available spaces. We do not believe that oxidation of the silicates occurred *in-situ*, because kamacite in the metal-rich band has the same composition as in the host (~2.4% Si), and the enstatite laths in troilite pockets, which obviously crystallized from a melt, are low in FeO. Rather at least some material of the inclusion must have been brought by the shock event from a more oxidized region of the parent-body (the surface?).

References: [1] Weisberg M. K. and Prinz M. (1998) *LPS XXIX*, abstract #1741.

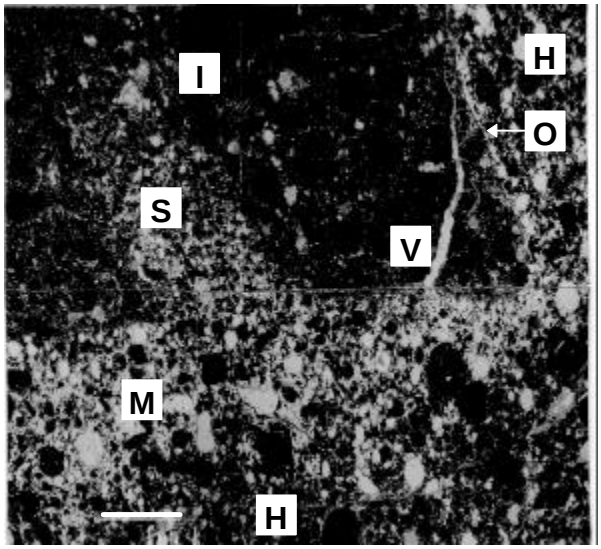

Fig. 1. Partial view of the inclusion (BSE image). H EH3 host; I inclusion; M metal-rich band; O oldhamite vein; V sulfide vein; S sulfide-rich region. Scale bar 1 mm.

PGA AND INAA STUDIES OF A NEW REDUCED L CHONDRITE. G. W. Kallemeyn, M. Ebihara and S. Latif, Department of Chemistry, Graduate School of Science, Tokyo Metropolitan University, 1-1 Minami-Ohsawa, Hachioji, Tokyo 192-0397 Japan. gregk@comp.metro-u.ac.jp

Introduction: Prompt-gamma analysis (PGA) and instrumental neutron activation analysis (INAA) have been performed on a recent find from Antartica: Queen Alexandra Range 94570. This meteorite was originally chosen for analysis because it was reportedly a new member of the Coolidge-Loongana001 grouplet. due to its low olivine Fa composition (Fa_{10-13}). Our analyses show that QUE94570 is not, in fact, a new member of this grouplet, but instead a new reduced-type L chondrite similar to Moorabie and Suwahib Buwah.

Analyses: Replicate samples of QUE94570 were run by PGA, along with samples of Coolidge and Loongana001 previously analyzed by INAA. PGA analyses were performed using a cold neutron beam for better sensitivity over traditional thermal neutron PGA. Elements of interest included B, Si and S. Later, the QUE94750 samples were also studied by INAA for some 27 additional elements.

Results: The compositional data clearly show that QUE94570 is not related to Coolidge and Loongana001. The latter two chondrites have highly enriched refractory lithophile element abundances relative to CI, whereas QUE94570 has abundances similar to ordinary chondrites (~0.9xCI). QUE94570 also has much higher Na and K abundances than Coolidge and Loongana, also more typical of ordinary chondrites. The abundance pattern for QUE94570 is quite similar to L chondrites, except for a depletion in common siderophiles (Ni, Fe, Co), which is likely the result of weathering. QUE94570 plots with the ordinary chondrites on a diagram of Zn/Mn vs Al/Mn (see Fig. 1). The abundances of B and S in QUE94570 from the PGA analyses are distinctly different from those in Coolidge and Loongana001. The latter two chondrites have very low S concentrations (3-4 mg/g) compared to QUE94570 (~29 mg/g), but have higher B concentrations (0.7-0.9 µg/g) than QUE94570 (~0.4 µg/g). The B and S concentrations in QUE94570 fall in the ranges of L chondrites.

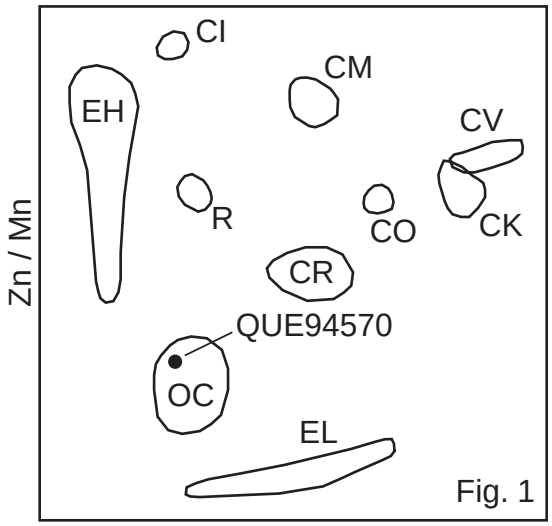

Fig. 1

Conclusion: Compositionally, QUE94570 appears to be an L chondrite that has lost some metal due to weathering. Because of this weathering effect, one cannot rule out the possibility that it is an LL chondrite, but other siderophile/chalcophile elements (Au, As, Zn) better support an L classification. It's very low olivine Fa value is not typical of normal L chondrites, but overlaps the ranges of reduced-type L chondrites such as Moorabie and Suwahib Buwah. Therefore, QUE94570 is likely a new member of this reduced L chondrite grouplet.

OXYGEN ISOTOPE EXCHANGE IN UNEQUILIBRATED ORDINARY CHONDRITES. J. C. Bridges[1], I. A. Franchi[2], A. S. Sexton[2], and C. T. Pillinger[2], [1]Department of Mineralogy, Natural History Museum, London SW7 5BD, UK, [2]Planetary Sciences Research Institute, Open University, Milton Keynes MK7 6AA, UK.

Introduction: Recent work has demonstrated that the most important control on the oxygen isotopic composition of UOC chondrules and clasts is their mineralogy. Feldspar/glass has preferentially exchanged with ^{16}O-poor gases whereas olivine/pyroxene has preserved more primitive isotopic compositions [1,2]. SiO_2-rich glass in chondrules has also exchanged more readily than crystalline feldspar [2]. Here we report isotopic analyses of mineral separations from whole meteorites - Parnallee (LL3.6), Dhajala (H3.8), Bremervörde (H3.9), Adrar 003 (L/LL3.2), Bovedy (L3) - to provide further constraints on the processes of isotopic exchange. Methods described in [1,2].

Results: All of the whole rock meteorites show that feldspar/glass has more ^{16}O-poor compositions than olivine/pyroxene. Ardrar 003 shows the greatest difference (8 ‰) in δ^{18}O values between feldspar/glass and olivine/pyroxene. The differences for Parnallee, Dhajala, Bremervörde and Bovedy are 4.3‰, 3.5‰, 2.8‰ and 2.5‰. A previous analysis of separates from Bremervörde chondrules [1] used very small sample sizes (< 0.2 mg), so we regard the results here as more reliable. The Ardar 003 feldspar/glass (δ^{17}O 9.5, δ^{18}O 13.1) is slightly more ^{16}O-poor than cristobalite-rich clasts [4]. Best fit lines for 3-isotope plots have been calculated for H, L, LL-group chondrules, separates and whole meteorite falls using data from [2,3]. These have slopes 0.68, 0.78, 0.77. Ardrar 003 and Bremervörde isotopic compositions are plotted on the figure.

Discussion: The purity of the mineral separates is similar for each of the meteorites so the large difference in isotopic compositions between feldspar/glass and olivine/pyroxene in Adrar 003 compared to the other meteorites may reflect its more highly unequilibrated state. The meteorites of highest petrographic subtype such as Bovedy, with the smallest difference in δ^{18}O values, may either be showing some isotopic equilibration or a low content of glass [2] in chondrule mesostases. The OC groups each have distinct mixing lines on isotope plots, which is consistent with their having exchanged with separate ^{16}O-poor gas reservoirs. These reservoirs may have formed by processes of chemical fractionation [5] in, as we suggest [1,2], parent bodies. However, the lack of slope 1.0 mixing lines (associated with non mass-dependent fractionation) suggests the ^{16}O-poor gases were mixed with an δ^{18}O-rich component prior to the chondrule-gas isotopic exchange. We believe low temperature, hydrous alteration of UOCs by high δ^{18}O fluids [3] is not a sufficient explanation for the absence of slope 1.0 mixing lines. If that where the case it would mean that ^{16}O-poor chondrules had undergone more extensive alteration than other chondrules - for which there is no supporting evidence.

References: [1] Bridges J. C. et al. (1998) *LPS XXIX*, 1401–1402. [2] Bridges J. C. et al. (1998) *EPSL, 155*, 183–196. [3] Clayton R. N. et al. (1991) *GCA, 55*, 2317–2338. [4] Bridges J. C. et al. (1995) *Meteoritics, 30*, 715–727. [5] Thiemens M. H. (1996) *Chondrules and the Protoplanetary disc*, (Hewins R. H. et al., eds.) Cambridge, 107–118.

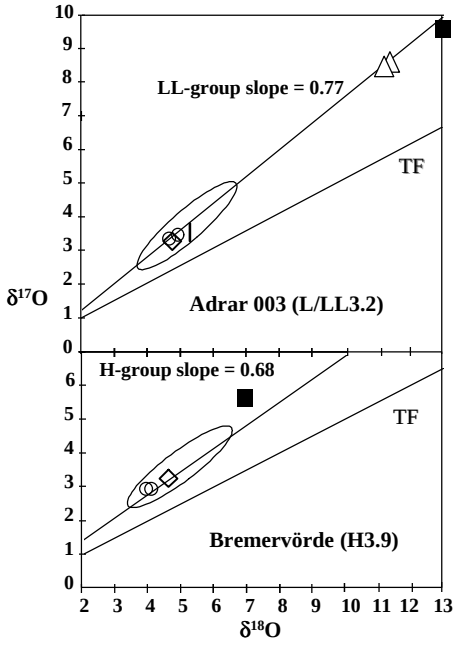

Fig. 1. Oxygen isotopic compositions of mineral separates from Adrar 003 and Bremervörde whole meteorites. Squares feldspar/glass, diamond bulk meteorite, circle olivine/pyroxene, triangles cristobalite-rich clasts from Parnallee [4]. Data for H,LL-group fields and best-fit lines from [2,3].

CHARACTERIZATION OF THE RUMURUTI CHONDRITE REGOLITH BRECCIA HUGHES 030 (R3-6) AND IMPLICATIONS FOR THE OCCURRENCE OF UNEQUILIBRATED LITHOLOGIES ON THE R-CHONDRITE PARENT BODY. A. Bischoff[1], D. Weber[1], R. Bartoschewitz[2], R. N. Clayton[3], T. K. Mayeda[3], L. Schultz[4], B. Spettel[4], and H. W. Weber[4]; [1]Institut für Planetologie, Wilhelm-Klemm-Str. 10, D-48149 Münster, Germany (bischoa@nwz.uni-muenster.de), [2]Meteorite Laboratory, Lehmweg 53, D-38518 Gifhorn, Germany; [3]Enrico Fermi Institute, University of Chicago, Chicago IL 60637, USA, [4]Max-Planck-Institut für Chemie, Saarstrasse 23, D-55122 Mainz, Germany.

Introduction: The Rumuruti (R) chondrite group has a new member: Hughes 030. This meteorite was recently recognized and classified as a Rumuruti chondrite regolith breccia [1] due to the brecciated texture of the rock and the contents of solar wind implanted noble gases.

Mineralogy: The olivine-rich rock consists of a variety of lithic clasts embedded in a fine-grained matrix. In this respect, Hughes 030 is very similar to Dar al Gani 013 [2]. Within equilibrated clasts olivine shows the typical R-chondritic composition ($Fa_{38–41}$). Chemically, olivine in the host matrix is very similar (Fig. 1; avg.: 40.6 mol% Fa; 0.16 wt% NiO). Two different types of unequilibrated lithologies occur as fragments in Hughes 030. One type of fragment has a chondritic texture consisting of various types of chondrules embedded in an olivine-rich matrix. The composition of olivine in chondrules varies from Fa_0 to Fa_{40}, whereas the matrix olivines (~$Fa_{43–48}$; avg. 45.5 mol%) are significantly richer in Fe than those in the host matrix (Fig. 1; fragment #1). The second type of unequilibrated clast consists of several low-Ca pyroxene fragments ($Fs_{5–25}$) and some zoned olivine grains embedded in Fa-rich matrix olivines (~$Fa_{54–60}$; avg. 56.0 mol%; Fig. 1 (#2)). This is the highest Fa-content for olivine in lithologies of R-chondrites reported so far. Previously, Jäckel et al. [2] also found that in some type 3 clasts from Dar al Gani 013 matrix olivines occur having higher Fa-contents (40–50 mol%) than typically found in other R-chondrites and in the matrix of equilibrated clasts.

Oxygen isotopes: Hughes 030 has an oxygen isotope composition ($ë^{18}O$ = 7.47; $ë^{17}O$ = 6.15) that is consistent with a R-chondrite classification. Both delta-values are somewhat higher than in other R-chondrites, which can be explained by weathering processes in the desert.

Chemistry: The chemical composition has been affected by weathering processes as indicated by significant enrichments in Ca (3.4 wt%), Br (5.94 ppm), and Ba (179 ppm) and severe loss of Co (254 ppm) and Ni (2700 ppm). The concentrations of most elements (e.g., Sc, Cr, Zn, As, Se, REE) are very similar to those in Rumuruti [3]. The Fe-concentration (23.0 wt%) in Hughes 030 is somewhat lower than in Rumuruti, which might also be affected by weathering (alteration of sulfides, Ni-loss).

Noble Gases: The ^{4}He-concentration in Hughes 030 is 9610 ($\times 10^{-8}$ cm^3STP/g) and a $^{20}Ne/^{22}Ne$ ratio of 5.24 was determined indicating the presence of significant concentrations of solar gases. The rock has the highest exposure age among all Rumuruti-chondrites (49 ñ 8 Ma).

Summary: Hughes 030 is a new member of the R-chondrite group. Based on the mineralogy of type 3 lithologies within this meteorite and within Dar al Gani 013 it is concluded, that primitive unbrecciated R-chondrites, which still have to be found, should have high Fa-contents in matrix olivines (>>40 mol%).

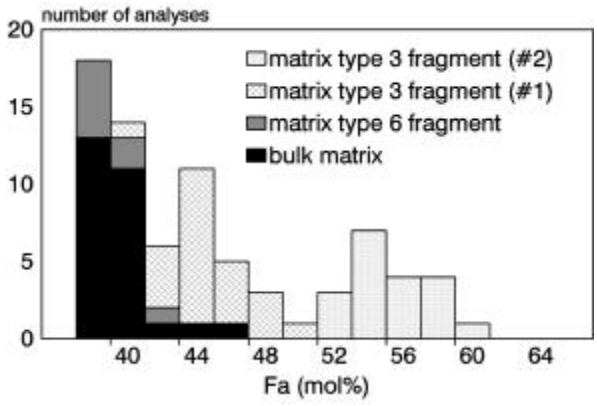

Fig. 1. Composition of matrix olivines in equilibrated fragments, the host meteorite, and two types of unequilibrated lithologies.

References: [1] Grossman J. N. (1998) *Meteoritics and Planet. Sci.*, this volume. [2] Jäckel A. et al. (1996) *LPS XXVII*, 595–596; [3] Schulze H. et al. (1994) *Meteoritics*, *29*, 275–286.

COSMOGENIC RECORDS IN THE DIDWANA-RAJOD METEORITE. [1]B. S. Paliwal[1], V. K.Vaya[1], A. D. Shukla[2], S. Chakraborty[2], K. M. Suthar[2], M. H. Dixit[2], P. N. Shukla[2], and N. Bhandari, [2]Department of Geology, J. N. V.University, Jodhpur 342 005 (bhandari@prl.ernet.in), [2]Physical Research Laboratory, Navrangpura, Ahmedabad 380 009, India.

A single fragment, weighing about 1 kg fell at Rajod, near Didwana in Western Rajasthan on 12th August, 1991 at about 10 p.m. IST. Mineralogical and petrological studies [1] indicate that the meteorite consists of enstatite, iron metal and troilite with abundant chondrules (0.1 to 5 mm), mostly with sharp boundaries. Chondrule fabric is highly varied showing exocentric, bar, swirling, radiating, porphyritic and ringed structures. A few highly turbid/glassy chondrules are also present. Metamorphic degradation in chondrules is generally low and occasionally moderate. Metallic phase is 24% (6% sulfide). Trace amounts of plagioclase and trydimite is seen.

Chemical analysis using ICPAES and AAS gives concentration of Fe (31.77%), Mg (14.08%), Al (1.05%), Ca (1.12%), K(0.086%) and Na (0.68%). Measurements of other major and trace elements are in progress now. Based on the presence of Orthoenstatite and the mg# (0.5), the chondrite can be classified as belonging to EH group.

We have also measured cosmogenic effects i.e. cosmic ray tracks and radionuclides in this meteorite. Tracks were measured in enstatites and olivines using standard techniques [2]. The track density varies in a narrow range around $6.7 \times 10^5/cm^2$ in a few spot samples taken from the surface of this meteorite, indicating nearly uniform ablation all around. The activity of cosmogenic radionuclides ^{22}Na and ^{26}Al are estimated, by whole rock gamma ray spectrometry[2], to be 64 ± 5 and 66 ± 5 dpm/kg respectively. Near absence of ^{60}Co indicates low thermal neutron exposure, suggesting that the meteoroid was a small body in space.

References: [1] Paliwal B. S. et al. (1997) *Current Science, 73,* 499–502. [2] Bhandari N. et al. (1998) *Meteoritics and Planet. Sci., 33,* in press.

FURTHER STUDIES OF ANTARCTIC R CHONDRITES. G. W. Kallemeyn, Department of Chemistry, Graduate School of Science, Tokyo Metropolitan University, 1-1 Minami-Ohsawa, Hachioji, Tokyo 192-0397 Japan (gregk@comp.metro-u.ac.jp).

Introduction: The R chondrite group is a noncarbonaceous chondrite group with members characterized by high states of oxiDation and $\Delta^{17}O$ values higher than any other chondrites. More than half of the known R chondrites have been found in Antarctica. Recently, three new R chondrites were discovered during the 1995-96 hunting season in Antarctica: Mt. Prestrud 95410, 95411 and 95412. They were tentatively paired as one fall. Another chondrite found during the same collection period, Mt. Prestrud 95404, was originally classified as a CV3 chondrite, but oxygen isotope data by Clayton and coworkers suggested that it was also an R chondrite. Samples of PRE95404 and PRE95411 are currently being analyzed by instrumental neutron activation (INAA). Preliminary results appear to show that both have typical R chondrite compositions and are likely paired.

Analyses: Interior chips of each chondrite (~500 mg) were gently crushed to smaller pieces and divided into two separate samples for analysis. One set has been analyzed for 27 elements by INAA, while the other is still to be run. Further analysis of the samples by prompt-gamma methods is also planned.

Results: The initial splits PRE95404 and PRE95411 have remarkably similar compositions for bulk and trace elements. Only the Au concentrations for the two samples differ by more than 5% relative. Because of this similarity, further discussion of mean PRE95411 will refer to the combined mean composition of both meteorites. The Mg-normalized lithophiles of mean PRE95411 range from ~0.9–1.0 × CI. Abundances of refractory and common siderophiles are also near CI levels. These are values typical of other R chondrites. Also, as with other R chondrites, the abundances of Se and Zn are consideraby higher than those in ordinary chondrites. The Au abundances in PRE95404 and PRE95411 are quite variable and depleted relative to the Rumuruti fall. This is typical of most of the other Antarctic R finds, and probably represents electrochemical redistribution aided by water from melting ice.

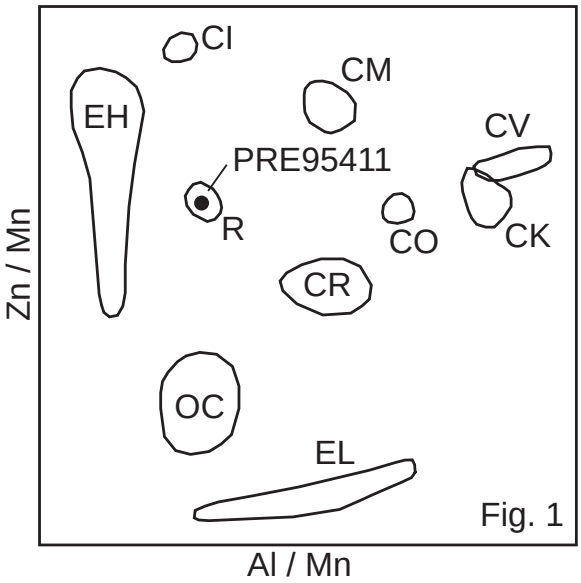

Fig. 1

Conclusion: Both PRE95404 and PRE95411 fall in the compositional range of the R chondrites, and they are undoubtedly R chondrites. This is clearly seen for mean PRE95411 in a plot of Zn/Mn vs Al/Mn (see Fig. 1). The remarkably similar compositions of the two chondrites, along with the close proximities of their finds suggests they are paired with each other, and therefore also likely paired with PRE95410 and PRE95412.

PETROLOGY AND GEOCHEMISTRY OF LARGE METAIGNEOUS INCLUSIONS FROM L CHONDRITES. D. W. Mittlefehldt[1] and M. M. Lindstrom[2], [1]Lockheed Martin SMSS, 2400 NASA Road 1, Houston TX 77058, USA (david.w.mittlefehldt1@jsc.nasa.gov), [2]NASA Johnson Space Center, Houston TX 77058, USA (marilyn.m.lindstrom1@jsc.nasa.gov).

Introduction: Ordinary chondrites often contain inclusions of igneous-textured material. Some of them are impact melts of the chondrite parent body [1], but some are foreign materials with distinct textures, O-isotopic, and bulk compositions [e.g. 2-4]. Approximately 30% of large inclusions in ordinary chondrites are of "planetary" or uncertain origin [5]. We began a survey of large antarctic L6 chondrites in an effort to locate these interesting materials for petrologic and geochemical study.

Petrology: The ten inclusions are roughly cm-sized and generally rounded in shape; some appear spherical. In most cases, the gross textures are like those of droplet chondrules; barred olivine (BO) and porphyritic olivine pyroxene (POP) textures dominate. One granular, meta-POP clast contains a small relict BO chondrule. The clast matrixes are granular and the margins are partially intergrown with the host, indicating that the inclusions were metamorphosed along with the host chondrite. Mafic mineral compositions are essentially those of equilibrated L chondrites; olivine - $Fa_{24.3\text{-}25.0}$, low-Ca pyroxene - $Wo_{1.4}En_{77.3\text{-}78.4}Fs_{20.2\text{-}21.3}$, high-Ca pyroxene - $Wo_{45.2\text{-}46.0}En_{46.7\text{-}47.0}Fs_{7.2\text{-}7.8}$.

Geochemistry: Splits of the inclusions free of host chondrite were analyzed by INAA. Eight inclusions have Na/Sc ratios and nine have Hf/Sc ratios identical to ordinary chondrite chondrules, but none of them have chondritic Sm/Sc ratios. Most of the inclusions have L chondrite-normalized Sm/Sc of 0.2-0.6. Most inclusions have REE patterns with slight LREE-depletions and positive Eu anomalies. Because splits of the inclusions were analyzed, sample heterogeneity problems are a worry. Specifically, we avoided the margins with the host chondrite when sampling. If phosphates were preferentially at the inclusion margins, we would have under-sampled them. We have identified phosphates, the likely major host for Sm, in the interiors of three of the inclusions so far. These have REE patterns like those of the majority of the inclusions, suggesting under-sampling of phosphates is not controlling the Sm/Sc ratio. One sample (POP texture) has an unusually high Sm/Sc ratio and a REE pattern expected of chondritic phosphates, suggesting its REE budget is controlled by phosphates.

The siderophile element distributions are also distinct from those of ordinary chondrite chondrules. Chondrules show wide ranges in Ir/Co ratios (factor of ~20), but narrower ranges in Ni/Co and Au/Co (factor of ~5 for each). This is taken as evidence for a refractory siderophile element component heterogeneously distributed among chondrules [6]. The inclusions also show a wide range in Ir/Co (factor of ~60) and a narrow range in Ni/Co (factor of ~2). The Au/Co ratio, however, roughly correlates with the Ir/Co ratio. This suggests that the siderophile elements in the inclusions are in two components, a noble metal component containing most of the Ir and Au, and a transition metal component containing most of the Co and Ni. This does not appear to be a result of antarctic weathering redistributing the more easily oxidizable siderophile elements, as inclusions with essentially identical and low Co and Ni contents have widely different Ir and Au contents.

Discussion: Macrochondrules are the most common type of large inclusion in ordinary chondrites [5]. Because our inclusions are rounded to spherical, have chondrule-like textures and L chondrite mineral compositions, the first order question is; Are they simply chondrules with pituitary malfunctions? The answer appears to be—Maybe. The compositional characteristics of these inclusions (non-chondritic Sm/Sc, different Ir-Au distribution) argue that they are not overly large chondrules. However, if the phosphates are concentrated along the inclusion margins, we would have systematically under sampled them, explaining the Sm/Sc ratios. This would not explain the siderophile evidence. A study of a large number of igneous inclusions in L chondrites has shown that most of them are impact melts of the L chondrite parent body [1]. This is a possible scenario for the formation of many of the inclusions studied here. However, the fractionated Sm/Sc ratios would imply that either the inclusions are not bulk melts of L chondrites, or that sample heterogeneity is a problem. At present, we do not think any of the inclusions are unusual "planetary" type materials. Continued petrologic and geochemical study of these inclusions will be geared to sorting out these issues.

References: [1] Rubin et al. (1983) *Meteoritics, 18,* 179. [2] Hutchison et al. (1988) *EPSL, 90,* 105. [3] Sack et al. (1994) *JGR, 99,* 26029. [4] Mittlefehldt et al. (1995) *Proc. NIPR Symp. Ant. Met., 8,* 251. [5] Bridges & Hutchison (1997) *MAPS 32,* 389. [6] Grossman & Wasson (1982) *GCA 46,* 1081.

NEW OBSERVATIONS OF THE PROPERTIES OF THE LUMPARN IMPACT STRUCTURE, ÅLAND ISLANDS, SW. FINLAND. A. Abels[1], P. Mannola[2], M. Lehtinen[3], L. Bergman[4], and L. J. Pesonen[5], [1]Institut und Planetologie, Universität Münster, D-48149 Münster, Germany (abels@uni-muenster.de), [2]Outokumpu Mining Oy, FIN-02201 Espoo, Finland, [3]Finnish Museum for National History, University of Helsinki, FIN-00014 Helsinki, [4]Geological-Mineralogical Institute, Åbo Akademi, FIN-20500 Turku, Finland; [5]Laboratory for Paleomagnetism, Geological Survery of Finland, FIN-02151 Espoo, Finland.

The Lumparn impact structure [1, 2] represents an almost land-locked bay situated in the Åland main island, SW-Finland (center co-ordinates: 60°08,7'N, 20°07,8'E). The approximately 100 km^2 large bay is roughly rhomb-shaped and contains only few small islands in its periphery, thus representing an unusual feature in the archipelago of SW-Finland.

The target rock is a porphyritic to coarse-grained Rapakivi granite, around 1.57 Ga in age [3,4]. In the NE-part of the bay a limestone shoal exists, a tiny part of which crops out at low water. Drilling revealed that the limestone is at least 40 m thick and that it overlies a breccia, which appears to occupy most of the sea-bottom over the whole bay [5,6]. The breccia unit consists solely of crushed Rapakivi granite and it is in places over 50 m thick, but drilling did not reach the basement [1,6]. The brecciated material shows decorated PDFs and mosaicism in quartz, kink bands in biotite, granularism in zircon, mosaicism in feldspar and zircon, planar fracturing in feldspar, as well as glassy fragments with fluidal textures [2,6]. We tend to view the succession as autochthonous, but the rather alternating clast size distribution points to a more complex development, possibly including re-deposition

Macroscopic hints for impact are visible on the shores in form of conically striated surfaces as well as several breccia patches and dykes. Furthermore, some star-like fracture sets (0.3–0.9 m in diameter), centered on perpendicular situated faults, were observed. As this fracture type is not known from anywhere else in the region it may be impact-originated.

The diameter of the structure is not well defined. Seismic and bathymetric data suggest canyons and ridges, which can be interpreted as forming a 7 km large, rounded structure in the center of the basin [5]. Despite the apparent size, however, no central uplift is visible in these data. This could be due to post-tectonic movements, because even the outline of the bay is clearly coincident with the dominant fault directions (N-S, NW-SE) in the region [3]. In addition, the seismic profiling indicates post-impact tectonic movements which affected the above mentioned limestone [5]. In aeromagnetic maps (flight-altitude 150 m) the bay is characterized by a weakly subdued relief extending slightly beyond the shore lines.

The minimum age of the impact (~450 Ma) is given by the lower part of the limestone shoal, which has been dated to the higher part of the Lower Ordovician [7]. Lower Cambrian acritarchs, found in the topmost fine-sandy part of the breccia [7], may not be positioned *in-situ*. As no Jotnian rocks was encountered in the drillings, the impact event postdates ~1250 Ma. Preliminary paleomagnetic results hint to an impact in the late Vendian (~580 Ma). If these age relationships are correct, Lumparn would be the ninth confirmed impact structure within the late Vendian and early Paleozoicum in Fennoscandia-Baltica. Although an increased meteoroid or comet flux can not be excluded, we assume that this concentration is rather an effect of early Paleozoic transgressional sediments, which protected the structures from being erased.

References: [1] Svensson N.-B. (1993) *Meteoritics* 28/3 *(Suppl.)*, 445. [2] Lehtinen M.(1994) *Luonnon Tutkija, 98*, 16–20. [3] Bergman L. (1981) *Expl. Geol. Map of Finland*, sheets 0034+0043, 1012 and 1021; Geol. Surv. Finland, 72 pp. [4] I. Laitakari et al. (1996) Geol. Surv. Finland, *Spec. Paper 21*, 59–97; [5] B. Winterhalter (1982) *Geol. Surv. Finland Bull., 317*, 115–130. [6] P. Mannola (1996) M. Sc.-Thesis, Åbo Akademi, Turku, Finland, 64 pp. [7] R. Tynni (1982) *Geol. Surv. Finland Bull., 317*, 35–94.

A GEOGRAPHIC INFORMATION SYSTEM-BASED CHARACTERIZATION OF THE SÖDERFJÄRDEN IMPACT STRUCTURE, W. FINLAND. Andreas Abels[1], Lauri J. Pesonen[2], Alexander Deutsch[1], Lutz Bischoff[3], Martti Lehtinen[4]; [1]Inst. for Planetology, Univ. Münster, D-48149 Münster, Germany <abels@uni-muenster.de>; [2]Lab. for Paleomagnetism,. Geol. Surv. Finland, FIN-02150 Espoo, Finland; [3]Geol. Inst., Univ. Münster, D-48149 Münster; [4]Finnish Museum of Nat. History, Univ. Helsinki, FIN-00014 Helsinki, Finland.

In order to reevaluate properties and formation of the Söderfjärden impact structure [1], W. Finland, we have applied the Geographic Information System (GIS) software ILWIS 2.1©. The database contains airborne electromagnetic (AEM) and magnetic (AM) data, Landsat-5-TM data, a Digital Elevation Model (DEM) as well as published results of gravity and seismic surveys [2].

The surface expression of Söderfjärden consists of a forested hilly rim that surrounds a lower agriculturally utilised plain. The structure, which has an average rim-crest-diameter of ~6.6 km [3], is situated in Paleoproterozoic granitoids. Drillings revealed a central uplift (max. 287 m high, diameter: ~1.2 km) ~30–50 m below the surface [2,4]. The uplift is surrounded by a downfaulted moat, which is filled with Cambrian sediments [4] and the whole basin is covered by ~30–75 m thick glaciogenic material [2,4]. The impact event occured probably in the Lower Cambrian [4]. The structure is associated with a negative gravity anomaly of up to –6 mGal [2].

A combined interpretation of the DEM and AM data shows, that morphological gaps in the rim are due to prominent faults, some of which are traceable for several kilometers. Selective erosion of a previously continuously elevated rim and possibly post-impact tectonic activity are reponsible for these ruptures. The fault trends are clearly coincident with the dominant fault directions in the region. The same faults, extrapolated to the interior of the crater, are also responsible for the polygonal shape of the inner crater walls, especially indicated by the outline of the AEM anomaly and the morphologically plain. An explanation is a slumping process, in which first uplifted parts of the rim slided back into the excavated crater preferently along pre-exsisting faults which acted as separation planes. This leads to rather straight bounderies of the final crater basin.

The increased electromagnetic response within the crater is mainly caused by the thick water-bearing sediment filling. In addition, several drainage channels are present at the surface. The polygonal shape of the anomaly and the relatively uniform intensity over the whole basin suggest a only minor contribution of impact-induced fracturing and brecciation. The eastern periphery of the topographic plain, covered with Quaternary material, lies beyond the outline of the AEM anomaly. There basement rocks occur probably at relatively shallow depths (<30 m). Furthermore, the crater is characterized by an overall magnetic low which is roughly congruent with the AEM anomaly. A sharply increased magnetic response with an amplitude of ~50 nT at the crater center is probably due to impact lithologies with a newly aquired magnetisation [3]. This anomaly is most distinct in the eastern part of the central uplift.

The seimic and gravity data indicate a certain asymmetry of the crater basin [2]. The eastern moat-rim-transition is considerably shallower than the western slope. A similar, but less distinct difference is visible in the magnetic data, i.e., the SW slope is relatively sharp, whereas the NE transition appears more gradual. Non-uniform slumping might be the reason. The western rim has preserved a steep slope, because no material slided back into the excavated basin, whereas in other rim sections slumping partly filled the moat up. This may explain also the missing allochthonous breccia unit in a drill core which penetrated the whole sedimentary pile in the western moat [4], although the absence of even extensive autochthonous brecciation remains a puzzling phenomenon [3].

References: [1] Lehtovaara J. J. (1992) *Tectonophysics, 216,* 157–161. [2] Laurén L. et al. (1976) *Geol. Surv. Finl. Bull., 297,* 5–38. [3] Abels A. et al. (1998) *LPS XXIC,* Abstract #1264. [4] Lehtovaara J. J. (1982) *Bull. Geol. Soc. Finl., 54,* 35–43.

COMPARISON BETWEEN CARBONATE TEXTURES IN CHICXULUB IMPACT ROCKS AND SYNTHETIC EXPERIMENTS. A. P Jones[1], S. Heuschkel[2], P. Claeys[2]
[1]Geological Sciences, University College London, WC1E 6BT, England, [2]Museum of Natural History, Humboldt-University, D-10115 Berlin, Germany

The Chicxulub impact structure on the Yucatan peninsula, Mexico, is most likely the cause for the mass extinction at the K/T boundary. Because of the Yucatan platform target rock composition—3 km thick sedimentary layer of carbonates and anhydrite, overlying a Pan African age crystalline basement—huge amounts (>1013 kg) of CO_2, H_2O vapor and sulfate aerosols were released to the atmosphere, inducing probable climate changes and subsequent mass extinction. It is thus important to clearly understand the behavior of carbonate and sulfate sediments under high pressure shock conditions. The Chicxulub impactite samples from well Yucatan 6 (N13, 1100–1103 mbsl) are very carbonate rich, both in clasts content and matrix composition [1,2]. Microscopic examination of thin sections show limestone fragments with preserved fossils, recrystallized quartz clasts and angular fragments of calcite with distinctive feathery textures; these are comprised of radiating to parallel aggregates of numerous fine-scale elongated calcite areas sometimes showing zoned or irregular extinction. Similar textures are found in synthetic experiments with carbonates over a wide range of P and T where they are diagnostic of quenched carbonate liquids (which do not quench to glass). We interpret the feathery calcite to represent quenched calcite liquid. Quench feathery calcite (QFC) is abundant and forms up to >15% of the impact breccia. We suggest that the carbonate melts formed during P-release and quenched by admixing with cold breccia before emplacement and move-out. This implies that large volumes of carbonate were melted, but not decarbonated. Only calcite melting at very shallow pressures would exsolve CO_2 since even very low pressures (>90 Atm.) prevent decarbonation. Rock-forming carbonate textures, lapilli, and chondrule-like spherules associated with silicate glass in the ejecta blanket show further evidence of the existence of carbonate melts. Minimum melting of calcite with water (~650°C), quenching of dry calcite liquid (>1310°C) and vapor deposition (?>> 1310°C) imply large temperature ranges at low pressures. If our textural interpretations are correct , then this is the first recognition of massive impact melting of carbonates; the volumes of CO_2 produced by decarbonation should consequently be re-evaluated.

References: [1] Heuschkel S. et al. (1997): *Eos, 78,* 398. [2] Claeys P. et al. (1998): *LPS XXIX*, abstract #1361.

CARBON CHEMISTRY OF SUEVITES AND TARGET ROCKS AT THE RIES CRATER, GERMANY. J. I. Abbott[1], R. M. Hough, I. Gilmour, and C. T. Pillinger, [1]Planetary Sciences Research Institute, The Open University, Walton Hall, Milton Keynes. MK7 6AA, UK (J. I. Abbott@open.ac.uk).

Introduction: The Ries Crater in Germany is a well-preserved 15 ma, 24Km diameter crater, which has been described extensively [1]. As part of a continuing study of the distribution of impact diamonds within the Ries impact structure, we have analysed samples from a number of impact litholgies in order to characterize the C content and isotopic composition of the target rocks and the suevites (polymict impact breccia) derived from them. To study the contribution of different target rock lithologies, such as sedimentary rocks or the prevariscan metamorphic basement complex, to the composition of the diamonds and SiC in suevites, samples of lithic fragments and glass were isolated from the nondemineralised suevites and core material and analysed for bulk C isotopes. In addition acid demineralised residues of crater suevites (343' to 494') from the 1973 Nordlingen drill core, contain polycrystalline diamond aggregates (aggregate size typically <100μm), silicon carbide (<10μm) and graphite (<200μm).

Results: The bulk C isotopic data and C content for the no-demineralised Ries samples is summarised in table 1. The composition of the whole rock suevites closely matches that of the sedimentary rocks, whilst the basement rocks have compositions matching graphite from the Ries (-26.0‰). The data indicates that a mixing of sedimentary carbon primarily as carbonates with basement derived graphite, results in the composition of the suevite itself. Diamonds and silicon carbide have been previously reported from suevite from the Ries crater [2, 3]. Diamonds from these suevites have a C isotopic composition ($\delta^{13}C$) of -16‰ to -17‰, similar to the isotopic composition of the bulk suevite samples presented here. Diamonds from the Ötting Quarry glass bomb have a carbon isotopic composition of -25.2‰ to -26.0‰ [4] which compares well with the bulk compositions of the glass bomb, basement samples and graphite extracted from the glass itself (-25.20‰).

Conclusions: Carbon isotopic measurements of a range of samples from the Ries crater, suggest that diamonds in the suevites are derived from either a mixture of C sources or a heterogenous single C source such as graphite [2]. In addition the basement graphite provides a suitable C source to give the lighter C isotopic compositions for diamonds found in the shock-produced glasses. From the $\delta^{13}C$ isotopic composition of the Seelbronn suevite and its constituents compared to the Ötting suevite, the source material for the Seelbronn suevite appears to have contained a heavier C source.

Table 1. Summary of C isotopic compositions and contents for Bulk Ries Crater samples.

Sample (Whole rock)	**$\delta^{13}C$**	**%C**
Ötting Suevite	-11.902	1.573
Seelbronn Suevite	-7.890	3.880
Nordlingen Core 1059	-13.987	0.121
Nordlingen Core 494	-18.229	0.130
Nordlingen Core 384	-13.941	0.430
Nordlingen Core 343	-15.387	0.406
Itzingen Quarry	-25.032	0.024
Ötting Quarry samples		
Glass (Bomb)	-28.072	0.038
Glass (Bomb)	-27.909	0.020
Glass (z=4)	-13.631	0.401
Lithic (Basement)	-20.945	0.368
Lithic (Sedimentary)	-11.847	4.067
Lithic (Sedimentary)	-11.529	1.154
Lithic (Sedimentary)	-10.445	3.505
Seelbronn Quarry Samples		
Glass	-10.625	0.722
Lithic (Basement)	-8.191	0.287
Lithic (Sedimentary)	1.950	2.490
Lithic (Sedimentary)	2.384	2.939
Lithic (Sedimentary)	-9.198	2.944

References: [1] Von Englehardt W. (1997) *Meteoritics, 32*, 545–554. [2] Hough R. M., Gilmour I., Pillinger C. T., Arden J. W., Gilkes K. W. R., Yuan J., and Milledge H. J. (1995) *Nature, 378*, 41–44. [3] Rost R. et al. (1978) *Dokladi AN SSSR, 241*, 695–698. [4] Abbott J. I. et al. (1996) *Meteoritics, 31*, A5.

POSSIBLY BACK-REACTED CARBONATES FROM IMPACT CRATERS: EVIDENCE THROUGH MAGIC ANGLE SPINNING NUCLEAR MAGNETIC RESONANCE SPECTROSCOPY. R. Skála[1] and J. Rohovec[2], [1]Department of Mineralogy, Czech Geological Survey, Geologická 6, CZ-15200 Praha 5, Czech Republic (skala@cgu.cz), [2]Department of Inorganic Chemistry, Faculty of Science, Charles University, Hlavova 2030, CZ-12843 Praha 2, Czech Republic.

Introduction: Ahrens and Gregson [1] presented Hugoniot data for calcite and calcite-rich rocks. Lange and Ahrens [2] speculated on the role of CO_2 released during impact events in early Earth's atmosphere. Boslough et al. [3], Kotra et al. [4], Lange and Ahrens [2], Martinez et al. [5] and Tyburczy and Ahrens [6] pointed out based on shock experiments that shock compression of carbonates results in degassing which starts at about 10–20 GPa. Evidence for limestone and/or dolomite decomposition in natural impacts was presented recently by study of chemistry of impact glasses from the Meteor Crater, Arizona, USA [7,8]. Love and Ahrens [9] found that in addition to partial vaporization of $CaCO_3$ the melting is induced at about 80 GPa pressure along the Hugoniot. They also did not exclude that melting of $CaCO_3$ can be achieved upon isentropic release from lower shock pressures of about 50 GPa. Miura and Okamoto [10] on the basis of experiments with limestones and marbles supposed that C is formed at the expense of calcite during the impact.

On the other hand, Martinez et al. [11], Bell [12], and Bell and Hörz [13] using common shock-recovery experiment setups showed that even under shock loads up to 60 GPa, 40 GPa, and 60 GPa respectively, carbonate-rich materials do not decompose and CO_2 is not released.

Miura [14] determined the unit cell dimensions of calcite from powder data for limestone samples from the Ries impact crater in Germany. He distinguished two types of calcite – one formed under reducing conditions of the vapor plume and the other under oxidizing conditions outside it. Unfortunately, he did not provide experimental details. Moreover, his cell dimensions are systematically lower than those published in literature [15].

Agrinier et al. [16], Deutsch et al. [17], and Martinez et al. [5] has speculated on possible role of back-reaction of carbonates. This back-reaction in carbonates is supported also by observations by Liu and Schmitt [18], who did not find any significant change in the Earth's partial CO_2 pressure at the moment of K/T impact.

During the study of the system $CaCO_3$ under elevated static pressures, high pressure metastable polymorphs $CaCO_3$ (II) and $CaCO_3$ (III) were produced and characterized [19,20]. Ahrens and Gregson [1] speculated that there are several phase transitions to these metastable $CaCO_3$ polymorphs in the region below 10 GPa during shock compression of $CaCO_3$.

Experiments on natural materials: In course of recently solved research project (Grant Agency of the Czech Republic, No. 205/95/098) focused on shock-induced phenomena in natural carbonate lithologies more than 100 samples of rock-forming carbonates (i.e. calcite- and/or dolomite-rich rocks) were studied by means of powder diffraction in detail being previously selected from a set of roughly 200 samples. These samples represented material from following impact craters on the Earth: Haughton, Kalkkop, Kamensk, Kara, Karla, Manson, Mishina Gora, Morokweng, Puchezh-Katunki, Ries, Steinheim, and Vepriaj. None of the samples studied did reveal either the presence of sometimes expected high-pressure polymorphs or traces of decomposition.

Nevertheless, several samples from fallback breccia lens or suevites not only have extremely broadened reflections in powder patterns but they appeared to be very intensively altered in thin sections. Some of them were also examined using ^{13}C MAS NMR spectroscopy. This technique has revealed up to 10-fold increase in chemical shift peaks compared to unshocked standards.

Conclusion: Extremely high broadening of chemical shift peaks in ^{13}C MAS NMR spectra of some studied materials indicating high degree of structure disorder together with finely dispersed character of calcite grains in those materials may allow us to speculate that those materials were probably decomposed during the impact event but almost instantaneously back-reacted again. Such behavior when confirmed on larger amount of samples and even experimentally could be of crucial importance with respect to currently widely accepted hypotheses of global warming due to greenhouse effect after large impacts into carbonate targets.

References: [1] Ahrens T. J. and Gregson V. G. Jr. (1964) *JGR, 69,* 4839–4874. [2] Lange M. A. and Ahrens T. J. (1986) *EPSL, 77,* 409–418. [3] Boslough M. B. et al. (1982) *EPSL, 77,* 409–418. [4] Kotra R. K. et al. (1983) *LPS XIV,* 401–402. [5] Martinez I. et al. (1994) *EPSL, 121,* 559–574. [6] Tyburczy J. A. and Ahrens T. J. (1986) *JGR, 91,* 4730–4744. [7] Hörz F.et al. (1998) *LPS XXIX.* [8] Mittlefehldt D. and Hörz F. (1998) *LPS XXIX.* [9] Love S. G. and Ahrens T. J. (1998) *LPS XXIX.* [10] Miura Y. and Okamoto M. (1997) IGCP Project 384, Excursion Guide and Abstracts, Tallinn, Estonia, 38–40. [11] Martinez I. et al. (1995) *JGR, 100, B8,* 15465–15476. [12] Bell M. S. (1997) *Meteoritics and Planet. Sci., 32,* A11. [13] Bell M. S. and Hörz F. (1998) *LPS XXIX.* [14] Miura Y. (1995) *Meteoritics, 30,* 550–551. [15] Reeder R. J. (1990) in Carbonates: Mineralogy and chemistry: *Reviews in Mineralogy, v. 11,* (R. J. Reeder, ed.), second printing, pp. 1–47. [16] Agrinier P. et al. (1998) *LPS XXIX.* [17] Deutsch A. et al. (1998) *LPS XXIX.* [18] Liu Y.-G. and Schmitt R. A. (1993) *LPS XXIV,* 883–884. [19] Biellmann C. et al. (1993) *Eur. J. Mineral., 5,* 503–510. [20] Carlson W. D. (1990) in Reeder, R. J., ed., Carbonates: Mineralogy and chemistry: *Reviews in Mineralogy, 11,* second printing, 191–225.

CAN EXPONENTIAL CREEP OF OLIVINE EXPLAIN THE FORMATION OF THE RING AROUND CHICXULUB? E. P. Turtle[1] and H. J. Melosh[2], Lunar and Planetary Laboratory, University of Arizona, Tucson AZ 85721-0092 ([1]turtle@lpl.arizona.edu, [2]jmelosh@lpl.arizona.edu).

Seismic data [1] have revealed the structure of a portion of the Chicxulub crater and the surrounding crust. These data provide strong evidence supporting the interpretation of Chicxulub as a terrestrial multi-ring basin. The seismic profiles show a flat-floored basin ~1 km deep and ~65 km in radius within which lies a peak ring 40 km in radius. Exterior to the basin at a radius of almost 100 km is a scarp 400–500 m high which appears to be the surface expression of a shallow-dipping, circumferential, normal fault that penetrates the entire crust and offsets the Moho by ~1 km [1]. These data provide the first peek at the deep structure associated with a multiring crater. Although faults are predicted by the ring tectonic theory [2] that was proposed to explain the formation of rings around large craters, neither the shallow dip (30°–40°) nor the depth observed for the fault around Chicxulub were expected. Therefore, the seismic data provide fundamental information concerning the three-dimensional nature of a multiring basin, information which is essential to performing accurate numerical simulations of crater collapse and ring formation.

We have used finite-element modeling to simulate crater collapse and to demonstrate the formation of rings according to the ring-tectonic theory [2]. This theory predicts that rings form around craters in targets consisting of two rigid layers between which lies a layer with a significantly lower effective viscosity. Our simulations of crater collapse have demonstrated that inward motion in a low-viscosity layer with either a Newtonian rheology or a low-cohesion, low-angle of internal friction plastic rheology, can generate extensional stresses sufficient to fracture the overlying rigid layer [5,6]. When we introduce faults in the upper rigid layer, substantial offset (as much as several hundred meters depending on the depth to and the thickness of the low-viscosity layer) can occur on at least one of the faults. These results are promising, but the number of unknown parameters makes it difficult to discriminate which models are the most accurate. Furthermore, aside from the fact that it is consistent with ring formation, there is little reason to expect crustal or mantle material to depart from their more rigid power-law rheologies.

The Chicxulub seismic survey provides information that can be used to assess the accuracy of simulations of crater collapse under various conditions. It may also elucidate the mechanism that accounts for the development of a low-viscosity layer. The depth of the fault observed around Chicxulub indicates that in the context of the ring-tectonic theory inward flow must have occurred within the mantle suggesting a possible explanation for this behavior: olivine has been observed to exhibit an exponential rheology when subjected to high stresses [7,8]. For stresses below 200 MPa, the strain rate of olivine follows a power-law dependence on the applied stress, but above this threshold the strain rate increases exponentially with increasing stress. In our simulations stresses of this magnitude are regularly achieved in the mantle around the collapsing transient crater. Therefore, we have incorporated the transition to an exponential rheology into our finite-element model to investigate whether it can explain the formation of the ring fault observed around Chicxulub. Current results are inconclusive, but we are undertaking a suite of simulations encompassing a broader array of parameters and we will present our conclusions at the conference.

References: [1] Morgan J. et al. (1997) *Nature, 390,* 472–476. [2] Melosh H. J. and McKinnon W. B. (1978) *GRL, 5,* 985–988. [3] Turtle E. P. and Melosh H. J. (1997) *Conf. on Large Meteorite Impacts and Planetary Evolution (Sudbury 1997),* 60. [4] Turtle and Melosh (1998) *LPSC XXIX*. [5] Goetze C. (1978) *Phil. Trans. R. Soc. Lond. A., 288,* 99–119. [6] Tsenn M. C. and Carter N. L. (1987) *Tectonophysics, 136,* 1–26.

DIRECT SYNTHESIS OF DIAMOND IN THE LABORATORY AND IN IMPACT CRATERS. P. S. DeCarli, SRI International, Menlo Park CA 94025, USA (pdecarli@unix.sri.com).

The purposes of this paper are to summarize current knowledge on direct (uncatalyzed) synthesis of diamond and on diamond graphitization, to present criteria for the recognition of impact diamond in various settings, and to present calculations of the ranges of shock conditions over which impact diamond may be formed and survive.

Laboratory studies [1,2] of shock synthesis and direct static synthesis have shown that the minimum conditions necessary for diamond formation depend on the initial crystallinity of the source carbon. Highly ordered graphite may be transformed to diamond via a quasi-martensitic mechanism at pressures above about 15 Gpa and simultaneous temperatures above 1300 K. These impact diamonds are polycrystalline, with varying degrees of preferred orientation and strain birefringence, and they often have the morphology of the parent graphite. Their X-ray patterns may show some of the reflections of Lonsdaleite. The upper pressure limit for formation and survival of impact diamond is controlled by the requirement that the post shock temperature of the diamond and surrounding material be low enough (<2000 K) to retard graphitization. Since the internal energy increase of shock compression depends on thermodynamic loading path, the necessary shock conditions will vary according to the nature of the matrix material. For graphite in a nickel iron meteorite, the peak temperature range of 1300–2000 K corresponds to peak iron pressures in the range between 60 Gpa and 120 Gpa. For graphite in a gneiss, the peak gneiss pressure should be in the range between about 27 Gpa and 40 Gpa.

Impact diamond may also be formed from porous disordered Cs. Data from numerous experiments and calculations are in accord with static results; very high shock temperatures (>3000 K) are required. The diamond must form in hot spots caused by shock interactions around pores; this diamond must be quenched before pressure release if graphitization is to be avoided. This latter form of impact diamond occurs in the form of micron-size equi-axed polycrystalline particles. In some laboratory experiments, we have also made large quantities of nanodiamonds that closely resemble Allende diamond On the basis of laboratory experiments with various cokes and Acheson graphites, one would expect that the best natural source carbons would be relatively low in H.

References: [1] Bundy F. P. and Kasper J. S. (1967) *J Chem Phys, 46,* 3437–3446. [2] DeCarli P. S. (1995) *Mat. Res. Soc. Symp. Proc., vol. 383,* 21–31.

LARGE IMPACT CRATER FORMATION: THERMAL SOFTENING AND ACOUSTIC FLUIDIZATION. B. A. Ivanov, Institute for Dynamic of Geospheres, RAS, Leininsky Prospect 38-6, Moscow, Russia 117939 GSP 1 (baivanov@glasnet.ru).

Introduction: The largest terrestrial impact craters (Chixculub, Sudbury, Wredeford) have a typical complex morphology with a prominent central uplift. The collapse of a transient cavity depends on strength properties of rocks around the crater. Two main phenomena change the normal dry friction behavior of shattered rocks: thermal softening [1, 2] and acoustic fluidization [3, 4]. We study an importance of these mechanisms with the numerical modeling of the Sudbury structure formation.

Modeling: To estimate material displacement during cratering, two simple mechanic models were applied. These are (i) the standard rock description (internal friction, Hugoniot Elastic Limit, thermal softening close to the melting point); and (ii) the modified test models with artificially decreased internal friction to simulate the possible acoustic fluidization). Details of the numerical modeling is published in [5]. The example of the final crater structure is shown on the Fig. 1.

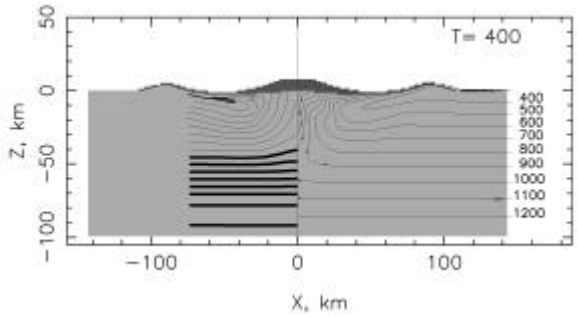

Fig. 1. The position of the marked, initially horizontal layers (left side) and isotherms (right side, labels show temperature in K) at T = 400 seconds after the impact for the model friction coefficient equal to 0.0625.

Results: Both models produce a complex crater with a central uplift. However, the thermal softening only is unable to result in a fluid-like collapse flow field under the transient cavity. The avalanche of the cavity walls overruns the cavity bottom uplift, and a lot of melt is buried under the apparent floor of the crater.

Acoustic fluidization of the upper crust allows the bottom uplift before the cavity wall collapse, giving more natural picture of the impact melt distribution. The problem is to estimate the level of lithostatic pressure which is enough high to suppress the acoustic fluidization.

References: [1] O'Keefe J. D. and Ahrens T. J. (1993) *JGR, 98*, 17011–17028. [2] O'Keefe J. D. and Ahrens T. J. (1998) LPSC XXIX, CD-ROM, #1822. [3] Melosh H.J. (1979) *JGR* 84, 7513-7520. [4] Melosh H. J. (1989) *Impact cratering: A geologic process*. Oxford University Press, 245 pp. [5] Ivanov B. A. and Deutsch A. (1998) Sudbury impact event: Cratering mechanics and thermal history. *Geol. Soc. Amer. Pap*. (in press).

POSSIBLE 770-METER DIAMETER IMPACT CRATER DETECTED BY SATELLITE; YEMEN ARAB REPUBLIC. R. G. Blom[1], J. F. McHone[2], and R. E. Crippen[1], [1]M/S 300-233 Jet Propulsion Laboratory, Pasadena CA 91109 (ronald.blom@jpl.nasa.gov), [2]Geology Department, Arizona State, Tempe AZ 85287-1404 (jmchone@asu.edu).

Introduction: During analysis of enhanced Landsat Thematic Mapper (TM) satellite images of eastern Yemen for the Mahra Archaeological Project, a 770-m diameter circular feature was detected at 18D 9M North by 50D 4M East. Subsequent study of Shuttle Imaging Radar-C/X-SAR radar images, and a brief field reconnaissance support, but do not confirm, that the feature may be an impact crater.

Remote Sensing Data: The Mahra Archaeology Project is a regional study to document ancient desert trade routes. In the course of this work remote sensing data for most of eastern Yemen have been analyzed. On the images, the proposed crater appears as a 770 meter diameter circular feature centered on a small wadi (dry river channel) which clearly antedates the craterform. No similar features were detected in study of Landsat scenes covering about 300,000 sq km of Yemen. Reduced resolution, black and white Shuttle radar data are shown in Figure 1. Landsat image products analyzed include both a standard Landsat "geology" composite of bands 1, 4, and 7, and a ratio composite of bands 3/1, 5/4, and 5/7. The crater is immediately obvious on the ratio composite, and completely obscure on the band composite. Thus it is possible that undiscovered craterforms might yet be detected elsewhere in previously examined Landsat TM data thru re-processing and re-analysis. The full resolution color Landsat image shows the circularity of the feature, reveals evaporites and aeolian fill within the craterform, and shows a deposit of sand as a wind tail to the west of the craterform caused by the wind shadow from the rim. Shuttle Imaging Radar-C/X-SAR images are available for limited areas in Yemen. Fortuitously, the craterform is covered. The image shown (Fig 1) is composed of X band data. The circularity of the feature is also obvious on the radar image, which also reveals a radar bright, or rough, annulus outside the craterform. Thin, aeolian deposits are largely transparent to the radar in this dry environment.

Field Examination: In January 1997 a one day diversion of our archaeological expedition was made to visit the craterform. We departed from Thamud, about 100 km south of the craterform and the nearest permanent habitation. We suggest "Thamud Craterform" to designate this feature. Although sharp on the remote sensing images, the feature is unremarkable in the field. The crater is bisected by a wadi, and so is filled with sediment and evaporites, further mantled with windblown sand. There is a barely perceptible raised rim about 1 m high. No overturned rims, shatter cones, or meteoritic material were observed during a complete circuit and transect of the craterform. Although the rim has topographic expression, it seems quite eroded. Due to the massive (nonlayered) character of the early Tertiary carbonate target rocks and the apparent erosion, no overturned rims or stratigraphic inversion was observable. Although shattercones have been observed in carbonates [1], none were observed at the Thamud craterform. Thus there is no field confirmation that the feature is an impact crater at present.

Discussion: Other potential explanations for this circular feature include a sinkhole or volcanic maar crater. Neither seems likely. Although this is a carbonate terrane, there are no known sinkholes in the region. A single, isolated, circular, 770-m sinkhole seems unlikely. Also, while there are volcanic landforms in Yemen, there are none anywhere nearby and no volcanic material was observed in the field. With regards to age of the feature, it is older than about 6000 yr as Neolithic material was found inside the craterform. However it seems unlikely that it is millions of years old. The subdued but slightly raised rim around the craterform, and an external annulus of coarser material suggest neither deep erosion nor exhumation. This craterform is clearly older than the nearby very young Wabar craters (21D 30M N by 50D 28M E, [2]) which are well preserved in the aeolian sands of the Rub al Khali. Additional field work is required to determine the true nature of the Thamud Craterform. Since the expected excavation depth for an impact crater of this diameter is of the order of 100 m [3], a gravity survey would likely disclose if the craterform is filled with low density sediment.

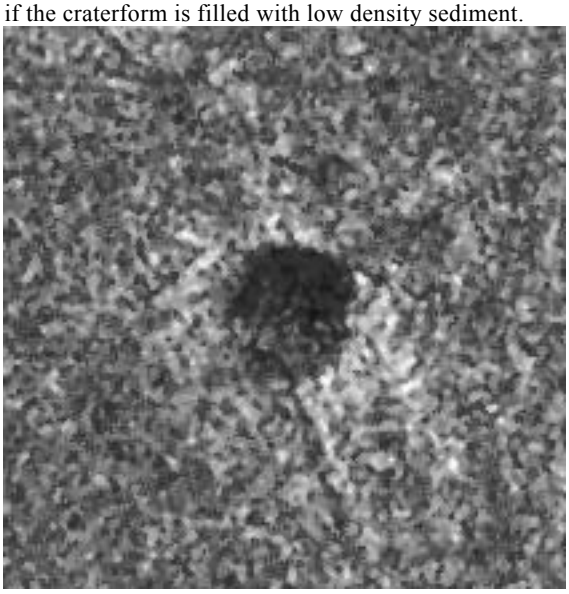

Fig. 1. X-SAR image of 770 m dia "Thamud" craterform feature at 18°09'N;50°04'E, Yemen Arab Republic.

Acknowledgments: Mahra Archaeology Project supported by J. M. Kaplan Fund and nWave International. RGB and REC supported by J PL, California Institute of Tech nology and NASA. JFM supported by a NASA grant to R. Greeley.

References: [1] Shoemaker et al. (1961) USGS Prof. Paper 424-D, 365–368. [2] Hodge P. W. (1994) Meteorite craters and impact structures of the Earth. [3] Melosh (1989) *Impact Cratering*, Oxford.

PLANAR DEFORMATION FEATURES IN QUARTZ GRAINS FROM THE MANSON IMPACT STRUCTURE, IOWA. P. C. Buchanan and C. Koeberl, Institute of Geochemistry, University of Vienna, Althanstrasse 14, A-1090 Vienna, Austria.

The Manson structure is a buried, 36-km diameter meteorite impact crater located in north-central Iowa [1]. Evidence of impact origin includes circular shape, a pronounced central uplift of ~10 km diameter, geophysical anomalies, and planar deformation features (PDFs) in a variety of minerals, including quartz, feldspar, and apatite [1,2]. To delineate the subsurface structure of the Manson crater, twelve boreholes were drilled in 1991-1992; two boreholes previously were drilled in 1953 [1]. Samples of cores from seven of these boreholes (M1, M4, M7, M8, M10, M11, and 2A), which range in location from the center of the structure to 14 km from the center, were analyzed for PDFs in quartz. These samples include basement and supracrustal rocks from the lower levels of some boreholes and various types of breccias from shallower levels. This study was an attempt to extend to other boreholes the work of Short and Gold [2], who reported orientations of PDFs in quartz grains from various levels of boreholes 2A and M1, which are located at distances of 2.5 and 3 km, respectively, from the center of the structure. The purpose of this study was to determine if PDF data could elucidate the spacial distribution of shock pressures that rocks in this impact structure experienced.

As also noted by Short and Gold [2] for their samples, few basal sets of PDFs are present in the rocks analyzed for this study. All of our samples display maxima at ω orientations with variable proportions of π orientations. A few sets of PDFs with normals oriented at angles greater than 35° to the c-axis are also present. Basement rocks from borehole 2A, which is located 2.5 km from the center of the structure, have a maximum at ω orientations with another small, but significant, maximum at π orientations. In contrast, basement rocks from borehole M8, which is located 5.5 km from the center of the structure, display a maximum at ω orientations without a maximum at π orientations. Supracrustal rocks from below breccias in the M4 borehole, which is located 14 km from the center of the structure, do not provide enough data to be statistically significant. However, they are unusual because they display a high proportion of PDFs with angles greater than 35°. Breccias from shallow levels in all boreholes display a predominance of ω orientations with or without small maxima in π orientations.

As noted by Short and Gold [2], the degree of shock experienced by samples taken from close to the center of the Manson impact structure was relatively high. Based on the research of Robertson and Grieve [3], the scarcity in quartz grains of PDFs with basal orientations and the predominance of ω and π orientations for all the samples analyzed in this study suggest that these rocks experienced relatively high shock pressures. The presence of a small maximum in π orientations for PDFs in basement rocks from borehole 2A and the absence of a similar maximum in samples of basement rocks from borehole M8 may be the result of a slight decrease in shock pressure with distance from the center of the structure. Orientations of PDFs in quartz grains from breccias in all of the boreholes analyzed in this study are consistent with mixtures of materials that have experienced shock pressures similar to those experienced by basement rocks in boreholes 2A and M8.

Acknowledgment: Supported by the Austrian Fonds zur Förderung der wissenschaftlichen Forschung (project START Y-058).

References: [1] Koeberl C. et al. (1996) *GSA, Spec. Paper, 302*, 145-219. [2] Short N. M. and Gold D. P. (1996) *GSA, Spec. Paper, 302*, 245-265. [3] Robertson P. B. and Grieve R. A. F. (1977) in *Impact and Explosion Cratering* (Roddy D. J. et al., eds.) Pergamon, NY, 687-702

SURFACE CRATERS ON SIKHOTE-ALIN IRONS; IMPACT PRODUCED. J. F. McHone[1] and M. Killgore[2], [1]Department of Geology, Arizona State University, Tempe AZ 85287-1404 , [2]Southwest Meteorite Laboratory, P.O. Box 95, Payson AZ 85547.

Introduction: Recent collecting expeditions into the Sikhote-Alin strewnfiel have produced several individual and fragmented irons decorated with round-floored circular depressions surrounded by high-relief rims. Previous reports attribute most delicate surface features to aerodynamic sculpturing, effervescence of volatile components, or plucking of xenoliths. We interpret some of these features as impact craters sustained during the final moments of a specimen in flight.

Background: On the morning of February 12, 1947, a brilliant fireball appeared in the clear sky over the Sikhote-Alin Mountains of eastern Siberia and, in less than 10 seconds, more than 50 tons of Fe meteorites slammed into uninhabited, snow-covered taiga forest.

Formal expeditions began arriving almost immediately so that, over the next several years, more than 100 impact pits and craters had been charted, more than 30 tons of pristine irons had been collected, and a uniquely preserved, bountiful collection of cosmic material had become accessible for systematic scientific scrutiny [1,2].

Breakup and Fusion: The original Sikhote-Alin Iron bolide, a coarsest octahedrite, began fragmenting high within the atmosphere along weaker internal planes defined by crystal boundaries. Recovered specimens occur mostly in three distinct geomorphic forms: larger masses bounded by recognizable geometric planes and usually with defined regmaglypts; twisted and jagged, shrapnel-like fragments with occasional regmaglypts or partial fusion crusts; and most commonly, small, irregularly shaped individuals completely sheathed in a distinct high-gloss metallic fusion crust. Fusion crusts on all geomorphic forms commonly are decorated with delicately sculptured patterns, which include swirls of grooves and ridges, adhered or "spattered" metal beads, patches of scoriaceous froth and bubbles, and occasional pits or shallow holes with angular walls. A thick ground cover of snow, estimated to be at least 60 cm deep during the impact event, has been credited with cushioning the impact landing of smaller pieces and preserving their delicate surfaces. Most of these features are readily attributed to processes accompanying high-velocity atmospheric flow: erosion of weaker components, frictional heat, volatilization, and plucking of single crystals.

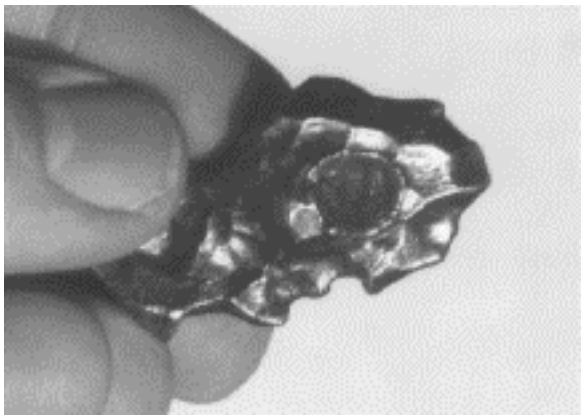

Fig 1. An individual Sikhote-Alin iron meteorite with well developed fusion crust and an 8 mm diameter impact crater on its surface.

Impact craters: During an examination of newly available, small (~100 g) individual and fragmented Sikhote-Alin Irons we have observed an unreported type of surface morphologic feature. Solitary, round-floored circular depressions 1–8 mm in diameter and ringed by high-relief rims occur on fusion-crusted individuals and on at least one shrapnel fragment. We interpret these features as impact craters resulting from high velocity collisions between meteoritic particles during the latest stages of atmospheric flight. Although crater-like bubbles might develop within a fusion crust, during skin heating by atmospheric friction, craters emplaced on fusion-free shrapnel fragments had to have formed later, after atmospheric penetration had already violently disrupted a larger body. Local contitions during the Sikhote-Alin event included thousands of Fe projectiles infalling into an environment already populated with high-speed Fe and rock ejecta fragments from craters still being formed on the ground.

References: [1] Krinov E. L. (1966) *Giant Meteorites*, Pergamon., 397 pp. [2]Krinov E. L. (1960) *Principles of Meteoritics*, Pergamon, 535 pp.

IMPACT STRUCTURES IN THE WILLISTON BASIN. R.A.F. Grieve[1], K. Kreis[2], A.M. Therriault[1], and P.B. Robertson[1], [1]Geological Survey of Canada, Ottawa, Canada, ATherria@NRCan.gc.ca. [2]Saskatchewan Energy and Minerals, Regina, Canada.

Three "new" buried impact structures have been identified in the Williston Basin in Canada. The Elbow structure (106°45'W; 50°58'N) is 8 km in diameter, circular in plan, with a ring depression and an uplifted core of fractured and brecciated target rocks [1]. The structural form is that of a complex impact structure. It has been drilled for hydrocarbons although there is no current production. Originally, the Elbow structure was thought to results from salt tectonics [2] or cryptovolcanism [1]. Sampling of drill hole material indicates the presence of quartz grains with decorated planar deformation features (PDFs; Fig.1a).

The Maple Creek structure (109°20'W; 49°51'N) is barely visible at the surface, where repeated sections of the Upper Cretaceous Bearpaw Formation are very poorly exposed. A structural anomaly was noticed by Whitaker [4] and subsequent Vibroseis seismic profiles indicated structural disturbance to ~ 1 km depth and a slightly elliptical zone ~ 6 km in diameter with an annular trough and a central core ~ 2 km in diameter. Drilling indicates structural complexity in the core, with brecciation and repetition of beds [5]. Interpretation of seismic data suggests a structural uplift of ~ 500 m. A number of possible origins had been suggested, including impact, but all were considered equivocal [5]. Although the bulk of the lithologies in the central uplift are shales, there are a few sandy lenses in the Upper Cretaceous Lea Park Formation with rare quartz displaying decorated PDFs (Fig. 1b).

The Viewfield structure (103°04'W; 49°35'N) is considered to be a 2.4 km simple crater formed in Jura-Triassic time (~ 200 Ma), based on geophysical and drill hole data [6]. Target rocks consist of Mississippian strata, of which at least 200 m are missing in the center of the structure and replaced by young Watrous Red Beds (WRB). In the rim, Mississippian carbonates are found sandwiched between Lower WRB. There are 50 producing hydrocarbon wells, with estimated primary reserves of 10.5 MMBO and 4.5 BCFG [7]. An impact origin for the structure was suggested by Sawatzky [6]. Detrital quartz grains in the WRB display decorated PDFs (Fig. 1c). The specific nature of these grains and their very limited occurrence in materials overlying and filling the crater suggest they were washed into the Lower WRB.

These three "new" structures bring to five the number of known impact structures in the Williston Basin. Three (Newporte, Red Wing, and Viewfield) are hydrocarbon producers. Another possible impact structure (Heidt, North Dakota) is a producer, as is the 25 km diameter Steen River structure, Alberta [7]. Impact structures in this area of North America are important targets for hydrocarbon exploration. The early identification of their impact origin bears on exploration strategies.

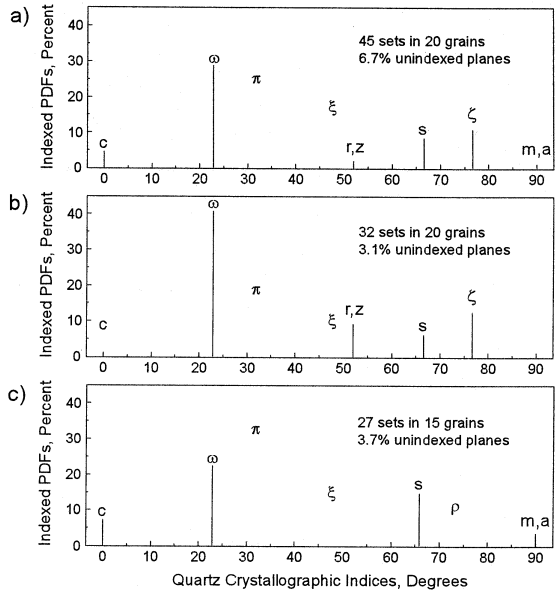

Fig. 1. Frequency of indexed PDFs in quartz from (a) Elbow, (b) Maple Creek, and (c) Viewfield. Standard U-stage and indexing techniques were used.

References: [1] de Mille G. (1960) *J. Alberta Soc. Pet. Geol.*, *8*, 154-162. [2] Goudie M.A. (1956) *Oil in Canada, April 30*, 18-20. [3] Grieve R.A.F. *et al.* (1996) *Meteoritics & Planet. Sci.*, *31*, 6-35. [4] Whitaker S.H. (1976) *Sask. Res. Council Geol. Div. Map, 22*. [5] Gent M.R. *et al.* (1992) *Sask. Energy Mines Misc. Rep., 92-4*, 204-208. [6] Sawatsky H.B. (1972) *Can. Soc. Expl. Geophys. J.*, *8*, 22-401. [7] Donofrio R. (1997) *Oklahoma Geol. Surv. Circ., 160*, 17-29.

BERYLLIUM-10 IN MUONG NONG-TYPE TEKTITES. K. Aggrey[1], C. Tonzola[2], C. Schnabel[2], G. F. Herzog[2], and J. T. Wasson[3], [1]School of Theoretical and Applied Sciences, Ramapo College of New Jersey, Mahwah NJ 07430-1680, USA, [2]Department of Chemistry., Rutgers University of Piscataway, Piscataway NJ 08855-8087, USA (schnabel@rutchem.rutgers.edu), [3]Institute of Geophysics, University of California at Los Angeles, Los Angeles CA 90095, USA.

Introduction: The ^{10}Be contents of Australasian tektites show systematic regional variations. Splash-form tektites from Australia and southeast Asia contain on average 150×10^6 atom/g and 100×10^6 atom ^{10}Be/g, respectively [1]. This ^{10}Be formed in the atmosphere, fell with rain and dust, and was incorporated into sediments.

The Muong Nong-type or layered tektites are found in a band 1100 km long that runs from Hainan, China to Cambodia. Two very different models have been proposed for their origin: 1) they, like all other Australasian tektites, were ejected from one large crater somewhere in southeast Asia and traveled the shortest distances, ≤~500 km [4]; or 2) they, unlike all other Australasian tektites, were parts of melt-sheets, now largely destroyed, that formed when the accretional energy was spread out over a large area [5].

Scattered reports indicate that the Muong Nong-type tektites contain less ^{10}Be than other types. Few of the actual measurements or sample descriptions have been published, however. We present ^{10}Be measurements of five layered tektites and discuss some implications for tektite formation.

Results: The samples were collected in NE Thailand, Laos, Hainan Island, and Vietnam [5,7]. A distance of 640 km lies between the recovery sites of Non-Hung (Thailand) and Lingshui (Hainan Island). We separated Be from 500-mg samples and analyzed for ^{10}Be by accelerator mass spectrometry at Purdue University's PRIME Lab. Results follow (sample name, 10^6 atom ^{10}Be/g): (Huai-Sai, 41 ± 2); (Lingshui, 58 ± 3); (Muong Nong, 77 ± 5); (Non-Hung, 52 ± 2); (Vinh, 55 ± 3). The average for the five tektites is 57 ± 12. Figure 1 shows these results and others from the literature [1,6]. Average ^{10}Be contents of Muong Nong-type tektites are ~1/3 and ~1/2 those of Australian tektites and splash-form indochinites, respectively.

Discussion: The high ^{10}Be concentrations in Australites indicate formation from near-surface deposits. The lower ^{10}Be contents of southeast Asian tektites may reflect decay in an older source (^{10}Be half-life = 1.5 Ma), dilution by ^{10}Be-poor bedrock, a smaller proportion of adsorptive sediments, or a higher proportion of large grains.

Figure 1

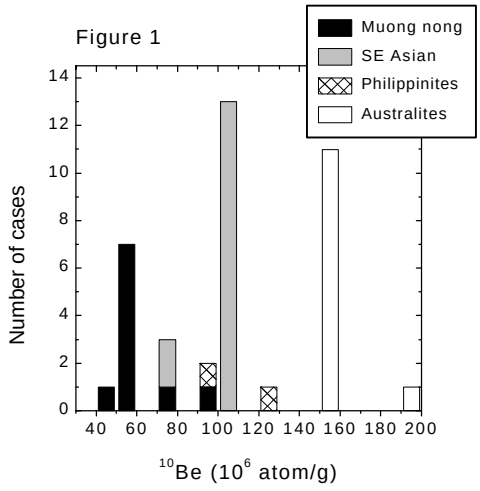

Low ^{10}Be in the one-crater model: Typical long-term deposition rates for plausible impact sites such as an alluvial fan or a major delta are cm/ky [8], implying column heights of ~25-250 m, i.e., depths marginally consistent with a likely crater depth of 2 km. Discontinuous deposition would, however, allow smaller column heights.

Dilution of a ^{10}Be-rich surface component with ^{10}Be-poor bedrock could also explain the observed range of ^{10}Be contents. For surface materials and bedrock that contain, respectively, ~$200\text{-}1000 \times 10^6$ and ~10×10^6 atom/g, we infer an admixture of at least 70% bedrock in layered tektites and 35% in Indochinites. Crater formation occurs within a few tens of seconds [9], leaving little time to produce uniform mixing of melts from different depths.

The lowering of ^{10}Be in Muong Nong-type tektites could reflect meter-scale heterogeneities like those seen in depth profiles of North China loess and other materials [2,3]. In this picture, we either attribute the lower ^{10}Be to chance or postulate that proto-Muong-Nong grains come preferentially from certain low-^{10}Be layers (e.g., loess), while other tektites contain more high-^{10}Be material (e.g., paleosols).

Finally, we note that by virtue of their higher surface to volume ratios, larger sedimentary grains contain less ^{10}Be per unit mass than smaller ones (e.g., [2]). Perhaps the Muong Nong-type tektites formed preferentially from larger grains.

Low ^{10}Be in the many-crater/melt-sheet model: The overall homogeneity of the ^{10}Be contents in Muong Nong-type tektites indicates either that the target material was everywhere fairly similar or, less likely, that the formation process efficiently mixed the ejecta from different impacts. The mixing arguments made above for the one-crater hypothesis apply here as well.

References: [1] Tera F. et al. (1983) *Carnegie Inst. Wash., Dept. Terr. Magnetism Yearbook*, 463–466. [2] Gu Z. Y. et al. (1997) *GCA, 61,* 5221–5231; Gu Z. Y. et al. (1996) *EPSL, 144,* 273–287. [3] Brown L. (1987) *Phil. Trans. R. Soc. Lond., A323,* 75–86; Pavich M. J et al. (1987) *GCA, 50,* 1727–1735; Brown E. T. et al. (1992) *GCA, 56,* 1607–1624. [4] Taylor S. R. (1996) *Meteoritics and Planet. Sci., 31,* 4–5; Koeberl C. (1992) *GCA, 56,* 1033–1064; Fiske P. S. (1996) *Meteoritics and Planet. Sci., 31,* 36–41; Schnetzler C. C. (1992) *Meteoritics, 27,* 154–165; Blum J. D. et al. (1992) *GCA, 56,* 483–492. [5] Wasson J. T. et al. (1995) *JGR, 100,* 14383–14390. [6] Raisbeck et al. (1988) *Chem. Geol., 70,* 120; Pal D.K. et al. (1982) *Science, 218,* 787-789. [7] Wasson J.T. (1991) *EPSL, 102,* 95–109; Fiske P. S. et al. (1996) *Meteoritics and Planet. Sci., 31,* 36–41. [8] Miall A. D. (1996) *The Geology of Fluvial Deposits*, Springer, p. 62. [9] Melosh H. J. (1989) *Impact Cratering*, Oxford, N.Y., p. 123.

EMPLACEMENT AND THICKNESS OF THE CHICXULUB EJECTA. S. W. Kieffer[1] and P. Claeys[2], [1]Kieffer and Woo Inc., P. O. Box 130, Palgrave, Ontario L0N1P0, Canada (skieffer@geyser.com), [2]Inst. fuer Mineralogie, Museum fuer Naturkunde, Invalidenstr. 43, D-10115 Berlin, Germany (philippe.claeys@rz.hu-berlin.de).

Estimates of the kinetic energy of the bolide that formed the Chicxulub impact structure vary because the density and incoming velocity are not known. However, plausible estimates cluster around 100 million megatons. The most recent estimate, constrained by seismic definition of the transient cavity and multiring structure, is 5×10^{23} J. Modeling of the cratering event and ejecta distribution are complex because of the complicated multicomponent, multiphase nature of the target (air, water, refractory silicate rocks, and less refractory carbonate and sulfate components), and because of the extreme scales that must be considered (tens of meters for plausible water thicknesses over the carbonate platform; kilometers for the meteorite and atmospheric thicknesses; hundreds of kilometers for the crater; and thousands of kilometers for the far-field effects). For an impact of this size, the continuous ejecta blanket can be expected to extend several hundred kilometers in radius. Evidence for this comes from observations on fresh planetary craters of various sizes, from smaller relatively fresh terrestrial impact craters, and from theory. Martian impact craters may have been formed under conditions most similar to Chicxulub: a gravity field approximately equal to that of the Earth; a substrate containing volatile components; and possibly with some finite atmosphere in place. Large rampart craters on Mars may therefore be the best planetary analog for estimating ejecta. The continuous ejecta for these craters typically extends to a distance equal to several radii. Fresh craters on all of the planets show ballistically emplaced discontinuous debris out to much greater distances in so-called "rays." For Chicxulub, recent seismic surveys have provided data that strongly indicate that the radius of the transient impact crater was ~45 km, and that the radius of the collapsed cavity was ~90–100 km. Thus, it is likely that the continuous ejecta blanket around Chicxulub extended out to at least 200 km by even the most conservative estimate, and it is plausible that a discontinuous blanket extended many hundreds of kilometers further. Volatile-lubricated debris flows might have also extended beyond the continuous ejecta blanket. Steep escarpments border the Yucatan continental shelf at distances as small as 200 km or even less and not greater than 450 km in all directions. Thus, it is clear that the ejecta blanket probably reached the escarpments and may have induced further slumping and mass flow on the escarpment slope. We estimate the thickness of the ejecta blanket at these distances, by using theoretical and laboratory work of Oberbeck [1] on the dynamics of a "ballistic curtain" combined with the field applications developed by Horz et al. [2] at the Ries. When combined with the estimates of erosion rates induced by ejecta emplacement during meteorite impacts from Simonds and Kieffer [3], our conclusions are (1) that there were probably hundreds of meters erosion during emplacement of the ejecta blanket, and that (2) that ejecta beyond the collapsed rim should consist of a significant component of admixed local material caused by secondary cratering in the ballistic curtain. Our estimated thicknesses are then compared with the ejecta thicknesses observed in the field at several proximal and distal KT sites in the Gulf of Mexico region. They are in reasonable agreement for radii less than three times the radius of the collapsed cavity, which is the maximum distance to which the theories have been validated. Beyond this distance, we obtain reasonable agreement with measured thicknesses out to distances of 1500 km if we assume that there is no admixed secondary ejecta.

References: [1] OberbeckV.R. (1975) *Rev. Geophy. Space Phys*, *13*, 337–362. [2] Horz et al. (1983) *Rev. Geophys. Space Phys.*, *21*, 1667–1725. [3] Simonds and Kieffer (1993) *JGR*, *98*, 14321–14337.

IMPACT EJECTA HORIZON NEAR THE CENOMANIAN-TURONIAN BOUNDARY, NORTH OF NAZARÉ, PORTUGAL. J. F. Monteiro, J. Munha, and A. Ribeiro, Departamento de Geologia, FCUL, University of Lisbon, Edifício C-2, Campo Grande, 1700 Lisboa, Portugal.

In this report we present new petrographic evidences that support the idea of a ejecta horizont found near the Cenomanian-Turonian boundary in a coastal site north of Nazaré [1]. If this is the ejecta from a meteorite impact, it must be related to the proposed Tore Sea-Mount impact crater, situated 300 Km to the west of the studied ejecta site [2,3].

The ejecta clasts show a homogeneous distribution along a narrow corridor (60 × 10 m) with a general trend N 60º E. The size of the clasts varies from millimetric up to 80 cm. Each clastic boulder corresponds to a polymitic breccia comprising a variety of different lithologies. Their shape are diverse, but rounded, spherical, and ellipsoidal forms predominate. Associated in small clusters, the fragments display dominant black to brownish-yellow colors. The most notorious macroscopic phases are iron sulfides, but other minerals such as quartz fragments and calcitic nodules are present. Solid hydrocarbons occur frequently as surface accumulations and impregnations occupying the pore spaces of the breccia. Optical (reflected and transmitted light) and SEM-EDX analysis indicate the occurence of pyrite, hematite, quartz, calcite, devitrified silica glass and diapletic glass.

Quartz shocked crystals are very common and we also observe features that resemble planar elements and shock lamellae in a very restricted number of quartz grains.

In the muddy-limestone matrix surrounding the great ejecta fragments we found microscopic spherules and irregular shard-like particles. The spherules consist entirely of diagenetic phases (mainly carbonate-replaced) and no relict minerals or pseudomorphed quench textures have been recognized. This may be because the spherules were initially composed entirely of glass or because the quench textures were destroyed during diagenetic stabilization. Some preserve the dumbbel-shaped typical of microtektites. Similar-sized spherules have been recorded from the K/T boundary [4] and have been interpreted as Chicxulub ejecta. The spherules were probably deposited as microtektite-like bodies consisting of glass and/or other diagenetically unstable phases. The discovery of these spherules and shard-like particles provides strong supporting evidence for the proposed impact-related origin of the north of Nazaré Cenomanian-Turonian ejecta horizon.

Acknowledgments: This research was supported by FCT grant PRAXIS XXI/BD/9542/96 to J.F. Monteiro.

References: [1] Monteiro J. F. et al. (1997) *LPS XXVIII*, 967. [2] Laughton A. et al. (1975) *Deep Sea Research*, 791–810. [3] Monteiro J. F. et al. (1997a) *Abstracts EUG 9*, 278, Strasbourg. [4] Smit J. et al. (1992). *Proc. of Lunar and Plant. Sci.*, vol. 22, p 87–100.

METALLIC SPHERULES AND A MICROTEKTITE SUPPORT THE INTERPRETATION OF A BURIED IMPACT CRATER BENEATH PANTHER MOUNTAIN IN THE CENTRAL CATSKILL MOUNTAINS, NEW YORK. Y. W. Isachsen, New York State Geological Survey/State Museum, Albany NY 12230, USA (e-mail: yisachse@mail.nysed.gov).

Introduction: Panther Mountain is located in the Catskill Mountains, a region of flat-lying Paleozoic sedimentary rocks that forms the eastern edge of the Allegheny Plateau. It is a circular mass, 10 km in diameter, located immediately west of Phoenicia, New York, and rises 800 m above the valley floor. The mountain is defined by an anomalous circular drainage pattern, vividly shown on Landsat images, that invites a geological explanation. Initial work included photogeology (Landsat and stereo airphotos), surface geologic study, shallow seismic refraction profiling, gravity and magnetic measurements, and gravity modeling [1].

Pervasive fluvial cross-bedding in the terrigenous strata of the region made it impossible to determine whether the feature is slightly domical, slightly basinal, or unwarped. However, it was clear that high joint density accounts for the greater erosion that produced the circular valley.

Gravity mapping defined a crudely-circular negative anomaly with a relief of 6 mGals, most anomalous for an area of flat-lying stratigraphy 3000 m thick. A measured gravity profile was satisfied by a computed profile of a shallowly-buried (~1 km) complex impact crater with a diameter of 10 km and a central uplift of brecciated and shattered rock ~1 km in thickness. The modeled crater, a syndepositional structure, would pass through the Middle and Lower Devonian section. The relatively high joint density that is responsible for erosion of the ring valley is attributed to the influence of the buried crater rim on the geometry of sedimentation, especially factors of differential compaction and cementation. The failure of fracture-controlled linear valleys north and south of Panther Mountain to extend across the mountain mass is explained by absorption of the regional stress energy by impact-produced brecciation below.

Investigation: The only direct access to subsurface information is provided by the 2000-m-deep Herdman gas test well located near the northern edge of Panther Mountain. The hole, produced by a percussion drill, yielded mainly 1–2-mm size rock cuttings. Such cuttings are customarily bagged for every 3–4-m depth interval, and used to construct the stratigraphic section. Before study, however, each bag of cuttings is placed in a liter beaker of water, stirred vigorously, and decanted, to remove the fine-grained "dust" fraction.

Some 600 bags of such washed cuttings were painstakingly searched for spherules and microtektites, using a binocular microscope with zoom lens. Thin sections were made of selected grain mounts to search for planar deformation lamellae in quartz and other features of shock metamorphism.

Observations: Seven magnetic spherules, measuring 0.2–0.8 mm were found at the depth interval 573–578 m in the Herdman well, and three at 902–904-m depth in the Armstrong well, 12 km to the west. A pale brown microtektite with gas bubble hollows was identified at 627–630 m in the Herdman well. No impact features were recognized in the thin secitons.

Interpretations: The washing of the samples probably removed most microtektites that might have been present, as well many of the very small spherules. The magnetic spherules found in the Herdman and Armstrong wells fall in the same stratigraphic interval and thus appear to represent the stratigraphic position of impact, which happens to be at or near the Middle-Upper Devonian boundary. The microtektite could also have originated at this position and become dislodged from the wall when the drill bit had reached the lower levels.

Future Work: Microprobe analyses will be made of representative spherules. Cuttings from several more distant deep gas test wells will be examined for further evidence of impact.

References: [1] Isachsen Y. W et al. (1994) *Northeastern Geology, 16,* 123–136.

A SURVEY OF CALCIUM-ALUMINIUM-RICH INCLUSIONS FROM R CHONDRITES: IMPLICATIONS FOR RELATIONSHIPS BETWEEN METEORITE GROUPS. S. S. Russell, Department of Mineralogy, The Natural History Museum, Cromwell Road, London SW7 5BD, UK (sarr@nhm.ac.uk).

Introduction: The newly identified rumurutiite (R) chondrite group is characterised by highly oxidised silicates ($Fa_{\sim 38\text{-}40}$), and high $\Delta^{17}O$ values [1–3]. No calcium-aluminium-rich inclusions (CAIs) so far have been described from this meteorite group. CAIs are refractory components that are believed to have formed early in solar system history [e.g., 4]. They are common constituents of carbonaceous chondrites, but are rare in ordinary chondrites and extremely rare in enstatite chondrites. The differences in abundance of CAIs between meteorite groups may reflect a localised formation site or distribution of CAIs, or differences in age between the chondrite groups. To investigate further the distribution of CAIs in the chondrite parent-body forming region, a search for CAIs from R chondrites was made.

Results: 5 polished thin sections from the R chondrites PCA 91002, ALH 85151 and PRE 95410 were inspected by SEM. Nine objects were found, between 30 µm and 200 µm in size, that exhibit many of the features of CAIs, such as the presence of Ca- and Al-rich minerals, an irregular shape, and rims. However, the common minerals of CAIs from carbonaceous chondrites, such as melilite, anorthite and magnesian spinel, are absent. Instead the objects are composed almost entirely of lower-temperature, secondary minerals, e.g., nepheline, sodalite, ilmenite, Na-rich plagioclase, and Fe-Cr-rich spinel. An example is shown in Fig. 1. This rounded inclusion is 130 × 90 µm across, and is composed of a core of Fe-rich spinel (FeO = 21%, Cr_2O_3 = 0.2%), enclosing rounded ilmenite grains. Sodalite and plagioclase surround the spinel. The inclusion is rimmed with pyroxene, that grades in composition from diopside (at the outside) to fassaite (Al_2O_3 = 16%; TiO_2 = 7.6%), and contains micron-sized blebs of Fe-rich pyroxene. By analogy to carbonaceous chondrite (CC) CAIs, the primary mineralogy of this CAI was probably magnesian spinel enclosing perovskite, with minor melilite and a diopside rim.

Location of alteration event: CAIs from R chondrites are always altered. Many of the alteration products observed, e.g., ilmenite and Fe-rich spinel, are also found in CAIs from high petrologic grade (>3.4) CO chondrites, where they probably formed as a result of metamorphic equilibration with Fe-rich matrix [5]. Since the R chondrites have comparatively high petrologic types of 3.8 to 4, the alteration of their CAIs probably also occurred on the parent body. The effects of metamorphism make it difficult to determine whether any alteration also occurred in the nebula, perhaps during the high temperature event that oxidised the R chondrite chondrules.

Implications for the relationship between chondrite groups: The abundance of CAIs in the various chondrite groups decreases from CC>RC>OC>EC. The abundance of CAIs in R chondrites argues against these meteorites having formed from the same material as OCs [as suggested by 6]. Instead, these observations imply that R chondrites are more closely related to carbonaceous chondrites, and strengthen the suggestion previously made [7] that the R parent body may have formed in between the ordinary and carbonaceous chondrite forming regions.

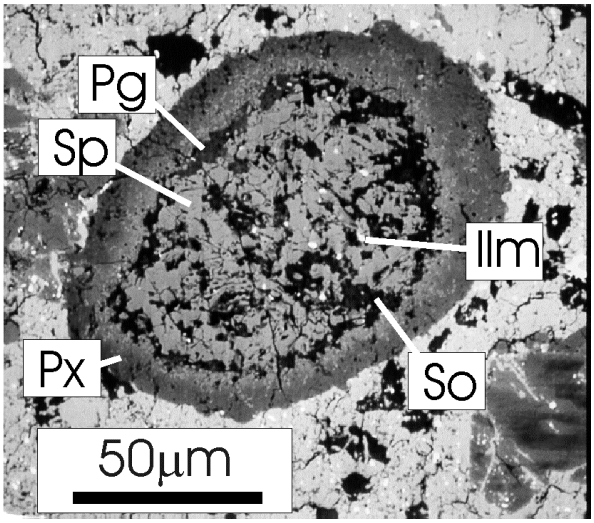

Fig. 1. A CAI from PCA 91002. Pg: plagioclase, Sp: Fe-rich spinel, Px: clinopyroxene, So: sodalite, Ilm: Ilmenite.

References: [1] Rubin and Kallemeyn (1994) *Meteoritics, 29,* 255. [2] Bischoff et al. (1994) *Meteoritics, 29,* 264. [3] Schultze et al. (1994) *Meteoritics, 29,* 275. [4] MacPherson et al. (1988) in *Meteorites and the Early Solar System* (J. F. Kerridge and M. S. Matthews, eds.), p. 746, Univ. of Arizona, Tucson. [5] Russell et al., (1998) *GCA, 62,* 689–714. [6] Weisberg et al. (1991) *GCA, 55,* 2657. [7] Kallemeyn et al. (1996) *GCA, 60,* 2243.

Accretion Shock Processing of Dust Aggregates in the Inner Solar Nebula.

T.V. Ruzmaikina, LPL, Univer. of Arizona, Tucson AZ 85721, USA.

Investigations of the accretional shock at the surface of the solar nebula [1,2] have shown that infalling gas may produces a strong shock. The shock might occupy the most part of the surface of the solar nebula or only a relatively small fraction of it, depending on the value of the angular momentum of the infalling gas, or on the presence (or absence) of density inhomogeneities in the infalling gas. However in all cases a significant fraction of in-falling matter passes through the shock. The heating and processing of solid grains in the accretional shock at (and beyond) the region of asteroid belt have been studied in some details [3-5]. It has been shown that the shock can result to the melting of silicate grains and chondrule formation, at least, at distances of the inner part of the asteroid belt. In this paper, I consider the shock processing of the grains at smaller heliocentric distances. For this purpose, the dissociation and ionization of the gas in the accretional shock is taken into account. These effects influence the structure of the shock at the inner part of the solar nebula. The dissociation and ionization include in the gas cooling at the hot gas in the postshock region. At the same time, the thermal ionization produces UV-radiation which heats and decelerates infalling gas, and includes in the heating of grains. Also, the structure of the shock could be affected by the magnetic fields presenting in the infalling gas because the magnetic pressure could pose restrictions on the maximal compression in the cooling postshock region, even in the case of rather weak field in the preshocked gas.

Partial or complete evaporation of dust aggregates might be appropriate for the formation of refractory inclusions in the accretional shock at the distances less than 1 AU. The grains coagulate again as the gas cools in the postshock region. The formed could be transported to the asteroidal belt by the turbulent diffusion. The necessity of transport explain their lower abundance in meteoritic material.

REFERENCES

[1] Ruzmaikina, T.V., and Maeva, S.V., (1986), *Astron. Vestnik* **20**, 212. [2] T.V.Ruzmaikina, I.V.Khatuncev, and T.V.Konkina, (1993). , *LPSC XXIV, (Abstracts)* , 1225-1226; and *to be submitted to Icarus.* [3] Boss, A.P., and J.A. Graham (1993), *Lunar Planet. Sci. XXIV*, 153–154. [4] Ruzmaikina, T.V., and Ip, W., (1994), *Icarus,* **112**, 430-447; and (1995), in *CHONDRULES AND THE PROTOPLANETARY DISK*, Eds. R.H. Hewins, R.H. Jones, E.R.D. Scott, *in press.* [5] Hood,L., and Kring, D., (1995), In *CHONDRULES AND THE PROTOPLANETARY DISK*, eds. R.H. Hewins, R.H. Jones, E.R.D. Scott, *in press*

IODINE-XENON ANALYSIS OF AN IGNEOUS CLAST FROM JULESBERG: EVIDENCE OF SHOCK DISTURBANCE. J. D. Gilmour[1], J. C. Bridges[2], R. Hutchison[2], and G. Turner[1], [1]Department of Earth Sciences, The University of Manchester, Manchester, M13 9PL, UK (Jamie.Gilmour@man.ac.uk), [2]Department of Mineralogy, The Natural History Museum, London, UK.

Excesses of ^{129}Xe in primitive meteorites are attributed to the in situ decay of ^{129}I ($t_{½}$ 17 Ma). However, efforts to interpret the initial ^{129}I/^{127}I ratio as a chronometer have not been entirely successful, in part due to the effect of shock [1]. We report the results of analysis of an igneous clast that records the shock-disturbance of the iodine-xenon system. This 10mm clast from Julesberg (L3) is a single olivine grain with inclusions of anorthite (~10 μm wide by 100 μm long) and low-Ca pyroxene [2]. The minerals are cogenetic and so incorporated material with identical ^{129}I/^{127}I and ^{129}Xe/^{132}Xe on formation.

During laser stepped heating initial iodine ratios are higher (earlier model ages) in low temperature releases (figure 1). The association of the major releases of iodine (measured as ^{128}Xe* produced during neutron irradiation) and ^{131}Xe* (barium-derived) suggests that anorthite is the common host phase since it is the most likely barium-bearing mineral and has been identified as a host of iodine [3]. The iodine/^{131}Xe* ratio is lower in the early releases, so mixing of a second iodine-bearing component at low temperature is not responsible for the seemingly earlier ages. Rather, the iodine-xenon chronometer has been disturbed - ^{127}I and ^{129}Xe$_{XS}$ have been mobilised from the lower temperature release sites. ^{127}I removal was slightly more efficient.

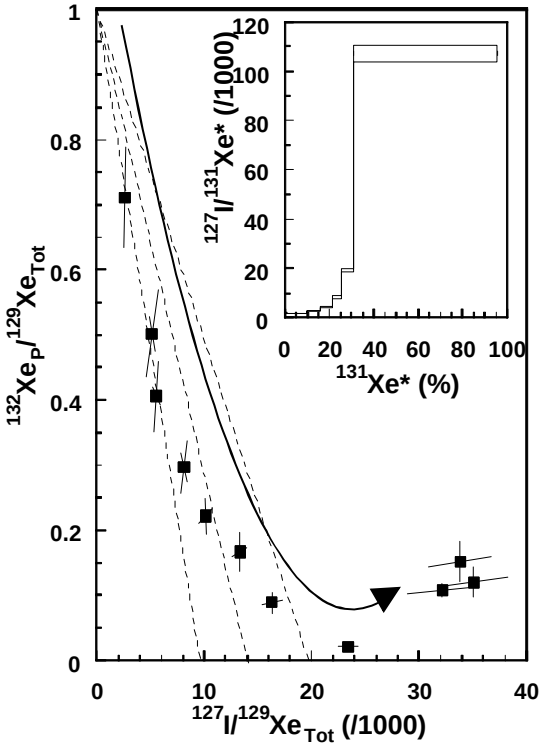

Fig. 1. With increasing release temperature (shown by the arrow) the apparent I-Xe age (intersection of the broken lines with the ^{127}I/^{129}Xe axis) of this sample decreases. The I to Ba (as ^{131}Xe*) ratio is lower in these releases, suggesting the effect is associated with iodine loss.

It seems that the disturbing event had greatest effect close to the (more readily degassed) grain surfaces - interpreting the fractional release pattern as a length scale (assuming a uniform Ba distribution) the bulk I/Ba value has been achieved within around 1 μm of the surface. This clast is shock stage S3 (the olivine exhibits parallel fractures and undulose extinction) and shock effects are enhanced at grain boundaries [4], so we attribute the disturbance of the iodine-xenon system to this shock event. Gas accompanying the major ^{131}Xe* release represents bulk anorthite unaffected by shock, and so may record the formation of the igneous clast ~20 Ma after Bjurböle. The three highest temperature releases possibly represent iodine (and ^{129}Xe$_{XS}$) implanted from anorthite to olivine during the same event. The varying effects of the shock on barium, iodine and xenon imply different potential barriers to their movement; significantly, both iodine and ^{129}Xe may be present as interstitials in the feldspar lattice while barium substitutes for calcium.

Our model has implications for the interpretation of the iodine-xenon system. Enhanced redistribution of iodine relative to xenon may produce falsely high ^{129}I/^{127}I accompanied by falsely low trapped ^{129}Xe/^{132}Xe. This clast is only weakly shocked and the effects may be greater in more strongly shocked samples. Finer grained material may also be more subject to disturbance, and redistribution of once-adjacent components would further hinder interpretation. These possibilities underline the difficulty in interpreting whole rock iodine-xenon data chronologically.

References: [1] Caffee M. W. et al.. (1982) *JGR, Suppl 87,* A318–A330. [2] Bridges J. C. and Hutchison R. (1997) *Meteoritics & Planet. Sci., 32,* 389–394. [3] Brazzle R. H et al. (1995) *LPS XXVI,* 165–166. [4] Stöffler D. et al. (1991) *GCA, 55,* 3845–3867.

NOBLE GAS AND METAL STUDIES IN THE VACA MUERTA MESOSIDERITE. B. Lavielle[1], E. Gilabert[1], M.R. Soares[2], M. A. Z. Vasconcellos[3], G. Poupeau[4], C. Canut de Bon[5], M.E. Cisternas[6], and R. B. Scorzelli[7], [1]URA 451 Centre National de la Recherche Scientifique, Centre d'Etudes Nucléaires de Bordeaux-Gradignan, Le Haut Vigneau, BP 120, 33175 Gradignan Cedex, France (lavielle@cenbg.in2p3.fr), [2]Instituto de Geociencias/UFRGS, [3]Instituto de Fisica /UFRGS, [4]UPRES-A 5025 of Centre National de la Recherche Scientifique, Universite Joseph Fourier, Grenoble, France, [5]Universidad de La Serena, Chile, [6]Universidad de Concepcion, Chile, [7]Centro Brasileiro de Pesquisas Fisicas, Rio de Janeiro, Brazil.

We report measurements of the noble gases He, Ne, Ar, Kr, and Xe in samples from 3 pebbles (sample weights: #1, 75.16 mg; #4, 90.74 mg; #7, 150.77 mg) by mass spectrometry. Extraction procedures required 2 temperature steps at 250° and 1800°C, respectively. At 250°C the amount of gas released was about 1% of the total for ^{4}He, 13% for ^{21}Ne, and less than 0.5% for Ar. Measured total concentrations of ^{3}He, ^{21}Ne, and ^{38}Ar range from 84 to 111, 18 to 27, 12 to 18 10^{-8} cm^3 STP/g, respectively, and reflect variations in chemistry rather than shielding depth effects. For Ne and Ar the trapped component is low (ratio ^{20}Ne/^{21}Ne=0.91 and ^{36}Ar/^{38}Ar=0.66) suggesting that the trapped gases were lost prior or during the exposure to cosmic-rays.

For Kr and Xe, the gas release at 250°C has an isotopic signature consistent with air composition. Most of the atmospheric Kr (70%) is released during the first temperature step, suggesting terrestrial atmospheric contamination. This two-step procedure allows a precise determination of the cosmogenic Kr component which is the main component released at 1800°C. For each sample, all krypton isotopes are analyzed, including ^{81}Kr (half-life 2.29×10^5 y). The dating method ^{81}Kr/^{83}Kr allows a determination of the exposure age, using the ratio ^{78}Kr/^{83}Kr as a shielding depth parameter. Such a calibration is less sensitive to the variation of the abundances of the target elements producing Kr [1], which appear to be 3–5 times higher in Vaca Muerta than in typical chondritic material. An average exposure age of 137 Ma is obtained, which agrees very well with the previous determination of 133 Ma, based on ^{36}Cl-^{36}Ar pair measured in metal separate [2]. Such an agreement also supports previous estimate of a terrestrial age lower than 2500 y based on ^{14}C measurement in Vaca Muerta [3].

We report on an investigation of Fe-Ni metal structures in the Vaca Muerta mesosiderite using Moessbauer spectroscopy, electron probe microanalyser (EPMA), and backscattered electron images (BSE). BSE image showed mainly two Fe-Ni regions, corresponding to the gamma high-Ni phase (tetrataenite) and the alpha-phase kamacite. The results of the chemical analysis of 10 positions using EPMA are in the range of 41.8–40.8 wt% Ni, 57.5–58.7 wt% Fe for tetrataenite and 4.7– 4.4 wt% Ni, 93.0–93.5 wt% Fe for kamacite. The Moessbauer spectra of the metallic Fe-Ni part of the meteorite showed a superposition of three subspectra (1) ordered gamma Fe-Ni phase (tetrataenite); (2) a low-Ni gamma Fe-Ni phase (antitaenite) [4]; and (3) kamacite. The Moessbauer hyperfine parameters indicate a very high degree of order of tetrataenite, which is consistent with the reported very slow cooling rates at low temperatures for the Vaca Muerta mesosiderite. Further studies are in progress.

References: [1] Gilabert et al (1995) *Meteoritics, 30,* 510. [2] Begemann F. et al. (1976) *GCA, 40,* 353–368. [3] Reedy R. C. et al. (1993) *Meteoritics, 28,* 421. [4] D. G. Rancourt and R. B. Scorzelli (1995), *J. Magn. Mater, 150,* 30.

METEORITES AT DOME C? A PROJECT FOR THE AUTOMATED SEARCH FOR METEORITES WITH A ROBOT OF PLANETARY EXPLORATION EQUIPPED WITH TWO RADARS. M. Maurette[1], M. Mellini[2], J. Silen[3], I. Tabacco[4], A. Morbidelli[5], and R.Chatila[6]. [1]CSNSM Bâtiment 104, 91405 Orsay-Campus, France, [2]Dipartimento Scienze Terra, Universitá Siena, 53100 Siena, Italy, [3]Department of Geophysics, Finnish Meterological Institute, P.O. Box 503, 00101 Helsinki, Finland, [4]DST-GEOFISICA, Via Cocognara, 20129 Milano, Italy, [5]Observatoire de la Côte d'Azur, B.P. 4229, 06034 Nice, France, [6]LAS/CNRS-Groupe RIA, 7 Av. Colonel Roche, 31077 Toulouse, France.

In the late 1970s theoretical models predicted that meteorites should not be deposited at the poles [1]. This conclusion has been subsequently invalidated by several studies. R.Harvey (personal communication) pointed out that ANSMET successfully collected meteorites at 260km from the South Pole (Mt Howe; 87°20'S, 149°30'W). A.Morbidelli and B.Gladman computed the orbits of meteorites which can be "fired" to the Earth during collisions between asteroids. All these meteorites have noticeable inclinations on the ecliptic plane. This feature when combined with the tilting of the rotation axis of the Earth on the ecliptic plane smears out any latitude effect for the capture of meteorites by the Earth.

In 1997 we submitted a project to both the French (IFRTP) and the Italian (CSNA) Polar Research Institute, which are jointly building the CONCORDIA Station at Dome C, in central Antarctica at ~2,000 km from South Pole. We want to detect meteorites buried up to a depth of 2 km at Dome C. For this purpose a robot (derived from a model conceived by the Russians for the exploration of Mars) will be equipped with two radars, already used in Antarctica by one of us (Tabacco), but will have to be modified with regard to their antennas and their system of exploitation. These radars, functionning at 60 MHz (pulse radar GSSI) and at 300-910 MHz (pulse radar GAS) would detect meteorites buried at depths of 0–30 m, and 100–2000 m, respectively. Our top priority (only funded at this date) is to determine the efficiency of detection of both radars for small meteorites during the 1999–2000 field seasons.

As the robot would have the potential to explore a surface area of ~20,000km^2 each year, the enormous ice layer extending to a depth ~2 km would be equivalent to a gigantic space collector of meteorites, exposed one year in space, with a total area exceeding that of Earth (the Earth captures about 30,000 meteorites per year).

Dome C presents unique advantages for the detection of meteorites: 1) the well known snow accumulation rate (~3 cm per year), as coupled to the negligible lateral flow of the ice, allows to relate the depth of burial of a given object to its time of fall on the firn surface; 2) morainic debris from the bed rocks buried under the ~4-km-thick ice sheet can hardly inject terrestrial rocks into the top ~2-km-thick ice layer. Thus, it can be safely assumed that all rocks buried in this layer will be meteorites; 3) the quick burial of meteorites will insure their preservation against cryogenic and biogenic weatherings; 4) the lack of crevasses and terrestrial rocks should produce a very low radar background highly favorable to the detection of small meteorites.

We thus expect: to measure the flux of large (>10kg) meteorites, which is essentially unknown, over a time scale ~50,000 years; to detect marked fluctuations in the meteorite flux over the same time scale; to recover a large fraction of the small meteorites buried up to a depth of 10m.

Acknowledgments: We thank G.Kurat for his constant interest.

References: [1] Wetherill G. (1976) *GCA*, *40*, 1297.

WOLD COTTAGE AND ITS INFLUENCE ON REPORTS OF THE PETTISWOOD AND EVORA METEORITES. C. T. Pillinger and J. M. Pillinger, Planetary Science Research Institute, Open University, Milton Keynes, MK7 6AA, UK.

Numerous authors have noted that the correspondence of Edward Topham with the editor of the Oracle newspaper, concerning the fall of the Wold Cottage meteorite, acted as a stimulus to others who had seen stones fall from the sky to report their experiences [1,2].

The first of these was by businessman Mr W^{m} Bingley [3] in an extensive letter to the editor of the Gentlemen's Magazine about something that fell over 20 years earlier when he was living at Pettiswood in Ireland. Bingley's account, and his attempt to offer an explanation for what he had quite obviously seen has every semblance of authenticity. Bingley's career as publisher and bookseller was one which would likely have brought him into contact with Topham and he makes the very interesting observation that "upon further investigation by the learned my cake and Captain Topham's loaf will be found to have been both baked in the same stupendous oven." Bingley therfore is another early believer that all meteorites were related.

A second circumstance always cited is refered to as a letter from the poet Robert Southey [4] writing home from a visit to Portugal. There are numerous reasons to question the veracity of this theory. At the period in question the poet was out of England avoiding the wrath of a benefactress aunt who he had offended by getting involved in a scheme to found a commune and subsequently clandestinely marrying. On his return to England he was somewhat financially embarrassed and just prior to entering training for the law submitted a manuscript for publication supposedly letters written home during his travels in Spain and Portugal. Some letters are addressed and dated; many others have no indication who they were sent to and when. The one containing information about the meteorite is in this category and like some other material in the book could be padding to make the work more substantial and acceptable to the publisher.

Southey needed the money from sales. Southey was out of Britain when Wold Cottage fell and did not return until shortly before his book was submitted and yet there are close parallels between the stories of Evora and Wold Cottage for example, Southey has an account of the local magistrate swearing testimonies (just as Topham did for his meteorites). The question which must be considered is did Southey, who is always credited with announcing the meteorites fall, indulge in a little opportunistic reporting?

References: [1] Pillinger C. T and Pillinger J. M. (1996) *Meteoritics and Planet. Sci.*,*31*, 589–605. [2] Burke J. G. (1986) *Cosmic Debris*, Univ. California. [3] Bingley W. (1796) *Gentleman's Magazine*, *66*, 726–728. [4] Southey R. (1797), letters written during a short residence in Spain and Portugal.

THE CWPI MODEL OF NEBULAR CONDENSATION: EFFECTS OF PRESSURE ON THE CONDENSATION SEQUENCE. M. I. Petaev and J. A. Wood, Harvard-Smithsonian Center for Astrophysics, 60 Garden Street, Cambridge MA 02138, USA.

Since pioneer work of [1] it is customary for a meteoriticist to think that an increase (or decrease) in total nebular pressure results in a corresponding change in condensation temperatures of the all minerals, so the equilibrium condensation sequence remains virtually unchanged. The only exception is the well-known olivine-metal reversal at ~7×10^{-5} bar [1]. To check if it is also true for the CWPI model [2], we performed condensation calculations in the range of pressures from 10^{-1} to 10^{-12} bar at two fixed ξ values of 0.1 %, and 1 % which are representative of condensation of the carbonaceous and enstatite chondrite minerals, respectively, from the nebula of solar composition [2].

We found that the effects of total pressure on the condensation sequence are three-fold: pressure variations (1) cause a corresponding increase or decrease in condensation temperatures of all phases, (2) result in appearance of additional phases in the condensation sequences, and (3) change the order in which minerals condense from the cooling gaseous phase.

At ξ = 0.1 % and $P_{tot}=10^{-5}$ bar [2] the condensation sequence includes corundum, hibonite, melilite, clinopyroxene, spinel, olivine, metal, orthopyroxene, plagioclase, Na_2SiO_3, troilite, tremolite, talc, and Na-phlogopite. In addition, grossite, Si-bearing metal, silicate melt, and $Na_2Si_2O_5$ appear in the condensation sequence at higher pressures, with the stability fields widening with increasing pressure. Graphite condenses at total pressures lower than ~10^{-8} bar. The metal-olivine reversal occurs at the nebular pressure of ~3×10^{-4} bar; clinopyroxene and plagioclase condense prior to olivine at pressures lower than ~2.5×10^{-5} and ~2.5×10^{-8} bar, respectively. At pressures lower than ~1.3×10^{-8} bar anorthitic plagioclase condenses before clinopyroxene.

At ξ = 1 % and $P_{tot}=10^{-5}$ bar the condensation sequence consists of corundum, hibonite, melilite, larnite, wollastonite, merwinite, clinopyroxene, olivine, spinel, metal, low-Ca orthopyroxene, silica, plagioclase, $Na_2Si_2O_5$, Na_2SiO_3, nepheline, monticellite, periclase, troilite, Na_2S, and oldhamite. Grossite, Si-bearing metal, silicate melt, and $NaAlO_2$ are added to the condensation sequence at higher pressures, and cordierite, graphite, and Na_2CO_3 appear at low pressures. The metal-olivine reversal occurs at the nebular pressure of ~4×10^{-4} bar. Other changes in the order of mineral appearance are more complex than those at ξ = 0.1 %, probably due to larger degree of chemical fractionation at higher ξ values. The most striking difference is that spinel condenses after olivine in the limited pressure range from ~1.5×10^{-6} to ~3×10^{-2} bar. At a pressure of ~2×10^{-2} bar anorthitic plagioclase and spinel appear almost simultaneously at the expense of melilite. High-Ca pyroxene and plagioclase condense prior to olivine at pressures lower than ~3×10^{-5} and ~1.3×10^{-9} bar, respectively.

While our results clearly show that pressure has substantial effects on the condensation sequences in the solar nebula, the most radical changes such as appearance or disappearance of new phases in the condensation sequences take place at pressures which are either too high, or too low compared to the range of ~10^{-4} - 10^{-8} bar predicted for the inner portion of a low-mass solar nebula [*e.g.*, 3]. Nevertheless, the presence of grossite-rich inclusions in some chondrites [4] suggests that the total nebular pressure must have been locally as high as 10^{-2} bar to stabilize grossite. (A similar effect might be achieved by increasing the dust/gas ratio by several orders of magnitude.) Variations of nebular pressures in the range characteristic of a low-mass nebula will change the order in which olivine, clinopyroxene, and plagioclase condense. Such variations might have been responsible for different alteration sequences observed in CAI's.

References: [1] Grossman L. (1972) *GCA, 36*, 597–619. [2] Petaev M. I. and Wood J. A. (1998) *Meteoritics & Planet. Sci.*, submitted. [3] Wood J. A. and Morfill G. E. (1988) *Meteorites and the Early Solar System*, 329–347. [4] Weber D. et al. (1995) *GCA, 59*, 803–823.

NEBULAR WATER DISTRIBUTION AND NEBULAR CHEMISTRY. K. E. Cyr[1], C. Sharp[2] and J. I. Lunine[1], [1]Lunar and Planetary Laboratory, Department of Planetary Sciences, 1629 E. University, University of Arizona, Tucson AZ 85721, USA (kimberly@lpl.arizona.edu, jlunine@lpl.arizona.edu), [2]Steward Observatory, 933 N. Cherry St., University of Arizona, Tucson AZ 85721 (csharp@as.arizona.edu).

Introduction: The distribution of water in the solar nebula is important both because water is extremely abundant and because it condenses out at 5 AU, allowing ice and vapor to affect the chemistry of the nebula and forming solar system bodies. In one of the few previous examinations of the distribution of nebular water, Stevenson and Lunine [1] modeled water vapor transport across the ice condensation front by eddy diffusion and the subsequent rapid condensation of ice. The ice was assumed to suffer little effect from gas drag or other transport processes and so remained in the condensation zone. The model predicted that the inner 5 AU of the nebula was swept clear of all water vapor in as little as 10^5 yr.

Water Distribution: However in relatively recent work, Cyr et al. [2] found that gas drag effects in the Stevenson and Lunine model had been underestimated and that ice particles could drift back inward of 5 AU significant distances and sublimate, re-injecting the nebula with water vapor. The expanded water transport model [2] numerically incorporates both the diffusive transport of water vapor and the aerodynamic gas drag on and subsequent drift of ice particles. The nebula is modeled post-collapse, during the 10^{6-7} year long quiescent phase of its evolution, and Cassen [3] temperature profiles were used. Similar to Stevenson and Lunine, results of the Cyr et al. model still predict an overall depletion in water vapor relative to solar abundance concentrations, however there is a zone of significant local vapor enhancement from 1–2 AU which gradually drops off out to 5 AU. At the start of the quiescent phase of nebular evolution, the nebula is relatively hot and the level of vapor enhancement is greatest; peak enhancement occurs over 1–2.5 AU and is on the order of 60% of solar abundances. As the nebula ages it cools; by 2×10^6 yr after the start of quiescent evolution, the zone of peak vapor enhancement occurs over 1–2 AU and peak enhancement is 40% of solar abundances.

Chemistry: This suggests that while there is still a tendency towards overall drying of the inner nebula relative to solar values, there is additionally a local "wet" zone of relative vapor enhancement which gradually shrinks radially and decreases in amplitude as the nebula evolves. Further, unlike Stevenson and Lunine, there is a radial dependence to the water vapor abundance and thus potentially to the relative reducing nature and C/O ratio in the inner nebula. Cyr et al. [4] considered the overall effect of the radial dependence of water depletion on nebular chemistry, using a chemical equilibrium code that computes abundances of nebular elements and major molecular C, N, S, etc. species. In particular, changes in local $[CO]/[CH_4]$ and $[N_2]/[NH_3]$ ratios due to the radially dependent decrease in oxygen fugacity were tracked and plotted. Assuming heterogeneous catalysis of the CO to CH_4 reaction, one can estimate a quench temperature as low as 520K [5]. At such low quench temperatures, given an oxygen abundance 60–40% of solar values $[CH_4]$ dominates [CO] by an order of magnitude; at oxygen abundances less than 20% of solar value which the Cyr et al. [2] model found at radial distance 4–5 AU, methane appears to dominate fully. The $[N_2]/[NH_3]$ ratio was not significantly affected by changes in oxygen fugacity.

Conclusions: While these results do incorporate a few simplifying assumptions, diffusion as the dominant vapor transport process and low quench temperatures, they do suggest that water vapor transport in a diffusive quiescent nebula could significantly affect nebular chemistry, potentially producing large variations in the reducing nature and chemical products of the inner nebula over nebular history. Other nebular processes that could have occurred, such as advective midplane gas flows and migration of giant planets, and their effects on the water transport and chemistry will also be discussed.

References: [1] Stevenson, D. J and Lunine, J. I. (1988) *Icarus, 75*, 146–155. [2] Cyr, K. E. et al. (1998) *Icarus* submitted. [3] Cassen, P. (1994) *Icarus, 112*, 405–429. [4] Cyr, K. E et al. (1998) in preparation. [5] Prinn, R. G. and Fegley Jr., B. (1989) *Origin and Evolution of Planetary and Satellite Atmospheres*, 78–136.

NEW CROSS SECTION MEASUREMENTS OF PROTON-INDUCED PRODUCTION OF HELIUM, NEON, AND ARGON IN IRON AND NICKEL IN THE ENERGY RANGE FROM 159 TO 1600 MEV. E. Gilabert[1], B. Lavielle[1], S. Neumann[2], M. Gloris[2], R. Michel[2], F. Sudbrock[3], and U. Herpers[3], [1]URA 451 CNRS, Centre d'Etudes Nucléaires, BP120, 33175 Gradignan CEDEX, France (gilabert@cenbg.in2p3.fr), [2]Center for Radiation Protection and Radioecology, University of Hannover, Germany; [3]Department of Nuclear Chemistry, University of Cologne, Germany.

The interaction of galactic and solar cosmic rays (GCR and SCR) with meteoroids in space leads to the production of a large variety of stable and radioactive nuclides. The observed abundances of these cosmogenic nuclides in meteorites provide important information regarding the irradiation histories of these objects, as well as on temporal changes in the flux of the GCR and SCR, respectively. Noble gas isotopes of He, Ne, and Ar are of great interest in this study, and the availability of accurate reaction data is essential.

In the course of a systematic investigation of proton-induced reactions, we report new cross section measurements of ^{3}He, ^{4}He, ^{20}Ne, ^{21}Ne, ^{22}Ne, ^{36}Ar, ^{38}Ar, and ^{39}Ar in Fe and Ni targets in order to complete and to improve our knowledge of these excitation functions. In particular the energy region between 159 MeV and 600 MeV was not studied in earlier investigations [1].

Proton irradiations were performed at the Theo Svedberg Laboratory (TSL), University of Uppsala, and at the Laboratoire National Saturne, Saclay, using the stacked-foil technique for proton energies lower than 200 MeV, and between 200 MeV and 1.6 GeV, respectively. Concentrations of noble gases were measured by mass spectrometry using the isotopic dilution method. Comparison with previous work [1,2] shows good agreements. However, some targets contained large amounts of atmospheric Ne and Ar and did not allow reliable determinations of ^{20}Ne, ^{22}Ne, and ^{36}Ar concentrations.

References: [1] Michel R. et al. (1995) *NIM, B103,* 183–222. [2] Baros F. and Regnier S. (1984) *J. Phys., 45,* 855–861.

MEASUREMENT OF CROSS SECTIONS FOR THE PROTON-INDUCED PRODUCTION OF HELIUM AND NEON ISOTOPES FROM MAGNESIUM, ALUMINUM, AND SILICON. I. Leya[1], H. Baur[1], H. Busemann[1], R. Wieler[1], M. Gloris[2], S. Neumann[2], R. Michel[2], U. Herpers[3], [1]Institute for Isotope Geology and Mineral Resources, ETH Zurich, NO-C61, CH-8092 Zurich, Switzerland,[2]Center for Radiation Protection and Radioecology, Universität Hannover, Am Kleinen Felde 30, D-30167 Hannover, Germany, [3]Abt. Nuklearchemie der Universität Köln, Otto-Fischer-Straße 12-14, D-50674 Köln, Germany.

Integral thin target cross sections for the proton induced production of He and Ne isotopes are one of the basic data for modeling the cosmic ray record in extraterrestrial matter. There are some cross sections available for proton energies >500 MeV [1], but for lower energies only a few and sometimes inconsistent data exist. We therefore measured the excitation functions for the proton induced production of He and Ne isotopes from Mg, Al, and Si.

For energies <200 MeV we used the well known stacked-foil-technique, since the influences of secondary particles on the production of He and Ne isotopes from Mg, Al and Si can be neglected in this energy range [2]. For irradiations with energies >200 MeV we use a new mini-stack set-up, since earlier experiments clearly demonstrated the influences of secondary particles on the production of residual nuclides in this energy range [1,3,4]. For more details about the mini-stack approach see Refs. [3,5].

The gases were extracted in a single heating step and purified on Zr-Ti- and Zr-Al-getters. Background Ar was separated by absorbing it on activated charcoal held at the temperature of boiling nitrogen. ^{20}Ne and ^{22}Ne were corrected for $^{40}Ar^{2+}$, $H_2{}^{18}O^+$ and $^{44}Co^{2+}$, respectively. The corrections were always below 0.5% [6].

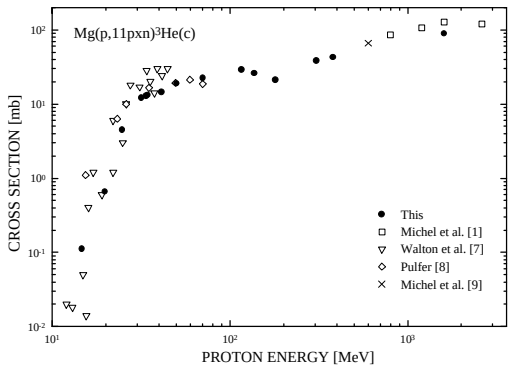

Fig. 1. Excitation function for the production of $^3He(c)$ from Mg. The error bars are always smaller than the symbol sizes.

In Fig. 1, we show the excitation function for the production of $^3He(c)$ from Mg. Prior to our measurements there was a complete lack of data between 70 MeV and 600 MeV and a considerable discrepancy between the cross sections given by Walton et al. [7] and Pulfer [8]. Our data are about 2 times lower than the results given by Walton et al. [7] but agree within 30% with the cross sections from Pulfer [8]. In the energy range between 70 MeV and 600 MeV integral cross section are presented for the first time.

We will present complete excitation functions for the proton induced production of He and Ne isotopes from Mg from the respective reaction threshold up to 1.6 GeV. For Al and Si our new data fill former gaps between 70 MeV and 600 MeV. As a result of our new measurements there now exists a complete and consistent data set for the proton-induced production of He and Ne isotopes from Mg, Al, and Si, which are the relevant target elements for the production of cosmogenic He and Ne in meteorites and the surface material of the moon. The new data allow us to further improve the model calculations with the goal the decipher exposure histories of meteoroids, especially the solar cosmic record in small meteoroids, cosmic dust and the upper few millimeters of lunar rocks.

Acknowledgments: The first author wishes to thank the Deutsche Forschungsgemeinschaft for financial support. The authors are grateful to the Laboratoire National Saturne/Saclay, France, the Svedberg National Laboratory/Uppsala, Sweden and the Paul Scherrer Institut/ Villingen, Switzerland for making available the irradiations.

References: [1] Michel R. et al. (1995) *Nucl. Instr. Meth. Phys. Res., B103,* 183–222. [2] Michel R. et al. (1997) *Nucl. Instr. Meth. Phys. Res., B129,* 153–193. [3] Leya I. (1997) Ph.D. thesis, Univ. Hannover, Lüpke M. (1993) Ph.D. thesis, Univ. Hannover. [5] Gloris M. et al. (1998) *Nucl. Instr. Meth. Phys. Res. B,* for submission. [6]Graf Th. et al. (1990) *GCA, 54,* 2511–2520. [7] Walton J. R. (1976) *JGR, 81,* 5689–5699. [8] Pulfer P. (1979) Ph.D. thesis, Univ. Bern . [9] Michel R. et al. (1989) *Analyst.,* 114.

VARIATIONS IN SOLAR-PROTON FLUXES OVER THE LAST MILLION YEARS. R. C. Reedy, Mail Stop D436, Los Alamos National Laboratory, Los Alamos NM 87545, USA (rreedy@lanl.gov).

Introduction: Nuclides made by solar cosmic rays (SCR) have been studied in many lunar samples. Measured concentration-versus-depth profiles now exist for many SCR-produced nuclides, covering the last ~10^4 (5730-year ^{14}C) to ~5×10^6 (3.7-Myr ^{53}Mn) years [e.g., 1]. The solar-proton fluxes and spectral shapes determined from these profiles vary among nuclides and often in results for a given nuclide. A question is whether real variations have been observed in these SCR results. Closely associated with this question is what are the uncertainties in the inferred solar-proton fluxes and spectral shapes.

Variations in the Results from SCR Records: Interpreting a measured profile involves many steps. The measured concentration-versus-depth profile must be corrected for all nuclides not made by SCR particles, mainly reactions induced by galactic cosmic rays. This inferred SCR profile is then used to determine the SCR flux and spectral shape. The main input is a set of reaction cross sections.

The SCR spectral shape is usually assumed to be an exponential in rigidity, with R_0 the shape parameter, although a range of spectral shapes, including power laws in energy and rigidity, can give good fits to a SCR profile [e.g., 2]. The incident flux of protons is traditionally given as the integral flux >10 MeV (J_{10}), which varies much with R_0 for a given SCR profile. However, for many nuclides, there is an energy, ~30–90 MeV, where the integral flux above that energy for all spectral shapes varies little. For ^{14}C, this energy was 57 MeV [2], near the energy for the peak in the O(p,x)^{14}C cross section. Usually the fluxes >30 MeV (J_{30}) and >60 MeV (J_{60}) vary much less than J_{10} for fitting SCR profiles, and thus there is more confidence in these fluxes.

Variations Among SCR Results: When one set of SCR measurements is interpreted by several groups, or when several different profiles for one nuclide are studied, resulting solar-proton fluxes and spectral shapes often vary widely. Several groups [e.g., 3–5] have studied SCR-produced 0.7-Myr ^{26}Al and 1.5-Myr ^{10}Be. Reported results for the last ~1 Myr range from R_0 = 75 MV and J_{10} = 100 protons/cm^2/s [4] to R_0 = 125 MV and J_{10} = 55 protons/cm^2/s [5]. However, these results all have J_{30} of 24-32 protons/cm^2/s and J_{60} of 7-12 protons/cm^2/s.

The R_0 and J_{10} determined for 0.3-Myr ^{36}Cl in three lunar samples varied much [6]. Most of these fits give J_{30} = 30 protons/cm^2/s and J_{60} = 12 protons/cm^2/s.

For ^{14}C [2] and 0.1-Myr ^{41}Ca [3], J_{30} are 42 and 56 protons/cm^2/s and J_{60} are 17 and 16 protons/cm^2/s, respectively, similar to such energies for recently measured SCR fluxes [1,2].

Conclusions: While a detailed analysis of the uncertainties in the results for solar-proton fluxes and spectral shapes in the past has not been done, the results will depend on the energies used, with J_{30} and J_{60} being better determined than J_{10} and R_0 (or other spectral-shape parameters). The J_{30} and J_{60} above for ~1 Myr (^{26}Al and ^{10}Be) are less than those for the last ~0.1 Myr (^{14}C, ^{41}Ca, and modern). Being less than the uncertainties in the cross sections for unfolding these data, now usually well determined [2,3,5,6], these variations in solar-proton integral fluxes >30 and >60 MeV over the last ~0.1 Myr and ~1 Myr look real.

References: [1] Reedy R. C. and Marti K. (1991) in *The Sun in Time*, p. 260, Univ. of Ariz. [2] Jull A. J. T. et al. (1998) *GCA*, in press. [3] Fink D. (1998) *GCA*, in press. [4] Nishiizumi K. et al. (1995) *LPS XXXVI*, 1055. [5] Michel R. et al. (1996) *NIM B113*, 434. [6] Reedy R. C. and Nishiizumi K. (1998) *LPS XXIX*, abstract #1698.

This work was supported by NASA and done under U. S. DOE auspices.

LOOSELY BOUND MATTER ON THE SURFACE OF SMALL BODIES – MODELS OF ITS MOTION.

M. Solc[1], R. Stork[1,2], [1]Institute of Astronomy, Charles University Prague, V Holesovickach 2, CZ–18000 Prague 8, Czech Republic (solc@mbox.troja.mff.cuni.cz), [2]Astronomical Institute, Academy of Sciences of the Czech Republic, Fricova 1, CZ–25165 Ondrejov, Czech Republic (stork@asu.cas.cz).

Since the early studies of regolith on the surface of asteroids [e.g. 1] many numerical simulations of impact ejecta motion were carried out in order to fit the meteoroid supply to other solar system bodies. Simultaneously, processes of producing meteoroids from cometary parent bodies were studied, e. g. in case of the Geminid meteoroid stream, it has been shown by Adolfsson and Gustafson [2] that meteoroids were released continuously for at least 3000 years ending ca 1600 AD. The source of meteoroids can be either the cometary activity or repeated collisions with smaller solid pieces of sufficient energy. We simulated the latter process in case of impacts energetic enough to release meteoroids but still under the limit of disrupting the target body.

Small bodies of diameter 1 to 10 km can develop only several centimeters to meter thick layer of regolith that is relatively fine grained and homogenous because the ejecta from each impact are spread almost uniformly over the surface. Moderate energetic impact can release not only the ejecta from the impact crater but also the regolith cover that can reach the escape velocity, too.

We developed a numerical code for simulating simplified collisional processes on such a low mass body in order to estimate the motion of the surface dust, sand and regolith lumps due to acceleration by shattering and tumbling motion of the target. Spherical shape of the target is assumed. Energy and momentum of the impacting projectile is varied so that the impact effect ranges from the erosion by excavation of crates to the disruption of the target. Other variable parameters are the collision parameter, thickness and structure of the surface layer, initial rotation state of the target etc. The resulting velocity distribution of escaping particles seems to be strongly directional dependent, which differs from what has been inferred by Adolfsson and Gustafson [2] who argued that the released particles did predominantly start on the illuminated side of Phaeton. Particular attention is further given to the way how the size distribution of lumps on the surface is modified when they are lifted up and released due to shaking of the target during the impact.

We will present results for a variety of initial conditions and collisional parameters, asteroidal masses and will discuss the implications of these results also in the context of cometary and asteroidal trails [3].

Acknowledgement: We acknowledge the support by Grant Agency of the Czech Republic (grant 96/205/0213)

References: [1] Chapman C. R. 1976: Asteroids as meteorite parent bodies: The astronomical perspective, Geochim. Cosmochim. Acta 40, p. 701-719; [2] Adolfsson L. G., Gustafson B. A. S. 1996: Dynamic and probabilistic relation between meteoroids and their parent bodies, ASP Conf. Ser. 104, p. 133-136; [3] Stork R. 1998: Optical and infrared observation of solid state interplanetary matter, PhD Thesis, Charles University Prague.

"BASALTIC" ASTEROIDS IN THE MAIN BELT: ARE THEY FRAGMENTS OF VESTA? T. H. Burbine, R. P. Binzel, and S. J. Bus, Department of Earth, Atmospheric, and Planetary Sciences, Massachusetts Institute of Technology, Cambridge MA 02139, USA (thb@astron.mit.edu).

Introduction: Asteroid 4 Vesta has been linked to the HED (howardite, eucrite, and diogenite) meteorites due to Vesta's distinctive basaltic spectrum in the visible and near-infrared [1,2]. A similar type of distinctive visible spectrum was subsequently identified [3] in a number of small (diameters <10 km) asteroids near Vesta. Out of ~1500 main-belt asteroids that have been observed as part of the Small Main-Belt Asteroid Spectroscopic Survey (SMASS) [4,5], less than 50 objects have been identified with this type of spectrum. Approximately 80% of the Vesta family [as defined by Zappalà et al., 6] have this distinctive spectrum. However, these small "basaltic" asteroids do tend to have much stronger ultraviolet (UV) absorption features than Vesta [7].

Observations: To better understand the composition of these small "basaltic" asteroids, we have observed a number of these objects in the near-infrared (0.9–1.65 μm) [8]. The observed small "basaltic" asteroids tend to have 1-μm features that are much stronger than Vesta's feature and continuum slopes that are much redder than Vesta's slope. Interestingly, the HEDs have spectral properties [9] that span the reflectance range from Vesta to the small "basaltic" objects. Some of the eucrites have UV feature strengths intermediate between Vesta and the small "basaltic" asteroids. The eucrites also have continuum slopes that range from relatively flat (like Vesta) to as red as some of the reddest "basaltic" asteroids. From the positions of their absorption features, the observed "basaltic" objects tend to have compositions similar to the howardites.

Distribution: Out of ~1500 asteroids observed in the visible, we have only found these "basaltic" asteroids between 2.2 and 2.5 AU. These objects tend to be relatively spread out in semimajor axis, but are more constrained in distribution in proper eccentricity and inclination. Using Gauss's equations for changes in orbital elements in response to an impulse velocity [10], we find that the distribution of these objects is consistent with a region defined by ejection velocities from Vesta up to 1 km/s. These velocities are much higher than the highest calculated velocities [11] for ejecting multikilometer-sized fragments from Vesta.

Conclusions: The continuum of spectral properties of HEDs that span the reflectance range between the small "basaltic" asteroids and Vesta indicates that the spectral diversity of the basaltic asteroids in the main belt is consistent with the diversity in the HEDs. The orbital distribution of these small "basaltic" asteroids is consistent with these objects being ejected from Vesta with velocities up to 1 km/s. The Hubble Space Telescope has also revealed a 460-km impact basin on Vesta consistent with an impact event which resulted in substantial excavation [12]. All of this observational and dynamical evidence appears consistent with these small "basaltic" asteroids being fragments of Vesta.

References: [1] McCord T. B. et al. (1970) *Science, 168,* 1445–1447. [2] Larson H. P. and Fink U. (1975) *Icarus, 26,* 420–427. [3] Binzel R. P. and Xu S. (1993) *Science, 260,* 186–191. [4] Xu S. et al. (1995) *Icarus, 115,* 1–35. [5] Bus S. J. (1998) Ph.D. dissertation, Massachusetts Institute of Technology. [6] Zappalà V. et al. (1994) *Astron. J., 107,* 772–801. [7] Hiroi T. and Pieters C. M. (1998) *Antarct. Meteorite Res., 11,* 165–172. [8] Burbine T. H. et al. (1998) *LPS XXIX*, Abstract #1459. [9] Gaffey M. J. (1976) *JGR, 81,* 905–920. [10] Marzari F. et al. (1996) *Astron. Astrophys., 316,* 248–262. [11] Asphaug E. (1997) *Meteoritics & Planet. Sci., 32,* 965–980. [12] Thomas P. C. et al. (1997) *Science, 277,* 1492–1495.

PECULIAR FEATURES OF α MONOCEROTID TV SPECTRA. R. Stork[1,2], J. Borovicka[1], J. Bocek[1], and M. Solc[2], [1]Astronomical Institute, Academy of Sciences of the Czech Republic, Fricova 1, CZ–25165 Ondrejov, Czech Republic (stork@asu.cas.cz), [2]Institute of Astronomy, Charles University Prague, V Holesovickach 2, CZ–18000 Prague 8, Czech Republic (solc@mbox.troja.mff.cuni.cz).

An outburst of α Monocerotid meteors was widely observed on November 22, 1995. Jenniskens et al. found that α Monocerotids penetrate deeper into the atmosphere than meteoroids of the Orionid stream or Perseid stream (meteoroids with similar velocity) and that their light curves do not show flares [2]. The Jenniskens' results imply that α Monocerotids are more compact than meteoroids in other showers and can therefore contain lower amount of volatile elements. We obtained four α Monocerotid spectra with our television system on the Ondrejov observatory [1,3]. The spectra allowed us to test the above mentioned hypothesis. We found that the sodium line Na I (589 nm) is very faint in all α Monocerotid spectra. The velocity of the meteoroids is 64 km/s but the spectra have a specific appearance different from both Perseids (61 km/s) and Orionids (67 km/s). The hypothesis concerning low amount of volatile elements could be confirmed, at least for sodium. The α Monocerotid TV spectra will be presented together with a comparative statistical analysis of all observed showers. The dependence of meteor spectra on velocity will be also discussed.

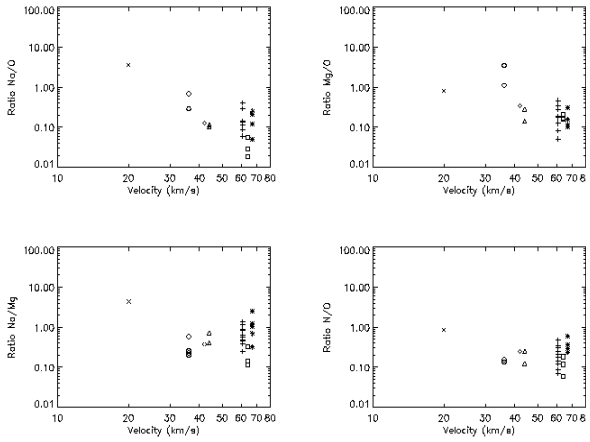

Fig. 1.

Figure 1 shows the ratio of the line intensities versus the meteor velocity. The measured spectral lines are Mg I-2 (517.8 nm), Na I-1 (589.2 nm), N I-1 (746.8 nm), O I-1 (777.4 nm). The plotted symbols correspond to the following meteor showers: asterisk — Orionids (67 km/s), square — α Monocerotids (64 km/s), plus sign — Perseids (61 km/s), triangle — δ Aquarids (44 km/s), diamond — Quadrantids (42 km/s), circle—Geminids (36 km/s) and x—very slow meteor (about 20 km/s).

The Na/O ratio decreases with increasing velocity. All showers agree with this dependence except of α Monocerotids. Their points lie significantly lower (please, note the logarithmic scale) and it indicates differences in meteoroids composition. The Na/Mg ratio also confirm low amount of sodium in the α Monocerotid spectra. The N and O lines are both atmospheric and their ratio should be constant, independent on velocity, as it has been approximately found.

Acknowledgments: Two of authors (R. Stork, M. Solc) acknowledge the support by Grant Agency of the Czech Republic (grant 96/205/0213)

References: [1] Borovicka J. and Bocek J. (1995) *Television spectra of meteors, Earth, Moon, and Planets, 71,* 237–244. [2] Jenniskens P. et al. (1997) *Ap. J., 479,* 441–447. [3] Stork R. (1998) *Optical and infrared observation of solid state interplanetary matter,* PhD Thesis, Charles University Prague.

MAGNETIC COSMIC SPHERULES FROM THE GREAT SAND SEA (WESTERN DESERT, EGYPT): A NEW EXAMPLE OF EOLIAN CONCENTRATION AND TRAPPING. A. M. Fioretti[1], G. Molin[2], G. Reniero[2], B. Piacenza[3], and R. Serra[4], [1]C. S. Geodinamica Alpina, C.N.R., I-35122 Padova (anna@dmp.unipd.it), [2]Dip.to Mineralogia e Petrologia dell'Universita', I-35122 Padova (gmario@dmp.unipd.it), [3]ENI-AGIP S.p.A. I-20097 San Donato Milanese (MI), [4]Dipartimento di Fisica dell'Universita' I-40126 Bologna, Italy (serra@df.unibo.it).

During a joint Italian-Egyptian expedition in the Western Desert (Egypt) dark "brush-strokes" fading into the usual golden colour were observed along the flanks of some sand dunes. In the southern part of the Great Sand Sea the long linear dunes run N-S and are separated by wide "corridors" whose floor is locally composed of Cretaceous sandstone. The prevailing wind blows southward and the dunes taper southward on a gently northward-deepening peneplain, on the Cretaceous Nubian Sandstone Formation.

The thin, millimetric black "veils" are mainly located on the distal part of the dunes. They are composed of fine black dust mixed with a little quartz sand. Several samples were collected on different dunes using a "home-made" magnetic rake device which provided a good concentration of magnetic particles. Optical investigations carried out under the stereomicroscope showed that the dark dust is mainly composed of subrounded to well-rounded opaque grains of high sphericity, mixed with minor amounts of quartz and silica glass grains. Among them, small, absolutely perfect spheres, with a smooth, polished surface and a metallic lustre are clearly manifest, representing less than 1% (visual estimation) of the total. Small amounts of magnetic particles from six different subsamples of dark sand were mounted on epoxy resin, sectioned, polished and studied by reflected light and SEM; chemical compositions were obtained by WDS-EMPA. The rounded opaque minerals are mostly terrestrial magnetite, ilmenite and hematite. The oxidised spherules are 100 to 200 microns long, with metal Fe-Ni eccentric cores 40 to 100 microns long. The external shells show typical dendritic structures (Figure).

Spherules with very different core compositions are found (e.g. $Fe_{80}Ni_{20}$ - Fe_5Ni_{95}) within each of the six samples, whereas the oxides constituting the shells show more uniform, Ni-depleted, compositions. Both texture and chemical composition [2], [3], [4] indicate that these spherules are micrometeorites.

We suggest that these micrometeorites, together with magnetite, hematite and ilmenite, which have high density were concentrated by an eolian mechanism. As the micrometeorites represent less than 1% of the black sand, the contemporaneous presence of magnetite, hematite and ilmenite in this area clearly played an essential role in revealing the micrometeorite concentration. The apparent contradiction that the heavier grains are found in the distal part of the dunes probably indicates that, in this area, only the light quartz grains can be windblown to a greater distance, causing selective concentration of the heavier dark grains. The bedrock, gently uprising in the prevailing wind direction, therefore constitutes a gravitational trap for the densest sand particles.

Whether these micrometeorites represent a concentration of superficial falls, are reworked spherules trapped in the sandstone which gave rise to the sand of the dunes or a combination of both is not yet clear.

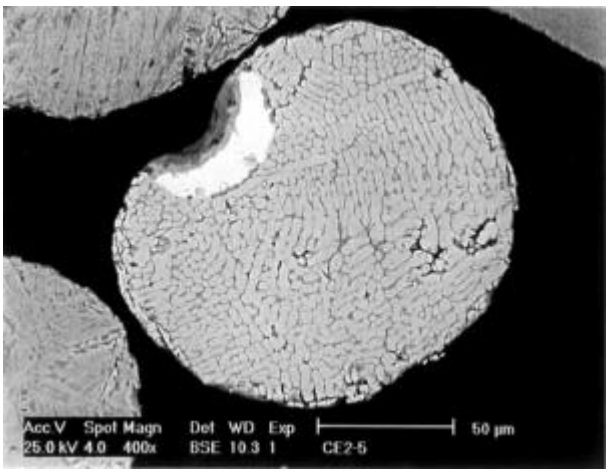

Acknowledgments: We are grateful to the Luigi Negro Foundation (Verderio Superiore, Lecco, Italy), Museum of Natural History of Milan (Italy) and Egyptian Geological Survey and Mining Authority (Cairo, Egypt) which organized and supported the expedition during which the micrometeorites were recovered. We thank V. de Michele for precious suggestions.

References: [1] De Michele eds. (1997) *Silica 96 Proceedings*, Pyramids snc - Milan (Italy) Publisher. [2] Blanchard M.B. et al. (1980) *EPSL*, **46,** 178-190. [3] Bi D. et al. (1993) *Geochim. Cosmochim. Acta* **57**, 4129-4136. [4] Kosakevitch A. & Disnar J.R. (1997) *Geochim. Cosmochim. Acta* **61,** 1073-1082.

CARBON AND POTASSIUM MAPPING AND CARBON BONDING STATE MEASUREMENTS ON INTERPLANETARY DUST. G. J. Flynn[1], L. P. Keller[2], C. Jacobsen[3], and S. Wirick[3], [1]Department of Physics, State University of New York–Plattsburgh, Plattsburgh NY 12901, USA, [2]MVA, Inc., 5500 Oakbrook Parkway, Norcross GA 30093, USA, [3]Department of Physics, State University of New York–Stony Brook, Stony Brook NY 11794, USA.

We previously employed the Scanning Transmission X-Ray Microscope (STXM) in two modes, one to map the distribution of C and a second to determine the C bonding state at selected spots using X-ray Absorption Near Edge Structure (XANES) spectroscopy, on Interplanetary Dust Particles (IDPs). A new stack-imaging capability, eliminating problems previously experienced due to sample drift during the acquisition of C-XANES spectra, allows us to take full advantage of the ~50 nm spatial resolution of the STXM for spectroscopy.

In the stack-imaging mode, the absorption of focused, monochromatic X-rays is measured at each pixel on a thin-section. Typically 150 to 200 absorption images are taken over the range 270 to 310 eV, with an energy spacing of ~0.1 eV in the pre-edge region. The images are aligned, correcting for sample drift during the sequence. The C-XANES spectrum is extracted either at a point by examining the image-stack along a single pixel, or over a region of interest by adding the pixels corresponding to that region in each image. At each energy, the reference intensity (on the substrate) and sample intensity are measured on the same image, rather than in two successive spectra which are sometimes offset slightly in energy due to nonreproducibilities in the monochrometer motion (a problem being addressed in a redesign of the STXM).

We analyzed three IDPs using the new stack-imaging technique. Transmission Electron Microscope (TEM) examination indicates L2008F7 is a hydrated IDP dominated by Mg-rich saponite, and containing fine-grained Fe-Ni-sulfides and Mg-Fe carbonates. It has a thin, discontinuous magnetite rim, indicating moderate entry heating. SEM-EDX indicates L2009F7 contains ~14 wt.% C. The stack-image analysis of L2008F7 identified individual, submicrometer, C-rich grains and larger regions, up to several micrometers in size of C-rich material. These C-rich regions exhibit peaks at 285 eV, 286.5 eV, and 288.2 eV, very similar to peaks from organic C in other samples.

L2011*B2 (Cluster 7) is a compact IDP dominated by coarse-grained, low-Ca pyroxene with inclusions of low-Ni sulfides. No tracks were observed in the TEM, and a thin magnetite rim indicates the particle was heated on atmospheric entry. L2011*B2 has a relatively high K content. The L-lines of K occur at ~297 eV and ~299.8 eV. By comparing images taken at 297 eV and 295 eV, we mapped the K distribution. Potassium is apparently concentrated in the pyroxene, though we are investigating possible contamination. Both C and K were detected in some individual pixels, indicating C is intermixed with pyroxene on the ~100-nm scale. This fragment has C-rich regions around its perimeter, possibly suggesting that C was mobilized during entry heating and redistributed on the exterior. The C has similar C-XANES spectra in both sites, exhibiting peaks at 285.1 eV, 286.6 eV, and 288.5 eV, again indicating organic C.

L2009*E2 (Cluster 7) is a D-rich cluster fragment, with regions having D/H ~400‰. Other fragments from this cluster have D/H up to 11,000‰ [1]. L2009*E2 is anhydrous, dominated by olivine and pyroxene, Glass with Embedded Metal and Sulfides (GEMS) and C (~3 × CI). The stack-image analysis identified numerous C-rich regions, up to micrometer size. Unlike the other two IDPs, which show only a single C-XANES spectrum wherever C is detected, L2009*E2 exhibits several C-XANES spectra. Peaks occur at 285.2 eV, 287 eV and 288.2 eV. In some spots the 288.2 eV peak occurs alone, while it occurs in combination with the 287 eV peak and a weak 285.2 eV peak in other spots. Thus, L2009*E2 appears to contain at least two distinct C species.

References: [1] Keller L. P. and Messenger S. (1998) *LPS XXIX*.

VOLATILE CONTENTS OF LARGE AND SMALL INTERPLANETARY DUST PARTICLES FROM L2036: COMPARISON OF ZINC AND HELIUM HEATING INDICATORS. G. J. Flynn[1], S. R. Sutton[2], K. Kehm[3], and C. M. Hohenberg[3], [1]Department of Physics, State University of New York–Plattsburgh, Plattsburgh NY 12901, USA, [2]Department of Geophysical Sciences, The University of Chicago, Chicago IL 60637, USA, [3]McDonnell Center for the Space Sciences, Washington University, St. Louis MO 63130, USA.

We have begun a comprehensive study of the volatile element and noble gas contents of three types of chondritic IDPs—small (~10 μm) IDPs, large (>25 μm) IDPs collected intact, and large IDPs which fragment on collection ("cluster particles")—from the same stratospheric collector. The objectives are to determine if these different types of IDPs have significantly different (1) chemical compositions, (2) atmospheric entry heating characteristics, and/or, (3) space exposure histories. Thus far, nine large IDPs collected intact and eight small IDPs from the L2036 collector have been examined.

Four large IDPs had Zn/Fe <0.3 × CI, an indicator of significant atmospheric entry heating [1], while five had Zn/Fe >0.3 × CI, suggesting little element loss during entry. The average element/Fe pattern of the five IDPs with Zn/Fe >0.3 × CI is flat, with elements having low nebula condensation temperatures (Cu, Ga, Ge, Se, Zn, and S) plotting between the CI and CM meteorites, while Br is enriched to ~13 × CI. This pattern has previously been reported for large IDPs from other collectors [2].

Three small IDPs had Zn/Fe <0.3 × CI, while five had Zn/Fe >0.3 × CI. The five with Zn/Fe >0.3 × CI show an average enrichment of elements having low condensation temperatures to ~3 × CI, with Br ~40 × CI, consistent with ~10 μm IDPs from other collectors [3]. Thus, even comparing particles from the same collector, large IDPs collected intact are chemically distinct from small IDPs, which are enriched in elements having low condensation temperatures compared to the most volatile-rich meteorites.

The large IDPs are ~2.5 times bigger and SEM images suggest they are generally more compact than the small IDPs. If both groups had similar atmospheric entry velocities, then modeling indicates the large IDPs would, on average, be heated ~400 K higher than the small IDPs. However, roughly the same fraction of large IDPs (4 of 9 = 44%) and small IDPs (3 of 8 = 38%) experienced significant Zn loss, suggesting similar heating histories.

These measurements provide the first opportunity to compare the degree of heating inferred from Zn and He contents measured on the same IDPs. Helium was measured on seven of the small IDPs. All three low-Zn IDPs had low He contents, while the four with Zn >0.3 × CI had significantly higher He abundances [4], indicating qualitative agreement between the two heating indicators.

The results for the six large IDPs on which He and Zn were measured are more complicated. The two with low Zn have low He contents. However, two of four with Zn >0.3 × CI also have low He contents [4]. Thus, He indicates 66% (4 of 6) of the large IDPs but only 43% (3 of 7) of the small IDPs were severely heated.

The conflict between these two heating indicators might result from the locations of Zn and He [4]. Zinc is distributed throughout, thus Zn loss measures interior temperature. However, solar He is implanted only a few monolayers into the surface. Thus, He content should monitor the surface temperature. Thermal gradients, possibly resulting from dehydration of clays or alteration of organics, have been suggested to inhibit Zn loss from the interior of large IDPs [5]. This mechanism is consistent with the observed difference between the two heating indicators.

References: [1] Flynn G. J. et al. (1993) *LPS XXIV*, 497–498. [2] Flynn G. J. et al. (1995) *Meteoritics, 30*, 505. [3] Flynn G. J. et al. (1996) in *Physics, Chemistry and Dynamics of Interplanetary Dust*, pp. 291–294, ASP Conference Series, V104. [4] Kehm K. et al. (1998) *LPS XXIX*. [5] Flynn G. J. (1995) *LPS XXVI*, 405–406.

THERMAL MODIFICATION OF SYNTHETIC NANODIAMONDS AS ANALOGUE OF METEORITIC DIAMOND GRAINS. A. P. Koscheev[1], I. A. Panin[1], and U. Ott[2], [1]Karpov Institute of Physical Chemistry, ul. Vorontzovo Pole 10, Moscow, 103064, Russia, [2]Max-Planck-Institut für Chemie, Becherweg 27, D-55128 Mainz, Germany (ott@mpch-mainz.mpg.de).

The low abundance of diamond micrograins in meteorites restricts the possibility to use them in simulation laboratory experiments which could provide information concerning their origin and properties. A promising candidate as an artificial analogue is ultradispersed detonation diamond (UDD) the mean size and IR spectra of which is similar to that of meteoritic diamond [1,2].

We have tried to develop an approach - using thermal treatment in vacuum and in oxygen - both in order to understand the differences between different types of UDD and as a means of modification in order to obtain a close analogue to the meteoritic diamonds.

The nanodiamonds used were several types of UDD powder produced by detonation processes in different Russian Research Centers with approx. the same mean crystal size of 3–4 nm but different composition and structure of surface functional groups as shown by IR spectra and in the gas release features during pyrolysis.

Mass spectra of volatiles released from UDD as received were measured in the dynamic mode during heating in vacuum up to 1100°C with a rate 11°C/min and revealed the presence of H_2O (100°–600°C), CO_2 (200°–600°C), CO (500°–900°C) and H_2 (above 800°C) as main components and a variety of minor species including hydrocarbons. The temperature profiles of CO and CO_2 depended strongly on the type of UDD used reflecting different oxidation states of their surfaces. This was confirmed by the IR spectra showing differences in the position of the prominent absorption band 1730–1780 cm^- assigned to C=O bonds [3,4].

Preheating of UDD in air at temperatures up to 450°C for 30 min affected both the IR spectra and the CO/CO_2 release curves (see Figure). In particular, a «low temperature» peak of CO release at 550°C appeared in addition to the «high temperature» peak at 750°–800°C. The C=O band shifted to 1790 cm^{-1} after preoxidation. Both gas release features and IR spectra of different UDD were very much alike after the 400°–450°C oxidation. Vacuum heating up to 650°C reduced the oxidation state of UDD which could be recovered by repeating the heating in air.

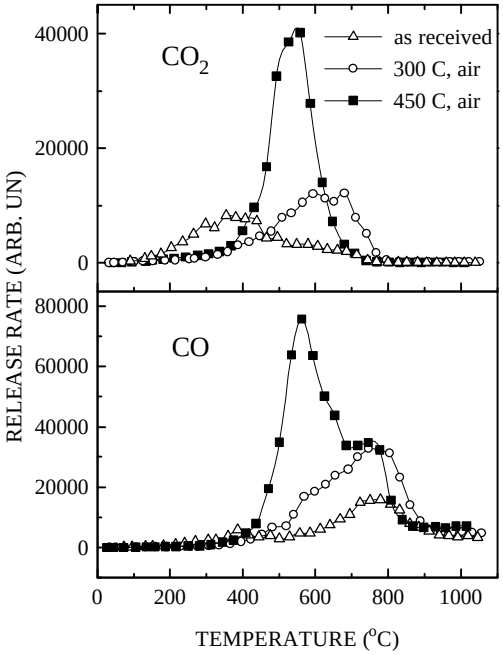

In general, the obtained result indicate the existence of two different types of C=O bonds on the surface of UDD and point to a simple method to modify the oxidation state of nanodiamonds, thus providing the possibility to change in a controlled manner their surface properties. This may be of relevance with regard to the interpretation of gas release patterns observed during pyrolysis of meteoritic nanodiamonds [5,6].

Acknowledgments: This work was partly supported by RFBR-DFG (Grant# 96-05-00038).

References: [1] Greiner N. R. et al. (1988) *Nature, 333,* 440–442. [2] Daulton T. L et al. (1996) *GCA, 60,* 4853–4872. [3] Lewis R. S. et al. (1989) *Nature, 339,* 117–121. [4] Mutschke H. et al. (1995) *Astrophys. J., 454,* L157–L160. [5] Verchovsky A. B. and Pillinger C. T. (1996) *LPS. XXVII,* 1361–1362. [6] Zadnik M. G. et al. (1998) *Meteoritics and Planet. Sci.,* this issue.

ISOTOPIC COMPOSITION OF ZR AND MO IN SINGLE SIC PRESOLAR GRAINS: AGB MODEL PREDICTION AND MEASUREMENTS. R. Gallino, *Dipartimento di Fisica Generale, Universita' di Torino, I-10125 Torino, Italy, gallino@ph.unito.it*, M. Lugaro, *Department of Mathematics, Monash University, Clayton, Victoria 3168, Australia, marial@thala.maths.monash.edu.au*, C. Arlandini, *Forschungszentrum Karlsruhe, Institut fur Kernphysik, D-76021 Karlsruhe, Germany, claudio@ik3.fzk.de*, M. Busso, *Osservatorio Astronomico di Torino, Torino, Italy, maurizio@otoxd6.to.astro.it*, O. Straniero, *Osservatorio Astronomico di Collurania, Teramo, Italy, straniero@astrte.te.astro.it.*

Abstract: We report the results of the s-process Zr and Mo isotopic abundance composition for AGB star models of solar metallicity and mass of 1.5 and 3 $M_{\odot}$, as compared with recent measurements of isotopic ratios in single presolar SiC grains [1,2]. We have made use of the stellar models described in [3], computed by the FRANEC code, while the s-process has been calculated by a post-processing in which the major neutron source is the ^{13}C burning radiatively [4,5]. We show that model predictions match all the single grain measurements, when we allow a range of variation for stellar parameters, thus confirming a multiplicity of AGB stars as source of SiC grains.

Introduction: There are many evidences that the origin of SiC grains found in carbonaceous meteorites, such as Murchison, has to be connected to AGB stars, which are evolved low mass stars burning alternatively H and He in shells. Thanks to third dredge-up episodes progressively mixing partial He-burning ashes into the envelope, in late phases AGB envelopes becomes richer in carbon than in oxygen: C/O>1, allowing the condensation of SiC dusts in their circumstellar regions feeded by strong stellar winds. Indeed, the emission line at 11.2 μm, characteristic of SiC, is a typical signature of C-rich AGB stars. As for trace heavy elements, their isotopic composition can be described as a combination of a normal component, close to solar, and of a pure s-component, which is to be connected to the s-process nucleosynthesis occurring in AGB stars in the He intershell and in thermal pulses [4]. So far, isotopic ratios of the heavy elements Sr, Kr, Xe, Ba, Nd, Sm and Dy have been measured in bulk SiC grains. Mo and Zr compositions were impossible to obtain because of isobaric interferences. The measurements in individual SiC grains provide an insight on single AGB star s-process nucleosynthesis. The different isotopic compositions found in single grains can be explained varying the ^{13}C supply in the intershell region, or considering AGB models with different initial stellar masses. Single grains show a multiplicity of AGB stars polluting the presolar system nebula, while the average behaviour of such a variety of AGB stars can be inferred by the analysis of SiC grains aggregates.

Results and Discussion: In Fig.1 we show our predictions for s-process ^{90,94,96}Zr and ^{92,95,96}Mo isotopic composition for two solar composition stellar models of different mass, combined with six different choices of the amount of ^{13}C, where the case *ST* (standard) refers to figure 1 of reference [5]. The open symbols are for compositions corresponding to C/O>1 in the envelope and little crosses are single grains measurements ($\pm 2\sigma$) from references [1,2]. The most model-dependent isotope is ^{96}Zr. It is produced only when the branching at ^{95}Zr is open, that is under condition of high neutron density. The maximum neutron density is very low during the radiative phases ($N_{n,max}(rad) \sim 10^7$ n/cm^3), but reaches high peak values ($N_{n,max}(conv) \sim 10^{10}$ n/cm^3) during the convective termal pulses when the second marginal neutron source, the ^{22}Ne, is activated. As a consequence we can obtain very different final amount of ^{96}Zr as function of the listed above stellar parameters. As clearly shown in Fig. 1, this results is confermed by the $\delta(^{96}Zr/^{94}Zr)$ found in individual SiC grains spreading from -400 to -1000. This measurements confirm our choice for low mass and about solar metallicity AGB stars as parents of presolar SiC grains, as well as our treatment for the evolution of the envelope composition, that strongly depend on mass loss and third dredge-up features. As for Mo, there is not a big spread of values and results are in very good agreement. Note that ^{95}Mo depends on the treatment of the branching at ^{95}Zr. The plots also show how the majority of the grains are expected to come from AGB stars experiencing a radiative neutron flux near to cases from *d2* to *ST*, as confirmed by the bulk SiC grain Ba and Sr measurements (see the Lugaro et al. abstract), while the case *u2* is to be considered an upper limit in the frame of single SiC grains. Note the the case *u2* is a best fit for reproducing the solar s-main component.

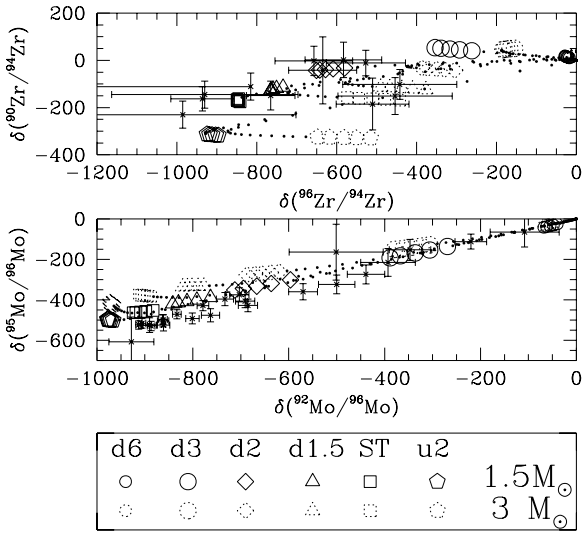

Figure 1: AGB envelope model predictions and individual SiC grains measurements from [1,2] of selected Zr and Mo isotopic composition.

References [1] Nicolussi, G. K. et al. (1997), Science,

in press. [2] Nicolussi, G. K. et al. (1998), submitted to Geochim. Cosmochim. Acta. [3] Straniero, O. et al. (1997), ApJ, 478, 332. [4] Gallino, R. et al. (1997), *Astrophysical Implications of the Laboratory Study of Presolar Materials*, ed. T. Bernatowicz & E. Zinner, (New York: AIP), 115. [5] Gallino, R. et al. (1998), ApJ, 497, 388.

Acknowledgments: M. Lugaro gratefully acknowledges the support of an Overseas Postgraduates Research Scheme grant by the Australian Government.

ISOTOPIC COMPOSITION OF HEAVY ELEMENTS IN SINGLE SIC GRAINS: AGB MODEL PREDICTION: THE CASE OF SR AND BA. M. Lugaro, *Department of Mathematics, Monash University, Clayton, Victoria 3168, Australia, marial@thala.maths.monash.edu.au*, R. Gallino, *Dipartimento di Fisica Generale, Universita' di Torino, Via P. Giuria 1, I-10125 Torino, Italy, gallino@ph.unito.it*, M. Busso, *Osservatorio Astronomico di Torino, Torino, Italy, maurizio@otoxd6.to.astro.it.*

Abstract: We report the results of the s-process Sr and Ba isotopic abundance composition for AGB star models of solar metallicity and mass of 1.5 and 3 $M_{\odot}$. We have made use of the stellar models described in [1], computed by the FRANEC code, while the s-process nucleosynthesis has been calculated by a post-processing in which the major neutron source is the ^{13}C burning radiatively [2]. Sr and Ba isotopic isotopic compositions have been measured so far only in bulk SiC grains [3-7]. We show how and why, while bulk SiC measurements can be reproduced by one standard choice of stellar parameters, we instead expect a wide range of isotopic composition for individual SiC grains measurements.

Introduction: The origin sites of SiC grains found in carbonaceous meteorites are most likely the dust rich envelopes of ABG stars. There, He-shell material is mixed into the convective envelope by third dredge-up episodes so that the resulting envelope composition is a mixture of s-processed (the socalled G-component) and solar composition (N-component) material. Both Ba and Sr in bulk SiC grains show a clear s-signature: their p-only isotopes (^{84}Sr and ^{130,132}Ba), which are destroyed by neutron captures, are present in very low amount, while the s-only isotopes of Ba (^{134,136}Ba) are the most abundantly produced. As for the s-only isotopes ^{86,87}Sr, a fraction ($\sim$ 50%) of their solar abundance comes from the s-process weak component produced in massive star, thus they could not, and do not, show in SiC a strong overproduction respect to ^{88}Sr, which is mainly produced by the s-process in AGB stars. The interesting point of presenting the Sr and Ba model predictions in AGB envelopes is the fact that both ^{88}Sr and ^{138}Ba are magic nuclei, which means that they have low neutron capture cross sections, so to act as bottleneck on the s-flux. As a consequence their production is very sensitive to the time integrated neutron flux (neutron exposure, τ) coming from the ^{13}C burning radiatively neutron source. This τ is quite large: $\sim$0.4 mbarn^{-1}, at least 10 times bigger as compared to the one released by the second marginal neutron source, the ^{22}Ne, which is activated for a very short time during the convective termal pulses. This latter neutron source however can strongly influence the production of branching-sensitive isotopes, such as ^{96}Zr and ^{134}Ba, which depend on the s-branching at the unstable isotope ^{95}Zr and ^{134}Cs, respectively, and also ^{86,87}Sr, both depending on the branching at ^{85}Kr. It is interesting to see how varying τ, $\delta(^{88}\mathrm{Sr}/^{86}\mathrm{Sr})$ and $\delta(^{138}\mathrm{Ba}/^{136}\mathrm{Ba})$ change so that while a typical value of τ can be considered as an average for SiC grain parent stars, reproducing Sr and Ba isotopic compositions in bulk SiC, a wider range of values must to be found in single SiC grains, as they are expected to condens in the winds of different AGB stars (see Gallino et al. abstract).

Results and Discussion: In Fig.1 we show our predictions for s-process ^{84,86,88}Sr and ^{135,136,138}Ba isotopic composition for solar metallicity in the envelope of ABG stars of different initial mass, combined with six different choices of the amount of ^{13}C supplied in the He intershell, where the case *ST* refers to figure 1 of reference [2]. Note that the case labeled as *u2* represents a best fit solution to the solar s-main component. The open symbols are for compositions corresponding to C/O>1 in the envelope, while small crosses are data for bulk SiC grains from references [5,6]. In terms of s-process nucleosynthesis results, the amount of ^{13}C is connected to the neutron exposure that is in good approximation proportional to ^{13}C/Z, where Z is the stellar metallicity. The amount of ^{13}C can vary from star to star and is determined by the amount of protons that can be diffused from the convective envelope into the He-shell during each third dredge-up: something that is still not fixed by stellar models, depending on rather difficult hydrodynamical treatment. As for Sr, what is puzzling is the apparent solar composition of ^{86,87,88}Sr [6]: the $\delta(^{87,88}\mathrm{Sr}/^{86}\mathrm{Sr})$ values measured in bulk SiC grains being close to zero. Our predicted $\delta(^{87}\mathrm{Sr}/^{86}\mathrm{Sr})$ depend almost only on the relative neutron capture cross sections and has a small range of variation (from -50 to +100), due to the way the neutron fluence freezes out at the quenching of the small ^{22}Ne neutron release, while $\delta(^{88}\mathrm{Sr}/^{86}\mathrm{Sr})$ varies greatly with the amount of ^{13}C (from -500 to 1000). Our predictions show how, whereas the average of the grains points to a given ^{13}C choice (*ST*) we actually expect individual SiC grains to show $\delta(^{88}\mathrm{Sr}/^{86}\mathrm{Sr})$ varying in a wide

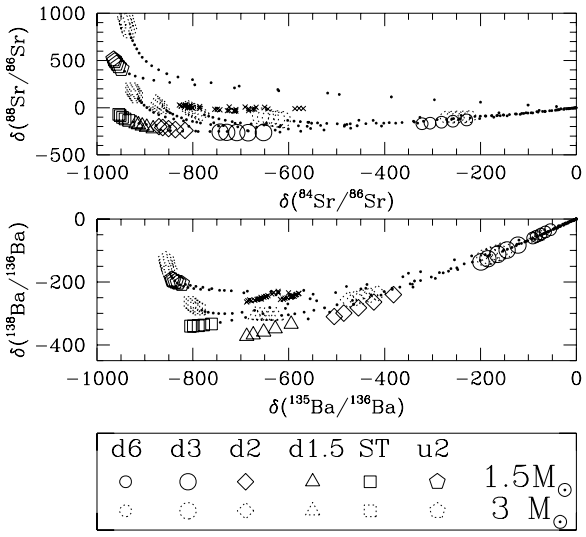

Figure 1: AGB envelope model predictions and bulk SiC grains measurements (small crosses) from [5,6] of selected Sr and Ba isotopic compositions.

range of values, from -300 to +1000. Analogous prediction holds to $\delta(^{138}Ba/^{136}Ba)$: in this case too we have a significative variation (from -400 to -100) with the ^{13}C, whereas the bulk grain measurements point again to the *ST* ^{13}C case. We have got model predictions for isotopic ratios of all heavy elements in AGB envelopes. In particular, besides Sr, and Zr, Ru is a candidate trace element to be measured in single SiC grains, as well as the heaviest W and Os, because of their possible condensation as carbides (likely in the form of subgrains). As for Ru, the two p-only isotopes $^{96,98}Ru$ are destroyed during the s-process. The same is true for the r-only ^{104}Ru, while ^{100}Ru is an s-only isotope. AGB envelope ratios of Ru, with ^{102}Ru as reference isotope, would correspond for the *ST* case to typical δ values of +1000 for ^{100}Ru, -500 for ^{101}Ru, -800 for $^{96,98,104}Ru$, with a linear spread for other cases, mimicking the Mo isotopic composition. An interesting isotope is ^{99}Ru, fed by the decay of radioactive ^{99}Tc both in the He shell and in the envelope. Measurement of $\delta(^{99}Ru/^{102}Ru)$ would range around -550 for the *ST* case, with some spread for different AGB initial masses. Because ^{99}Tc has a meanlife highly dependent on temperature [8], it might help to confirm our treatment of long-lived isotopes. Similar considerations hold for Os, where ^{184}Os is p-only, ^{186}Os s-only, and ^{192}Os r-only. As to W, there is an important branching feature at ^{185}W, substantially feeding the neutron-rich ^{186}W.

References [1] Straniero, O. et al. (1997), ApJ, 478, 332. [2] Gallino, R. et al. (1998), ApJ, 497, 388. [3] Ott U. & Begemann F. (1990), Lunar Planet. Sci. XXI, 920. [4] Ott U. & Begemann F. (1990), ApJ, 353, L57. [5] Prombo, C.A. et al. (1993), ApJ, 410, 393. [6] Podosek, F. et al. (1998), ApJ, in press. [7] Richter S. et al. (1992), Lunar Planet. Sci. XXIII, 1147. [8] Takahashi, K. & Yokoi, K, (1987), Atom. Data Nucl. Data Tables, 36, 375.

Acknowledgments: M. Lugaro gratefully acknowledges the support of an Overseas Postgraduates Research Scheme grant by the Australian Government.

SEARCH FOR METEORITES IN THE PATRIOT HILLS AREA, ELLSWORTH MOUNTAINS, WEST ANTARCTICA. P. Lee[1], W. A. Cassidy[2], D. Apostolopoulos[3], M. Deans[3], A. Foessel[3], C. Krause[4], J. Parra[5], L. Pedersen[3], K. Schwehr[1], and W. L. Whittaker[3], [1]NASA Ames Research Center, MS 245-3, Moffett Field CA 94035-1000, USA, [2]Department of Geology and Planetary Science, University of Pittsburgh, Pittsburgh PA 15260, USA, [3]The Robotics Institute, Carnegie Mellon University, Pittsburgh PA 15213, [4]Fuerza Aerea de Chile, [5]Museo Nacional de Historia Natural, Santiago, Chile.

Introduction: Between Dec. 30, 1997, and Jan. 25, 1998, a human search for meteorites was conducted at Patriot Hills (80°20"S, 81°20'W), Ellsworth Mountains, West Antarctica, as part of a site characterization study for the Robotic Antarctic Meteorite Search (RAMS) Project. The goal of the RAMS Project of the Robotics Institute of Carnegie Mellon University is to develop a robotic vehicle, using the NOMAD rover, capable of searching for meteorites in Antarctica autonomously. The Patriot Hills site was chosen because of its relative ease of access and because a wide variety of terrestrial rock types was known to be present [1]. A program of field tests of components and instruments to be integrated onto NOMAD in late 1998 was carried out at at Patriot Hills during the 97–98 field season in conjunction with the search for meteorites reported here.

Meteorite Search: The areas searched include both blue ice fields and moraines. The blue ice fields of Patriot Hills and nearby Independence Hills, Morris Cliff, Marble Hills, and Minaret Bowl were traversed and searched for meteorites by snowmobile and on foot. Two additional blue ice fields above Morris Cliff and between Mt. Simmons and Mt. Geissel (Independence Hills) were accessed by light aircraft and searched on foot. A total blue ice area of approximately 60 km^2 was covered, representing the bulk of the blue ice area available between Mt. Shattuck, Patriot Hills, and Minaret Peak. The polymict, allochtonous portions of the moraines associated with Patriot Hills, Independence Hills, Morris Cliff, Marble Hills, and Minaret Bowl were also searched. The total linear distance of moraine walked was approximately 35 km.

Result: No meteorite was found. Two explanations for this outcome are possible: (1) The relatively low altitude of the blue ice fields at Patriot Hills (800–1100 m vs >2000 m for typical meteorite concentration sites [2]) make for relatively warm summer peak temperatures leading to seasonal melting of surface ice. Meteorites exposed at Patriot Hills would likely be subject to rapid weathering and/or would not be able to be exposed at the surface without sinking deeper into the ice by melting the ice radiatively ; cryoconite holes, melt ponds, and refrozen ice are pervasive and attest to the significance of this temperature effect. (2) The history and sources of ice in the Patriot Hills area are unknown and might have been inadequate for concentrating meteorites. The blue ice fields might have been exposed as potential meteorite stranding surfaces only recently, and/or the upstream gathering area might not be extensive. None of the above explanations can be ruled out at present. However, regardless of the explanation, it can be safely concluded that the Patriot Hills site is not a productive search area for meteorites.

References: [1] Craddock C. et al. (1986) *Geologic Map of the Ellsworth Mountains*, GSA. [2] Cassidy W. A. (1991) in *The Geology of Antarctica*, pp. 652–666, Oxford Univ.

Acknowledgements: We are grateful to Gino Casassa of Universidad de Magallanes and Ralph P. Harvey of Case Western Reserve University for useful discussions. Thanks are also due to the National Aeronautics and Space Administration (NASA) and the Instituto Antartico Chileno (INACH) for their support.